

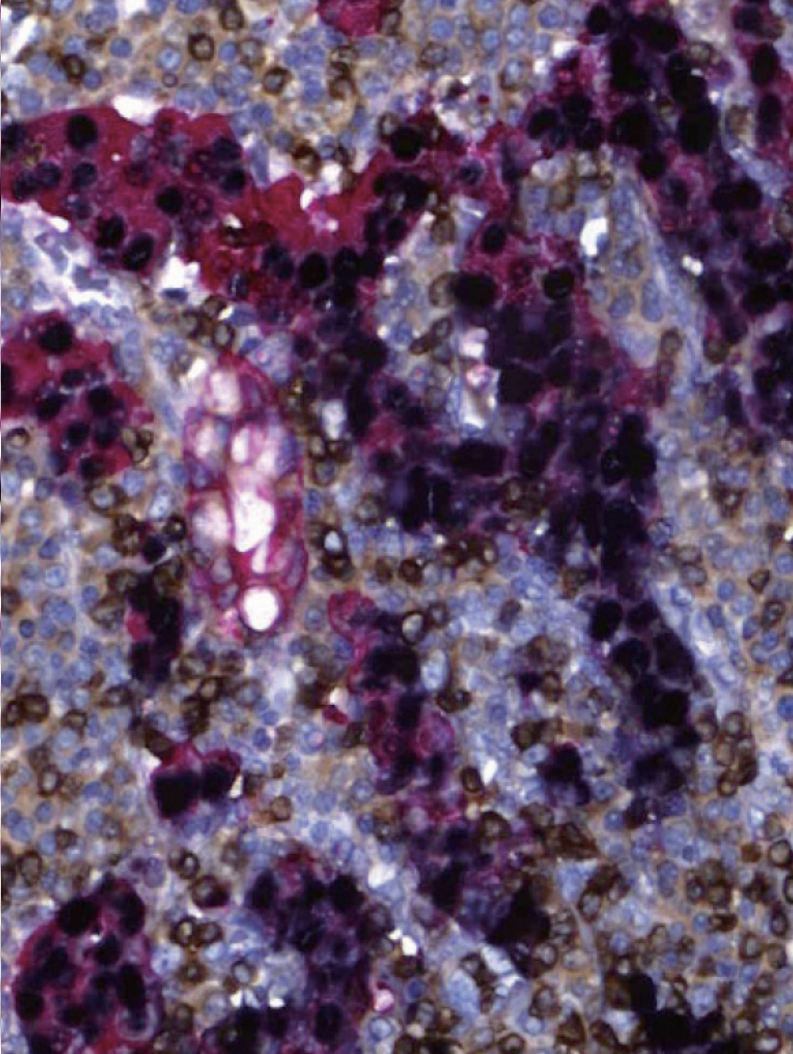
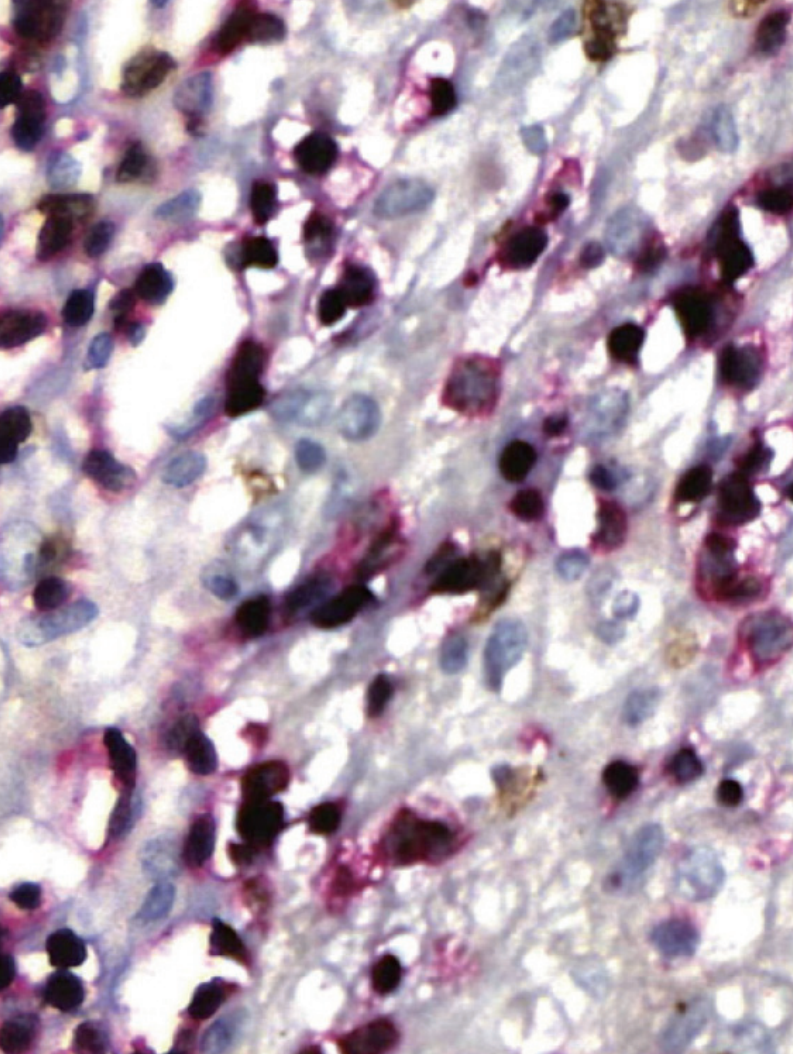
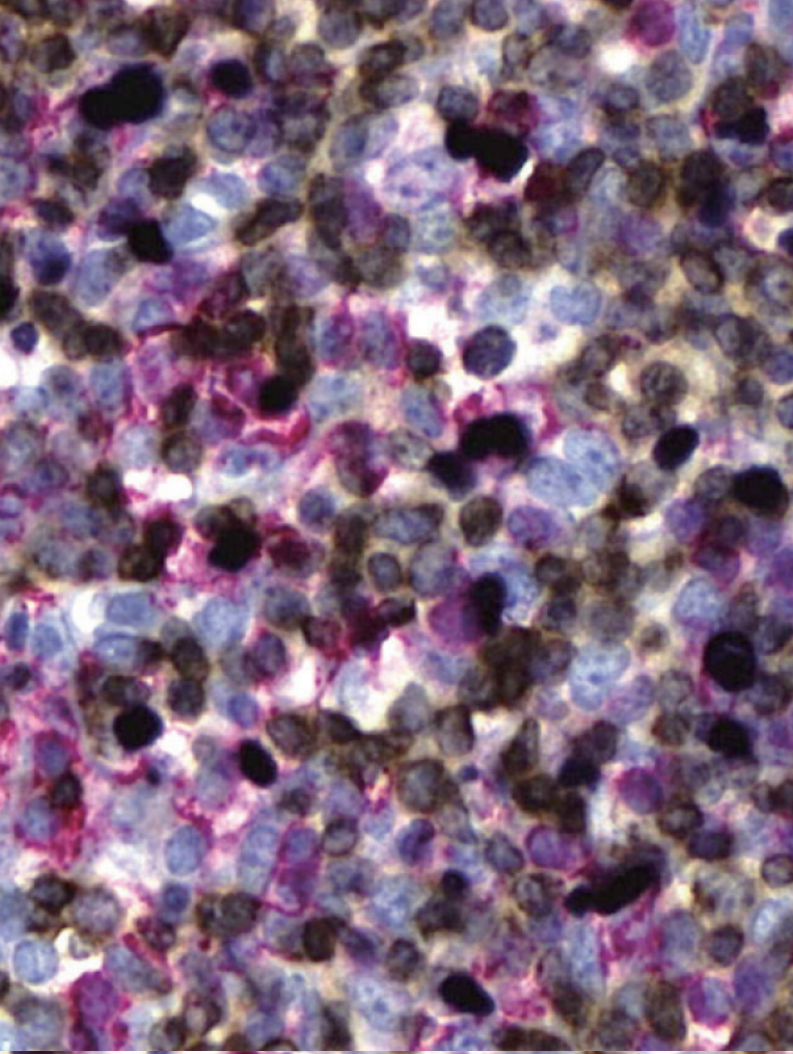
JPTM

Journal of **Pathology**
and **Translational Medicine**

September 2019
Vol. 53 / No.5
jpatholtm.org
pISSN: 2383-7837
eISSN: 2383-7845



*Application of the Optimized
Multistaining Protocol
to Various Epstein-Barr
Virus-Associated
Malignancies*



Aims & Scope

The *Journal of Pathology and Translational Medicine* is an open venue for the rapid publication of major achievements in various fields of pathology, cytopathology, and biomedical and translational research. The Journal aims to share new insights into the molecular and cellular mechanisms of human diseases and to report major advances in both experimental and clinical medicine, with a particular emphasis on translational research. The investigations of human cells and tissues using high-dimensional biology techniques such as genomics and proteomics will be given a high priority. Articles on stem cell biology are also welcome. The categories of manuscript include original articles, review and perspective articles, case studies, brief case reports, and letters to the editor.

Subscription Information

To subscribe to this journal, please contact the Korean Society of Pathologists/the Korean Society for Cytopathology. Full text PDF files are also available at the official website (<http://jpathol.tn.org>). *Journal of Pathology and Translational Medicine* is indexed by Emerging Sources Citation Index (ESCI), PubMed, PubMed Central, Scopus, KoreaMed, KoMCI, WPRIM, Directory of Open Access Journals (DOAJ), and CrossRef. Circulation number per issue is 700.

Editors-in-Chief

Jung, Chan Kwon, MD (*The Catholic University of Korea, Korea*) <https://orcid.org/0000-0001-6843-3708>
Park, So Yeon, MD (*Seoul National University, Korea*) <https://orcid.org/0000-0002-0299-7268>

Senior Editors

Hong, Soon Won, MD (*Yonsei University, Korea*) <https://orcid.org/0000-0002-0324-2414>
Kim, Chong Jai, MD (*University of Ulsan, Korea*) <http://orcid.org/0000-0002-2844-9446>

Associate Editors

Shin, Eunah, MD (*CHA University, Korea*) <http://orcid.org/0000-0001-5961-3563>
Kim, Haeryoung, MD (*Seoul National University, Korea*) <http://orcid.org/0000-0002-4205-9081>

Editorial Board

Avila-Casado, Maria del Carmen (*University of Toronto, Toronto General Hospital UHN, Canada*)

Bae, Young Kyung (*Yungnam University, Korea*)

Bongiovanni, Massimo (*Lausanne University Hospital, Switzerland*)

Choi, Yeong-Jin (*The Catholic University, Korea*)

Chung, Jin-Haeng (*Seoul National University, Korea*)

Fadda, Guido (*Catholic University of Rome-Foundation Agostino Gemelli University Hospital, Italy*)

Gong, Gyungyub (*University of Ulsan, Korea*)

Ha, Seung Yeon (*Gachon University, Korea*)

Han, Jee Young (*Inha University, Korea*)

Jang, Se Jin (*University of Ulsan, Korea*)

Jeong, Jin Sook (*Dong-A University, Korea*)

Kang, Gyeong Hoon (*Seoul National University, Korea*)

Kim, Aeree (*Korea University, Korea*)

Kim, Jang-Hee (*Ajou University, Korea*)

Kim, Jung Ho (*Seoul National University, Korea*)

Kim, Kyu Rae (*University of Ulsan, Korea*)

Kim, Se Hoon (*Yonsei University, Korea*)

Kim, Woo Ho (*Seoul National University, Korea*)

Ko, Young Hyeh (*Sungkyunkwan University, Korea*)

Koo, Ja Seung (*Yonsei University, Korea*)

Lee, C. Soon (*University of Western Sydney, Australia*)

Lee, Hye Seung (*Seoul National University, Korea*)

Lkhagvadorj, Sayamaa (*Mongolian National University of Medical Sciences, Mongolia*)

Moon, Woo Sung (*Chonbuk University, Korea*)

Park, Chan-Sik (*University of Ulsan, Korea*)

Park, Young Nyun (*Yonsei University, Korea*)

Shahid, Pervez (*Aga Khan University, Pakistan*)

Sung, Chang Ohk (*University of Ulsan, Korea*)

Than, Nandor Gabor (*Semmelweis University, Hungary*)

Tse, Gary M. (*The Chinese University of Hong Kong, Hong Kong*)

Tan, Puay Hoon (*National University of Singapore, Singapore*)

Yatabe, Yasushi (*Aichi Cancer Center, Japan*)

Yoon, Sun Och (*Yonsei University, Korea*)

Bychkov, Andrey (*Chulalongkorn University, Thailand Kameda Medical Center, Japan Nagasaki University Hospital, Japan*)

Chong, Yo Sep (*The Catholic University of Korea, Korea*)

Jain, Deepali (*All India Institute of Medical Sciences, India*)

Jun, Sun-Young (*The Catholic University of Korea, Korea*)

Lai, Chiung-Ru (*Taipei Veterans General Hospital, Taiwan*)

Liu, Zhiyan (*Shandong University, China*)

Paik, Jin Ho (*Seoul National University, Korea*)

Song, Joon Seon (*University of Ulsan, Korea*)

Zhu, Yun (*Jiangsu Institution of Nuclear Medicine, China*)

Consulting Editors

Huh, Sun (*Hallym University, Korea*)

Kakudo, Kennichi (*Kindai University, Japan*)

Ro, Jae Y. (*Cornell University, The Methodist Hospital, U.S.A.*)

Ethic Editors

Choi, In-Hong (*Yonsei University, Korea*)

Statistics Editors

Kim, Dong Wook (*National Health Insurance Service Ilsan Hospital, Korea*)

Lee, Hye Sun (*Yonsei University, Korea*)

Manuscript Editor

Chang, Soo-Hee (*InfoLumi Co., Korea*)

Layout Editor

Kim, Haeja (*iMiS Company Co., Ltd., Korea*)

Website and JATS XML File Producer

Cho, Yoonsang (*M2Community Co., Korea*)

Im, Jeonghee (*M2Community Co., Korea*)

Administrative Assistant

Jung, Ji Young (*The Korean Society of Pathologists*)

Jeon, Annmi (*The Korean Society of Cytopathology*)

Contact the Korean Society of Pathologists/the Korean Society for Cytopathology

Publishers: Lee, Kyo Young, MD, Hong, Soon Won, MD

Editors-in-Chief: Jung, Chan Kwon, MD, Park, So Yeon, MD

Published by the Korean Society of Pathologists/the Korean Society for Cytopathology

Editorial Office

Room 1209 Gwanghwamun Officia, 92 Saemunan-ro, Jongno-gu, Seoul 03186, Korea

Tel: +82-2-795-3094 Fax: +82-2-790-6635 E-mail: office@jpathol.tn.org

#1508 Renaissancetower, 14 Mallijae-ro, Mapo-gu, Seoul 04195, Korea

Tel: +82-2-593-6943 Fax: +82-2-593-6944 E-mail: office@jpathol.tn.org

Printed by iMiS Company Co., Ltd. (JMC)

Jungang Bldg. 18-8 Wonhyo-ro 89-gil, Yongsan-gu, Seoul 04314, Korea

Tel: +82-2-717-5511 Fax: +82-2-717-5515 E-mail: ml@smileml.com

Manuscript Editing by InfoLumi Co.

210-202, 421 Pangyo-ro, Bundang-gu, Seongnam 13522, Korea

Tel: +82-70-8839-8800 E-mail: infolumi.chang@gmail.com

Front cover image: Clockwise from upper left: EBV-positive diffuse large B-cell lymphoma; Extranodal natural killer/T-cell lymphoma, nasal type; EBV-positive gastric carcinoma with lymphoid stroma; Angioimmunoblastic T-cell lymphoma stroma (purple: EBER, brown: CD3, red: CD20, CD56, cytokeratin, CD30) (Fig. 2). p324-325.

© Copyright 2019 by the Korean Society of Pathologists/the Korean Society for Cytopathology

© Journal of Pathology and Translational Medicine is an Open Access journal under the terms of the Creative Commons Attribution Non-Commercial License (<https://creativecommons.org/licenses/by-nc/4.0>).

© This paper meets the requirements of KS X ISO 9706, ISO 9706-1994 and ANSI/NISO Z.39.48-1992 (Permanence of Paper).

This journal was supported by the Korean Federation of Science and Technology Societies Grant funded by the Korean Government.

CONTENTS

ORIGINAL ARTICLES

- 273 Human Papillomavirus Serologic Profiles of Selected Filipinos with Head and Neck Squamous Cell Carcinoma
Pia Marie Albano, Christianne Salvador, Jose Orosa, III, Sheryl Racelis, Modesty Leaño, Angelika Michel, John Donnie Ramos, Dana Holzinger, Michael Pawlita
- 280 High Expression of Galectin-1, VEGF and Increased Microvessel Density Are Associated with MELF Pattern in Stage I-III Endometrioid Endometrial Adenocarcinoma
Dmitry Aleksandrovich Zinovkin, Sergey Leonidovich Achinovich, Mikhail Grigoryevich Zubritskiy, Jacqueline Linda Whatmore, Md Zahidul Islam Pranjol
- 289 Clinicopathological Characterization and Prognostic Implication of SMAD4 Expression in Colorectal Carcinoma
Seung-Yeon Yoo, Ji-Ae Lee, Yunjoo Shin, Nam-Yun Cho, Jeong Mo Bae, Gyeong Hoon Kang
- 298 Reclassification of Mongolian Diffuse Gliomas According to the Revised 2016 World Health Organization Central Nervous System Tumor Classification
Enkhee Ochirjav, Bayarmaa Enkhbat, Tuul Baldandorj, Gheeyoung Choe
- 308 Primary Rhabdomyosarcoma of the Breast: Study of Three Cases at One Institution with a Review of Primary Breast Sarcomas
Junyoung Shin, Hee Jeong Kim, Dae-Yeon Kim, Gyungyub Gong, Kyung-Ja Cho
- 317 Multistaining Optimization for Epstein-Barr Virus-Encoded RNA In Situ Hybridization and Immunohistochemistry of Formalin-Fixed Paraffin-Embedded Tissues Using an Automated Immunostainer
Jae Nam Ko, Jin Kyoung Jung, Yun Ik Park, Hwa Jeong Shin, Jooryung Huh, Sol Back, Yu Jin Kim, Jae Ho Kim, Heounjeong Go

CASE REPORTS

- 327 Amoebic Encephalitis Caused by *Balamuthia mandrillaris*
Su Jung Kum, Hye Won Lee, Hye Ra Jung, Misun Choe, Sang Pyo Kim
- 332 Diffuse Involvement of Primary Colorectal Lymphoma Simulating Ulcerative Colitis
Ji-Ye Kim, Sun Hee Chang, Han Seong Kim, Mee Joo

337 Human Papillomavirus–Related Multiphenotypic Sinonasal Carcinoma with Late Recurrence

Bokyoung Ahn, Eojin Kim, Harim Oh, Yang-Seok Chae, Chul Hwan Kim, Youngseok Lee, Jeong Hyeon Lee, Yoo Jin Lee

341 Liquid-Based Cytology Features of Papillary Squamotransitional Cell Carcinoma of the Uterine Cervix

Yangkyu Lee, Younghwa Choi, Kiryang Lee, Youngeun Lee, Hyojin Kim, Ji-Young Choe, Hye Seung Lee, Yong Beom Kim, Haeryoung Kim

RETRACTION

345 RETRACTION: eNOS Gene Polymorphisms in Perinatal Hypoxic-Ischemic Encephalopathy

Instructions for Authors for *Journal of Pathology and Translational Medicine* are available at <http://jpatholm.org/authors/authors.php>

Human Papillomavirus Serologic Profiles of Selected Filipinos with Head and Neck Squamous Cell Carcinoma

Pia Marie Albano^{1,2,3}, Christianne Salvador⁴, Jose Orosa, III⁴, Sheryl Racelis⁵, Modesty Leño⁵, Angelika Michel¹,
John Donnie Ramos^{2,3}, Dana Holzinger¹, Michael Pawlita¹

¹Division of Molecular Diagnostics of Oncogenic Infections, Research Program Infection and Cancer, German Cancer Research Center (DKFZ), Heidelberg, Germany;

²Department of Biology, College of Science, University of Santo Tomas, Manila; ³Research Center for the Natural and Applied Sciences, University of Santo Tomas, Manila;

Departments of ⁴ENT Head and Neck Surgery and ⁵Pathology and Laboratories, Mariano Marcos Memorial Hospital and Medical Center, Ilocos Norte, Philippines

Background: The low prevalence of human papillomavirus (HPV) DNA and mRNA in biopsy samples of Filipinos with head and neck squamous cell carcinoma (HNSCC) has been reported previously. Here, the HPV serologic profiles of HNSCC cases were analyzed and associated with lifestyle and sexual practices. **Methods:** Serum samples were collected between May 2012 and September 2013 from HNSCC patients (n=22) in the northwest region of the Philippines, and age- and sex-matched clinically healthy controls. Antibodies to capsid and early oncoproteins of HPV16, 18, 31, 33, 45, 52, 58, 6, and 11 were analyzed using multiplex serology. **Results:** Most of the cases were males with tumors of the oral cavity or larynx. Two of the cases tested positive for at least one of the early oncoproteins (E6, E7, E1, and/or E2) of HPV16, and 11 did not display reactivity to any HPV early or late oncoproteins. Of the controls, four tested positive for at least one of the HPV16 early oncoproteins, and 10 were non-reactive to all HPV types. Titers to HPV16 E6 or E7 of the seropositive cases and controls were considerably lower than those typically observed in economically developed countries. **Conclusions:** The low HPV titers seen here are consistent with the results of molecular analyses for this population. Hence, the seropositivity of some of the HNSCC cases is likely an indication of prior exposure to the virus and not the presence of HPV-driven tumors.

Key Words: HPV antibodies; Head and neck squamous cell carcinoma; Philippines; Multiplex serology

Received: January 31, 2019 **Revised:** April 21, 2019 **Accepted:** May 12, 2019

Corresponding Author: Pia Marie Albano, PhD, Research Center for the Natural and Applied Sciences (RCNAS), Rm. 708 Central Laboratories, University of Santo Tomas, España Blvd, Manila, Philippines

Tel: +63-2-4061661 (loc 8545), Fax: +63-2-7314031, E-mail: psalbano@ust.edu.ph, p.albano2013@gmail.com

Human papillomavirus (HPV) has been demonstrated in more than 99% of cervical cancers and over 90% of their squamous intra-epithelial precursor lesions.¹ Moreover, molecular and epidemiologic studies have demonstrated that HPV, particularly HPV16, also plays a role in the pathogenesis of a subset of head and neck squamous cell carcinomas (HNSCC) particularly oropharyngeal squamous cell carcinoma (OPSCC).^{2,3} Biomarkers of HPV-driven cancers include DNA and mRNA detected in tumors using in situ hybridization and polymerase chain reaction-based assays, expressed cellular proteins (such as pRb, p53, and p16^{INK4a}) measured using immunohistochemistry, and serological markers indicative of cumulative viral exposure.

There is strong correlation between HNSCC and seropositivity to the E6 and E7 oncoproteins of HPV16.⁴⁻⁷ The risk of HPV-driven HNSCC is much greater in individuals positive for anti-

bodies to HPV16 E6 or E7 than in those positive for antibodies to HPV16 virus-like particles. Seropositivity to HPV18 E6, HPV33 E6, and HPV58 E7 are strongly associated with OPSCC and HPV52 E7 with oral cavity squamous cell carcinoma (OSCC).⁸ Due to the low prevalence of HPV16 E6 or E7 antibodies in healthy individuals without an HPV-related tumor, HPV antibodies are now being considered for monitoring for previous exposure, measuring prognosis, and monitoring treatment⁹⁻¹³ of HPV-associated cancers.¹⁴

The low prevalence of HPV DNA and mRNA among HNSCC cases from the northwest region of the Philippines was reported previously.¹⁵ In the current study, serum samples of HNSCC patients from the same region along with their age- and sex-matched clinically healthy controls were analyzed for antibodies to the capsid protein (L1), early oncoproteins (E6, E7), and other

early proteins (E1, E2) of the carcinogenic mucosal HPV16, 18, 31, 33, 45, 52, and 58 genotypes and the non-carcinogenic mucosal HPV6 and 11 genotypes to determine whether frequency of seropositivity and antibody titers are in concordance with molecular analyses. Moreover, the results of serologic analyses were correlated with lifestyle risk factors including sexual practices.

MATERIALS AND METHODS

Sample population and study site

The Mariano Marcos Memorial Hospital and Medical Center (MMMHC) in Ilocos Norte, Philippines, served as the study base. The study included cases of newly diagnosed, histologically confirmed primary tumors of the oral cavity (OSCC), oropharynx (OPSCC), or larynx (laryngeal squamous cell carcinoma [LSCC]) seen at MMMHC between May 2012 and September 2013. The study also required that the cases had no prior history of cervical dysplasia and/or cervical cancer. The cases were age- (\pm 2 years) and sex-matched with volunteer cancer-free controls recruited from the same communities where the study cases resided.

All participants completed a standardized questionnaire, either through self-administration or an interview with a member of the research group, that determined their alcohol consumption, tobacco use, and sexual practices. The clinical data of the patients were retrieved from medical records and histopathological reports. Blood was collected from both patients and controls at the time of the interview. The serum was separated and stored immediately at -80°C until use.

It must be noted that the freshly frozen biopsy samples of the HNSCC cases at this institution were previously analyzed for HPV DNA and mRNA.¹⁵ Only one of the cases tested positive for HPV DNA and RNA specifically to the low-risk HPV11.¹⁵

Multiplex serology

All serum samples were subjected to multiplex serology, a high-throughput technology that allowed the simultaneous quantification of specific antibodies against the major capsid protein (L1), the early oncoproteins (E6, E7), and other early proteins (E1, E2) of the carcinogenic mucosal HPV16 and HPV18 genotypes (L1, E1, E2, E6, and E7), the carcinogenic mucosal HPV31, HPV33, HPV45, HPV52, and HPV58 genotypes (E6, E7, and L1), and the non-carcinogenic mucosal HPV6 and HPV11 genotypes (E6, E7, and L1). The assay makes use of viral antigens bacterially expressed as glutathione

S-transferase (GST) fusion proteins.^{16,17} Spectrally distinct bead sets (SeroMAP Microspheres, Luminex Corp., Austin, TX, USA) carrying different viral antigens were individually washed and subsequently mixed. Each serum sample was diluted (1:100) in pre-incubation buffer (phosphate buffered saline with Chemi-Block), combined with the mixed beads, and incubated. The bound antibodies were detected with biotinylated anti-human secondary antibodies (goat anti-human IgG [H + L], IgA, and IgM) (Dianova, Hamburg, Germany) followed by conjugate streptavidin-R-phycoerythrin. With a Luminex 200 analyzer (Luminex Corp.), the reporter fluorescence of the beads was measured and expressed as the mean fluorescence intensity (MFI) of at least 100 beads per set per serum sample. For background determination, beads were loaded with GST alone. Net MFI values were categorized as either antibody positive (reactive) or negative (nonreactive) based on cut-off values of the mean \pm 3SD (standard deviation) excluding the positive outliers of the MFI values of 25 sera from self-declared sexually-naïve Indian girls aged 12–15 years old.^{4,18} Additionally, the minimal cut-off was set to 300 MFI for early HPV antigens and 400 MFI for L1 antigens.

Data analysis

IBM Statistical Package for Social Sciences (IBM SPSS, IBM Corp., Armonk, NY, USA) was used in the analysis of the data. The chi-square test of homogeneity was used to compare nominal data, and Fisher exact test was used to compare expected frequencies less than 5.00 (i.e., number of lifetime sex partners, performs oral-genital sex, engages in casual and/or commercial sex, engages in same-sex sexual activity, sex partner with history of sexually transmitted infection, and personal history of sexually-transmitted disease). The Mann–Whitney rank-sum test was used to compare median scores.

Ethics statement

The design, sampling, experimental protocols, questionnaires, and other pertinent documents were reviewed and approved by the Research Ethics Review Committee (RERC) of MMMHC. All participants gave their written informed consent.

RESULTS

This study considered a total of 22 HNSCC cases (13 OSCC, 2 OPSCC, and 7 LSCC) during the 16-month recruitment period. All HNSCC patients that visited MMMHC were invited to participate, but some of those diagnosed with late-stage cancer or of extreme age declined to participate. Moreover, two of the

cases were also not paired since it was difficult to recruit controls that matched their age (≥ 80 years old). There were more males ($n = 13$) than females, and the median age at initial diagnosis was 64 years old (range, 41 to 87 years). A majority of the cases had well-differentiated tumors ($n = 18$) and presented with the late stage of the disease ($n = 17$).

There were no significant differences between the cases and controls in terms of the number of lifetime sex partners ($p > .99$) and engagement in oral sex ($p = .332$). Although more controls engaged in casual or commercial sex ($p = .018$), more controls also used condoms for protection ($p = .029$). Very few of the participants, whether case or control, had more than five lifetime sex partners or engaged in oral sex (Table 1).

The HPV serologic profiles of the cases were the same from diagnosis to treatment. Among the 22 cases, only two (9%, both OSCC) showed reactivity to the E6 protein: one case to both HPV18 and HPV45 and one to HPV31. Four (18%, 2 LSCC and 2 OSCC) were reactive to the E7 protein: two cases to HPV33, one to HPV16, and one to HPV18. None of the cases showed dual reactivity to E6 and E7 of the same HPV genotype. One OSCC case was reactive to E2 of HPV18 and another was reactive to E1 of HPV18 and E2 of HPV16 (Table 2). Seven (31.8%, 4 OSCC and 3 LSCC) showed multiple reactivity to the L1 protein of HPV6, 11, 16, 18, 31, 33, 45, 52, and/or 58 (Table 2). Further, two of the LSCC cases were positive to HPV 11. Overall, only two (9%) of the cases were positive to at least one of the early proteins (E6, E7, E1, and/or E2) of HPV16, and 11 (50%) did not display reactivity to any of the early or late proteins of HPV.

Only three (15%) among the controls showed reactivity to either E6 or E7: one to the E6 protein of both HPV11 and HPV52 and two to E7 of either HPV16 or HPV33. One of the controls showed dual reactivity to E1 and E2 of both HPV16 and HPV18. Another control was reactive only to E2 of HPV16 (Table 3). Seven of the controls (35%) displayed multiple reactivity to L1 of HPV6, 11, 16, 18, 31, 33, 45, 52, and/or 58 (Table 3). Overall, 10 of the controls (50%) were not reactive to any of the HPV proteins, and four (20%) were positive to at least one of the HPV16 early proteins.

DISCUSSION

In this study, seropositivity to the early and late proteins of HPV was found in only half of the HNSCC cases and clinically healthy controls. None of the participants showed dual reactivity to the E6 and E7 proteins of HPV16, which is the most associated with HNSCC, particularly OPSCC.^{5,8,14,19} Increased titers of

Table 1. Clinico-epidemiologic profile of the cases vs controls ($n = 42$)

Characteristic	Case (n=22)	Control (n=20)	p-value ^a
Age (yr)	63 (41–87)	62 (39–74)	
Sex			
Male	13 (59)	11 (55)	
Female	9 (41)	9 (45)	
Tumor site			
Larynx	7 (32)	-	
Oral cavity	13 (59)	-	
Oropharynx	2 (9)	-	
Tumor grade			
Well-differentiated	18 (82)	-	
Moderately-differentiated	3 (14)	-	
Poorly-differentiated	1 (4)	-	
Tumor category			
Tis, T1, T2	5 (23)	-	
T3, T4	17 (77)	-	
Alcohol consumption			.516
Never	11 (50)	8 (40)	
Ever	11 (50)	12 (60)	
Tobacco use			.052
Never	3 (14)	8 (40)	
Ever	19 (86)	12 (60)	
Median age at first sexual intercourse (yr)	20.5 (19–24)	21 (17.5–25)	.870
No. of lifetime sex partners			>.99
0–5	19 (86)	17 (85)	
≥ 6	3 (14)	3 (15)	
Performs oral-genital sex			.332
Yes	3 (14)	5 (25)	
No	19 (86)	14 (70)	
No answer	0	1 (5)	
Engages in casual and/or commercial sex			.018
Yes	0	5 (25)	
No	22 (100)	15 (75)	
Engages in same-sex sexual activity			.099
Yes	0	3 (15)	
No	22 (100)	17 (85)	
Sex partner has history of STD			.003
Yes	0	1 (5)	
No	22 (100)	13 (65)	
Uncertain/no answer	0	6 (30)	
Personal history of STD			.221
Yes	0	2 (10)	
No	22 (100)	18 (90)	
Use of condom			.029
Yes	6 (27)	13 (65)	
No	16 (73)	7 (35)	

Values are presented as median (range) or number (%).

^aChi-square test of homogeneity was used to compare nominal data while Fisher's exact test was used to compare expected frequencies less than 5.00 (i.e., number of lifetime sex partners, performs oral-genital sex, engages in casual and/or commercial sex, engages in same-sex sexual activity, sex partner with history of sexually-transmitted disease [STD], and personal history of STD). Mann-Whitney rank-sum test was used to compare median scores.

Table 2. HPV serologic profile of the cases to the early and late proteins of low-risk (HPV6, 11) and high-risk (HPV16, 18, 31, 33, 45, 52, and 58) types

Case ID	Sex	Age at initial diagnosis (yr)	Tumor site	HPV DNA ^a	HPV mRNA ^a	Seropositivity	
						Early proteins (E6, E7, E1, E2)	Late proteins (L1)
18-1	M	49	LSCC	HPV11 L1 ^b	HPV11 E6 fl ^b	Negative	HPV11 ^b
09-1	F	59	OSCC	Negative	Negative	HPV18 E6, HPV45 E6 ^b	HPV16, 31, 33, 52, 58 ^b
11-1	F	65	OSCC	Negative	Negative	HPV31 E6 ^b	HPV31 ^b
22-1	M	78	OSCC	Negative	Negative	HPV18 E1, HPV16 E2 ^b	HPV11, 18, 31, 33, 45, 52, 58 ^b
07-1	F	53	OSCC	Negative	Negative	HPV33 E7 ^b	Negative
14-1	M	59	LSCC	Negative	Negative	HPV33 E7 ^b	Negative
17-1	M	41	LSCC	Negative	Negative	HPV16 E7 ^b	Negative
21-1	F	69	OSCC	Negative	Negative	HPV18 E7, HPV18 E2 ^b	Negative
06-1	F	70	OSCC	Negative	Negative	Negative	HPV58 ^b
15-1	M	59	LSCC	Negative	Negative	Negative	HPV33 ^b
19-3	M	69	LSCC	Negative	Negative	Negative	HPV6, 11, 16 ^b
01-1	M	87	OSCC	Negative	Negative	Negative	Negative
02-1	F	76	OPSCC	Negative	Negative	Negative	Negative
03-1	M	57	OPSCC	Negative	Negative	Negative	Negative
04-1	M	57	OSCC	Negative	Negative	Negative	Negative
05-1	M	77	OSCC	Negative	Negative	Negative	Negative
08-1	F	51	OSCC	Negative	Negative	Negative	Negative
10-1	F	69	OSCC	Negative	Negative	Negative	Negative
12-1	F	70	OSCC	Negative	Negative	Negative	Negative
13-1	M	55	OSCC	Negative	Negative	Negative	Negative
16-1	M	61	LSCC	Negative	Negative	Negative	Negative
20-1	M	68	LSCC	Negative	Negative	Negative	Negative

HPV, human papillomavirus; LSCC, laryngeal squamous cell carcinoma; OSCC, oral cavity squamous cell carcinoma; OPSCC, oropharyngeal squamous cell carcinoma.

^aMolecular analyses done earlier¹⁵; ^bPositive for HPV DNA, HPV mRNA, or HPV antibodies.

Table 3. HPV serologic profile of the controls to the early and late proteins of low-risk (HPV6, 11) and high-risk (HPV16, 18, 31, 33, 45, 52, and 58) types

Control ID	Sex	Age (yr)	Seropositivity	
			Early proteins (E6, E7, E1, E2)	Late proteins (L1)
06-0	F	71	HPV16 E1, HPV18 E1, HPV16 E2, HPV18 E2 ^a	HPV11, 18, 31, 33, 45, 52, 58 ^a
07-0	F	53	HPV16 E7 ^a	HPV11, 16, 18, 31, 45 ^a
03-0	M	59	HPV33 E7, HPV16 E1 ^a	Negative
12-0	F	72	HPV16 E2 ^a	Negative
20-0	M	65	HPV11 E6, HPV52 E6 ^a	Negative
08-0	F	54	Negative	HPV6, 11, 58 ^a
14-0	M	59	Negative	HPV11, 16, 31, 33, 45, 52, 58 ^a
15-0	M	61	Negative	HPV11 ^a
17-0	M	39	Negative	HPV11, 31 ^a
18-0	M	47	Negative	HPV 18, 58 ^a
02-0	F	74	Negative	Negative
04-0	M	55	Negative	Negative
05-0	M	74	Negative	Negative
09-0	F	58	Negative	Negative
10-0	F	68	Negative	Negative
11-0	F	63	Negative	Negative
13-0	M	53	Negative	Negative
16-0	M	64	Negative	Negative
19-0	M	66	Negative	Negative
21-0	F	66	Negative	Negative

^aPositive for human papillomavirus (HPV) antibodies.

HPV18 E6, HPV33 E6, and HPV58 E7 antibodies are strongly associated with OPSCC and HPV52 E7 with OSCC.⁸ The two OPSCC cases here were negative to all early and late HPV proteins; however, two of the OSCC cases were positive to HPV 52 L1 but not to E7 nor to any of the early proteins. The seropositive clinically healthy controls were primarily reactive to the early (E1 and E2) and late (L1) proteins. It must also be noted that antibody titers to HPV16 E6 or E7 in both the seropositive cases and controls were considerably lower compared to regions where the prevalence of HPV-driven HNSCC is high.^{5,8,14,19} Thus, the findings here correspond to the results of molecular analyses done earlier on biopsy samples of the cases.¹⁵

Among the cases, one (case 18-1) tested positive for both the DNA and mRNA of HPV11, a low-risk HPV type commonly associated with recurrent respiratory papillomatosis (RRP). The patient also registered very high titers of antibodies to the late, but not the early proteins of HPV11 (Table 2). It is worth noting that this patient had RRP prior to the diagnosis of LSCC. HPV11 sometimes causes cancer if genetic susceptibility and immune suppression allow the virus to persist with deregulated patterns of gene expression.²⁰ The other HPV11 L1 seropositive case (case 19-3) was negative for HPV DNA and mRNA and had no history of RRP, as indicated in his medical records (Table 2).

Antibodies to E6 and E7 of HPV18, 33, and 58 are associated with OPSCC and LSCC^{8,10,21} and HPV52 with a risk of OSCC and OPSCC.^{3,8} The HPV18 or 33 seropositive cases here were either OSCC or LSCC, and none had dual reactivity to at least two early proteins of the same HPV genotype, which has been suggested as a biomarker of HPV-driven HNSCC.^{5,13} Hence, the HPV seropositivity seen here may be a marker of recent HPV exposure.

It has been hypothesized that anti-E1 and E2 antibodies likely develop prior to full transformation, overexpression, and subsequent seroconversion to E6 and E7 because E1 and E2 are expressed at such low levels in HPV-transformed cells.¹¹ However, seropositivity to E6 and E7 is usually detectable only after tumor invasion, likely because a humoral response is generated only upon the release and spread of E6 and E7 oncoproteins into systemic circulation, which happens after a tumor vascular bed has been created followed by necrosis.⁵ Dual seropositivity to E6 and any one of the other early viral proteins (E7, E1, or E2) of one HPV type has a sensitivity of 95% and a specificity of 98%, indicating they could serve as reliable markers for diagnosis and prognosis of HNSCC.^{10,22,23}

The cases and controls in this study appeared to be sexually conservative (i.e., a small number of lifetime sex partners, do not

perform oral sex) compared to people from more economically developed regions. Thus, there was a lower risk of HPV-driven HNSCC, which is believed to be transmitted through sexual means.^{24,25} The characteristics of the cases here were more consistent with the features of HPV-negative HNSCC; the age at onset of their HNSCC was in the 6th to 7th decade of life, and a majority were tobacco and alcohol users. Dual seropositivity to E6 and E7 is much more common among young males with a greater number of lifetime sex partners,¹³ an observation that is consistent with the characteristics observed in patients with HPV-driven HNSCC.²⁶

This study included a limited number of cases from a single region of the country where HNSCC was most prevalent because there are no nationwide biobanks and participants were only recruited at the time this study was initiated. However, the cases were strictly age- and sex-matched with physician-assessed clinically healthy controls recruited from the same geographical location for comparison of HPV antibody titers.

Serological assays are not usually used in HPV diagnosis due to their low sensitivity and tumor-site specificity. However, HPV serologic markers can be used to assess previous exposure, measure prognosis, and monitor treatment.^{8,10-13} The current study was done to assess HPV exposure of HNSCC cases and their matched controls. The results of the serological analyses, lifestyle risk factors, and sexual practices of the HNSCC cases in this study complement the results of previous molecular analyses for presence of DNA and mRNA in tumors of retrospective HNSCC cases from the same region.¹⁵ Hence, it can be inferred that the low HPV titers seen among the participants were indicative of prior exposure and not due to presence of HPV-driven tumors.

A follow-up study involving a greater number of cases from both rural and urban areas in the Philippines should be conducted to determine any significant increase in the incidence of HPV-related HNSCC as verified using molecular and serologic analyses. In the present study, the median age of the cases (59 years old) and controls (59 years old) who were HPV seropositive was lower compared to the seronegative cases (68 years old) and controls (65 years old), indicating that the younger generations are more liberal. Given the strong influence of social media, Filipinos are becoming more sexually permissive, which increases their risk for HPV-driven HNSCC.

This study adds to the existing evidence that individuals without HPV-related tumors typically have low levels of HPV16 E6 or E7 antibodies. It supports the idea that HPV antibody testing can be used as a cheaper alternative to complex molecular marker

analyses in screening for HPV-driven cancers especially in countries where resources are limited.

ORCID

Pia Marie Albano: <https://orcid.org/0000-0002-5024-8819>
 Angelika Michel: <https://orcid.org/0000-0001-7684-4742>
 John Donnie Ramos: <https://orcid.org/0000-0001-9433-106X>
 Dana Holzinger: <https://orcid.org/0000-0002-5010-5236>
 Michael Pawlita: <https://orcid.org/0000-0002-4720-8306>

Author Contributions

Conceptualization: PMA, JO, JDR, DH, MP.
 Data curation: PMA, CS, SR.
 Funding acquisition: PMA, MP.
 Investigation: PMA, CS, JO, SR, ML.
 Methodology: PMA, AM, DH, MP.
 Project administration: PMA, JO, ML, JDR, DH, MP.
 Resources: PMA, CS, JO, SR, ML, MP.
 Supervision: JO, ML, JDR, DH, MP.
 Validation: DH, MP.
 Visualization: PMA, JDR, DH, MP.
 Writing—original draft: PMA, DH, MP.
 Writing—review & editing: PMA, DH, MP.

Conflicts of Interest

MP has received royalties for patents owned by DKFZ and research support through cooperate contracts between DKFZ and Roche and Qiagen in the field of HPV diagnostics. However, the funders had no role in study design, data collection and analysis, decision to publish, or preparation of the manuscript.

Funding

PMA was supported through grants from the Department of Science and Technology (DOST) and the Commission on Higher Education of the Philippines (CHED).

Acknowledgments

Our thanks go out to Ute Koch and Monika Oppenlaender for technical assistance.

REFERENCES

1. Monie A, Hung CF, Roden R, Wu TC. Cervarix: a vaccine for the prevention of HPV 16, 18-associated cervical cancer. *Biologics* 2008; 2: 97-105.
2. D'Souza G, Dempsey A. The role of HPV in head and neck cancer and review of the HPV vaccine. *Prev Med* 2011; 53 Suppl 1: S5-11.
3. D'Souza G, Kreimer AR, Viscidi R, et al. Case-control study of human papillomavirus and oropharyngeal cancer. *N Engl J Med* 2007; 356: 1944-56.
4. Kreimer AR, Pierce Campbell CM, Lin HY, et al. Incidence and clearance of oral human papillomavirus infection in men: the HIM cohort study. *Lancet* 2013; 382: 877-87.
5. Ribeiro KB, Levi JE, Pawlita M, et al. Low human papillomavirus prevalence in head and neck cancer: results from two large case-control studies in high-incidence regions. *Int J Epidemiol* 2011; 40: 489-502.
6. Wyss A, Hashibe M, Chuang SC, et al. Cigarette, cigar, and pipe smoking and the risk of head and neck cancers: pooled analysis in the International Head and Neck Cancer Epidemiology Consortium. *Am J Epidemiol* 2013; 178: 679-90.
7. Herrero R, Castellsagué X, Pawlita M, et al. Human papillomavirus and oral cancer: the International Agency for Research on Cancer multicenter study. *J Natl Cancer Inst* 2003; 95: 1772-83.
8. Michaud DS, Langevin SM, Eliot M, et al. High-risk HPV types and head and neck cancer. *Int J Cancer* 2014; 135: 1653-61.
9. Lang Kuhs KA, Pawlita M, Gibson SP, et al. Characterization of human papillomavirus antibodies in individuals with head and neck cancer. *Cancer Epidemiol* 2016; 42: 46-52.
10. Kreimer AR, Johansson M, Waterboer T, et al. Evaluation of human papillomavirus antibodies and risk of subsequent head and neck cancer. *J Clin Oncol* 2013; 31: 2708-15.
11. Anderson KS, Wong J, D'Souza G, et al. Serum antibodies to the HPV16 proteome as biomarkers for head and neck cancer. *Br J Cancer* 2011; 104: 1896-905.
12. Rubenstein LM, Smith EM, Pawlita M, Haugen TH, Hamšíková E, Turek LP. Human papillomavirus serologic follow-up response and relationship to survival in head and neck cancer: a case-comparison study. *Infect Agent Cancer* 2011; 6: 9.
13. Smith EM, Pawlita M, Rubenstein LM, Haugen TH, Hamsikova E, Turek LP. Risk factors and survival by HPV-16 E6 and E7 antibody status in human papillomavirus positive head and neck cancer. *Int J Cancer* 2010; 127: 111-7.
14. Smith EM, Ritchie JM, Pawlita M, et al. Human papillomavirus seropositivity and risks of head and neck cancer. *Int J Cancer* 2007; 120: 825-32.
15. Albano PM, Holzinger D, Salvador C, et al. Low prevalence of human papillomavirus in head and neck squamous cell carcinoma in the northwest region of the Philippines. *PLoS One* 2017; 12: e0172240.
16. Waterboer T, Sehr P, Pawlita M. Suppression of non-specific binding in serological Luminex assays. *J Immunol Methods* 2006; 309:

- 200-4.
17. Waterboer T, Sehr P, Michael KM, et al. Multiplex human papillomavirus serology based on in situ-purified glutathione s-transferase fusion proteins. *Clin Chem* 2005; 51: 1845-53.
 18. Clifford GM, Shin HR, Oh JK, et al. Serologic response to oncogenic human papillomavirus types in male and female university students in Busan, South Korea. *Cancer Epidemiol Biomarkers Prev* 2007; 16: 1874-9.
 19. Anantharaman D, Gheit T, Waterboer T, et al. Human papillomavirus infections and upper aero-digestive tract cancers: the ARCAGE study. *J Natl Cancer Inst* 2013; 105: 536-45.
 20. Egawa N, Doorbar J. The low-risk papillomaviruses. *Virus Res* 2017; 231: 119-27.
 21. Baboci L, Boscolo-Rizzo P, Holzinger D, et al. Evidence of the causal role of human papillomavirus type 58 in an oropharyngeal carcinoma. *Virology* 2013; 10: 334.
 22. Boscolo-Rizzo P, Pawlita M, Holzinger D. From HPV-positive towards HPV-driven oropharyngeal squamous cell carcinomas. *Cancer Treat Rev* 2016; 42: 24-9.
 23. Broglie MA, Jochum W, Michel A, et al. Evaluation of type-specific antibodies to high risk-human papillomavirus (HPV) proteins in patients with oropharyngeal cancer. *Oral Oncol* 2017; 70: 43-50.
 24. Lajer CB, von Buchwald C. The role of human papillomavirus in head and neck cancer. *APMIS* 2010; 118: 510-9.
 25. Smith EM, Ritchie JM, Summersgill KF, et al. Age, sexual behavior and human papillomavirus infection in oral cavity and oropharyngeal cancers. *Int J Cancer* 2004; 108: 766-72.
 26. Chaturvedi AK. Epidemiology and clinical aspects of HPV in head and neck cancers. *Head Neck Pathol* 2012; 6 Suppl 1: S16-24.

High Expression of Galectin-1, VEGF and Increased Microvessel Density Are Associated with MELF Pattern in Stage I-III Endometrioid Endometrial Adenocarcinoma

Dmitry Aleksandrovich Zinovkin, Sergey Leonidovich Achinovich¹, Mikhail Grigoryevich Zubritskiy²,
Jacqueline Linda Whatmore³, Md Zahidul Islam Pranjol⁴

Department of Pathology, Gomel State Medical University, Gomel; ¹Department of Pathology, Gomel State Clinical Oncological Dispensary, Gomel;

²Department of Pathology, Grodno Regional Clinical Bureau of Pathology, Grodno, Belarus;

³Institute of Biomedical and Clinical Science, University of Exeter Medical School, Exeter;

⁴William Harvey Research Institute, Barts & The London School of Medicine & Dentistry Queen Mary University of London, London, UK

Background: In this study, we investigate the expression of markers of angiogenesis and microvessel density (MVD) in cases of microcystic, elongated and fragmented (MELF) pattern, with its prognostic role in the survival of endometrioid endometrial adenocarcinomas (EA) patients. **Methods:** In this study, 100 cases of EA, 49 cases with MELF pattern and 51 without, were immunohistochemically stained for galectin-1, vascular endothelial growth factor (VEGF), and MVD. Morphometry and statistical (univariate and multivariate) analyses were performed to assess overall survival (OS) and disease-free survival. **Results:** The expression of VEGF ($p < .001$) and galectin-1 ($p < .001$), as well as MVD area ($p < .001$) and number of vessels/mm² ($p < .050$), were significantly higher in the +MELF pattern group compared to the -MELF group. A low negative correlation between MELF-pattern and the number of days of survival ($p < .001$, $r = -0.47$) was also found. A low positive correlation of MELF-pattern with galectin-1 expression ($p < .001$, $r = 0.39$), area of vessels/mm² ($p < .001$, $r = 0.36$), outcome of EA ($p < .001$, $r = 0.42$) and VEGF expression ($p < .001$, $r = 0.39$) suggests potential pathological relevance of these factors in the prognosis of EA. A univariate survival analysis indicated a role for all parameters of survival. Multivariate Cox proportional hazard regression analysis revealed that only area of vessels/mm² (hazard ratio [HR], 1.018; 95% confidence interval [CI], 1.002 to 1.033), galectin-1 (HR, 1.049; 95% CI, 1.025 to 1.074) and VEGF (HR, 1.049; 95% CI, 1.022 to 1.077) play key roles in OS. **Conclusions:** This study reports an increase in MVD, VEGF and galectin-1 expression in EA with MELF pattern and suggests that MELF pattern, along with the angiogenic profile, may be a prognostic factor in EA.

Key Words: Endometrioid endometrial carcinoma; MELF pattern; Galectin-1; Microvessel density; VEGF

Received: February 1, 2019 **Revised:** April 20, 2019 **Accepted:** May 13, 2019

Corresponding Author: Jacqueline Linda Whatmore, BSc (Hons.), PhD, Institute of Biomedical and Clinical Science, University of Exeter Medical School, Exeter, Devon EX1 2LU, UK
Tel: +44-(0)1392-722944, E-mail: J.L.Whatmore@exeter.ac.uk

Corresponding Author: Md Zahidul Islam Pranjol, BSc (Hons.), MSc, PhD, William Harvey Research Institute, Barts & The London School of Medicine & Dentistry, Queen Mary University of London, Charterhouse Square, London EC1M 6BQ, UK
Tel: +44-(0)207-882-2272, E-mail: z.pranjol@qmul.ac.uk

Although most early-stage endometrioid endometrial adenocarcinomas (EA) have an excellent prognosis, a minority of low-grade disease cases may have an aggressive clinical course.¹⁻⁴ EAs are histologically heterogeneous with myometrial invasion characterized by a microcystic, elongated and fragmented (MELF) pattern surrounded by myxoid and inflamed stroma. MELF pattern was first described by Murray et al. in 2003,⁵ but only a few studies since have reported on the biological potential of this histopathological lesion.

Most published studies have focused on the clinicopathological and immunohistochemical parameters of the cancer microenvironment in relation to the MELF pattern. However, the role of microvessels and angiogenic factors such as galectin-1 and vascular endothelial growth factor (VEGF) in the MELF pattern has not been described. Furthermore, the role of the specific fibromyxoid stromal changes in the prognosis of survival of patients with EA remains unclear.⁶ The MELF pattern is known to be associated with lymphovascular invasion and lymph node metastasis, but

no significant role of this lesion in relation to patient survival has been investigated.^{7,8} However, other studies have shown that the MELF pattern may play a negative role in the survival of patients suffering from EA.^{9,10}

In this study, we hypothesize that there is a significant association between the MELF pattern and microvessel density (MVD), as well as angiogenic factors such as VEGF and galectin-1, which play key roles in determining poor survival of patients. Therefore, we investigated the presence of galectin-1, VEGF, and microvessels in the tumor microenvironment using an immunohistochemical technique. We also analyzed the aforementioned association and report for the first time that these criteria may be used as possible prognostic factors of EA.

MATERIALS AND METHODS

Patients

This prospective study involved women with EA who were treated in 2015 in the Grodno and Gomel regions in the Republic of Belarus. The inclusion criteria for the study were a presence of stage I-III EA (International Federation of Gynecology and Obstetrics [FIGO], 2009), hysterectomy and an absence of malignant tumors in other locations during life. EA stage IV (FIGO, 2009), Lynch syndrome, palliative treatment, a presence of synchronous and metachronous malignancies and the presence of other specific growth patterns of EA were the exclusion criteria for this study.¹¹

The presence of the MELF pattern was confirmed independently by three pathologists (D.A.Z., S.L.A., and M.G.Z.). The pattern was identified by the presence of elongated, dilated (microcystic) and disrupted invasive tumor glands with peri-glandular fibromyxoid stromal reactions and single invasive tumor cells in the stroma around the pattern (Fig. 1).

A total of 100 out of 424 cases of EA during the study period were determined to be eligible for inclusion in this study. Patients were divided into two groups according to the presence or absence of MELF pattern. The first group included 49 subjects who had EA with stroma-specific MELF pattern (MELF positive group). The second group consisted of 51 patients who had no MELF pattern changes in the stroma (MELF negative group). The observation period was 36 months. All patients received treatment according to the National Protocols of Diagnostics and Treatment of Oncological Diseases of the Republic of Belarus. Clinicopathological characteristics of patients are presented in Table 1.

Immunohistochemistry

The primary antibodies used in this study were ready-to-use monoclonal mouse Gal-1 (Abcam, Cambridge, UK), anti-VEGF (Diagnostic Biosystems, Pleasanton, CA, USA), and anti-CD34 (Diagnostic Biosystems). An UnoVue HRP/DAB Detection System (Diagnostic Biosystems) was used for primary antibody visualization.

The method employed in this study has been described in our previous work.^{10,11} Briefly, sections of tissue (4 to 5 μ m thick) were deparaffinized and washed with distilled water. Antigen retrieval was performed using a microwave. The sections were then

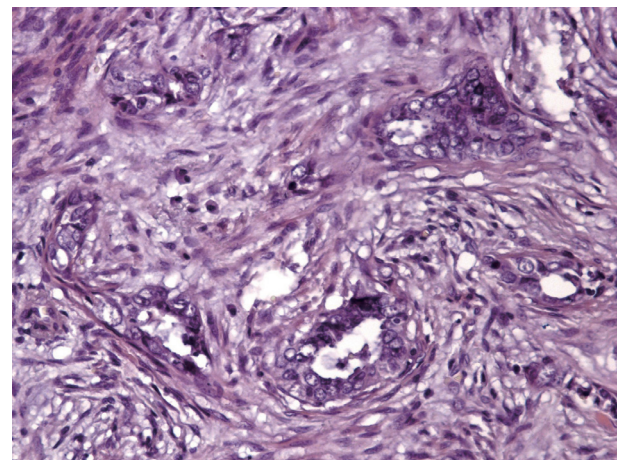


Fig. 1. Specific microcystic, elongated and fragmented pattern changes: endometrioid carcinoma showing eosinophilic glands with microcystic transformation embedded in fibromyxoid stroma and cancer cell complexes with some areas resembling vascular invasion.

Table 1. Clinicopathological characteristics of the patients

Characteristic	MELF-positive group (n = 49)	MELF-negative group (n = 51)	p-value
Age (yr)	64.2 ± 4.8	63.8 ± 5.2	.982 ^a
FIGO stage			.942 ^b
I	12	11	
II	23	25	
III	14	15	
Tumor grade			.855 ^b
G1	20	22	
G2	23	22	
G3	6	7	
Lymphovascular invasion			.115 ^c
Present	29	22	
Absent	20	29	
Myometrial invasion (%)			>.99 ^c
<50	10	9	
>50	39	42	

MELF, microcystic, elongated and fragmented; FIGO, International Federation of Gynecology and Obstetrics.

^aMann-Whitney U test; ^bKruskal-Wallis test; ^cFisher's two-tailed exact test.

allowed to cool and endogenous peroxidase blocking was performed in 5% hydrogen peroxide. Blocking of nonspecific antibody binding was carried out in 5% casein. Sections were washed and incubated in a moist chamber at room temperature with corresponding primary antibodies followed by incubation with anti-mouse horseradish peroxidase secondary antibodies. The reaction product was visualized after 3,3'-diaminobenzidine (DAB) staining for 5 minutes followed by Mayer's hematoxylin counterstaining.^{10,11}

Morphometry

The morphometrical analysis was carried out using package NIS-Elements. The tumor invasion zone was photographed using a microscope (Nikon Eclipse 50i, Nikon, Tokyo, Japan) with a digital camera (DS-Fi2) in 5 non-overlapping high-power fields (HPF; $\times 400$ magnification) of maximum expression for each marker. Expression of VEGF and galectin-1 in cell counting was analyzed using the function "measure." The number of positive cells was expressed as a percentage of the total number of cells in the epithelial component of the tumor.

MVD was presented as the area and number of vessels per mm^2 . The number of vessels was counted in 5 non-overlapping HPF in areas of "hot spots" and inverted into mm^2 using the formula:

$$N = \bar{X}_n \times 1000000/118947.07$$

where N = number of vessels per mm^2 ; $(\bar{X})_n$ = mean number of vessels; and $118947,07$ = area of one HPF (μm^2).

The area of the vessels was counted in 5 non-overlapping HPFs in regions of "hot spots" using the function "area." Area of vessels after the count was inverted into mm^2 using the formula:

$$S = \bar{X}_s \times 1000000/118947.07$$

where S = area of vessels per 1 mm^2 ; \bar{X}_s = mean area of vessels; and $118947,07$ = area of one HPF (μm^2).

Statistical analysis

Power analysis (power = 80%, $\alpha = 0.05$) during the pilot study, in which parameters were received from four cases with MELF pattern and four without the pattern in 5 HPF, revealed that the minimum number of subjects should be 18. The data were presented as the median, lower and upper quartiles. The Mann-Whitney test was used for comparing the study groups based on the evaluated criteria. The Spearman correlation test with Chaddock scale was used to perform correlation analysis. The hazard ratio (HR) with a 95% confidence interval (95% CI) was determined for overall survival (OS) and disease-free survival (DFS) using univariate and multivariate Cox proportional hazards regres-

sion models. A $p < 0.05$ was considered statistically significant. GraphPad Prism v.7.29 (GraphPad Software Inc., San Diego, CA, USA) and R Software v 3.4.0 were used for analysis (R Foundation for Statistical Computing, Vienna, Austria).

Ethics statement

Immunohistochemical study was undertaken at the Gomel State Medical University, Belarus, with informed consent from all patients and with ethical approval from the Institutional Review Board (Gomel State Medical University), Gomel, Belarus.

RESULTS

Galectin-1 expression in EA tissue

Galectin-1 was observed to be diffusely expressed by epithelial cancer cells, stromal cancer cells and vessels in both groups. However, the intensity of the expression of this marker in the MELF negative group was significantly lower ($p < .001$) than the MELF-positive group (Fig. 2A, B). The median galectin-1 expression in the MELF pattern-positive and -negative groups were 78.6 % (40.1%–88.3%) and 34.2% (24.4%–55.5%), respectively. The Mann-Whitney test showed statistically significant differences in galectin-1 expression in both groups ($p < .001$).

VEGF

The expression of VEGF was also observed across all cancer cells and stromal elements. In the MELF-negative group, predominantly moderate expression of this marker was observed (Fig. 2C). In the MELF pattern positive group, the expression was substantially intense (Fig. 2D). Median VEGF expression in the MELF-positive group was 81.4% (58.1%–86.3%) and in the group without MELF pattern was 53.0% (47.6%–75.4%). The VEGF expression difference between the two groups was statistically significant ($p < .001$).

Microvessel density

In various regions of the MELF pattern, a low number of vessels was observed. In the group without MELF pattern, vessels were situated in small groups, and lymphovascular invasion of EA was mostly absent (Fig. 2E). A significant number of microvessels was seen in the MELF pattern cases in "hot spots" regions with unusual lumens. This was often observed in areas of lymphovascular invasion (Fig. 2F).

We also measured the number of vessels per mm^2 in these tissue sections. We found that the median values in MELF-negative and MELF-positive groups were 101.6 vessels/ mm^2 (range,

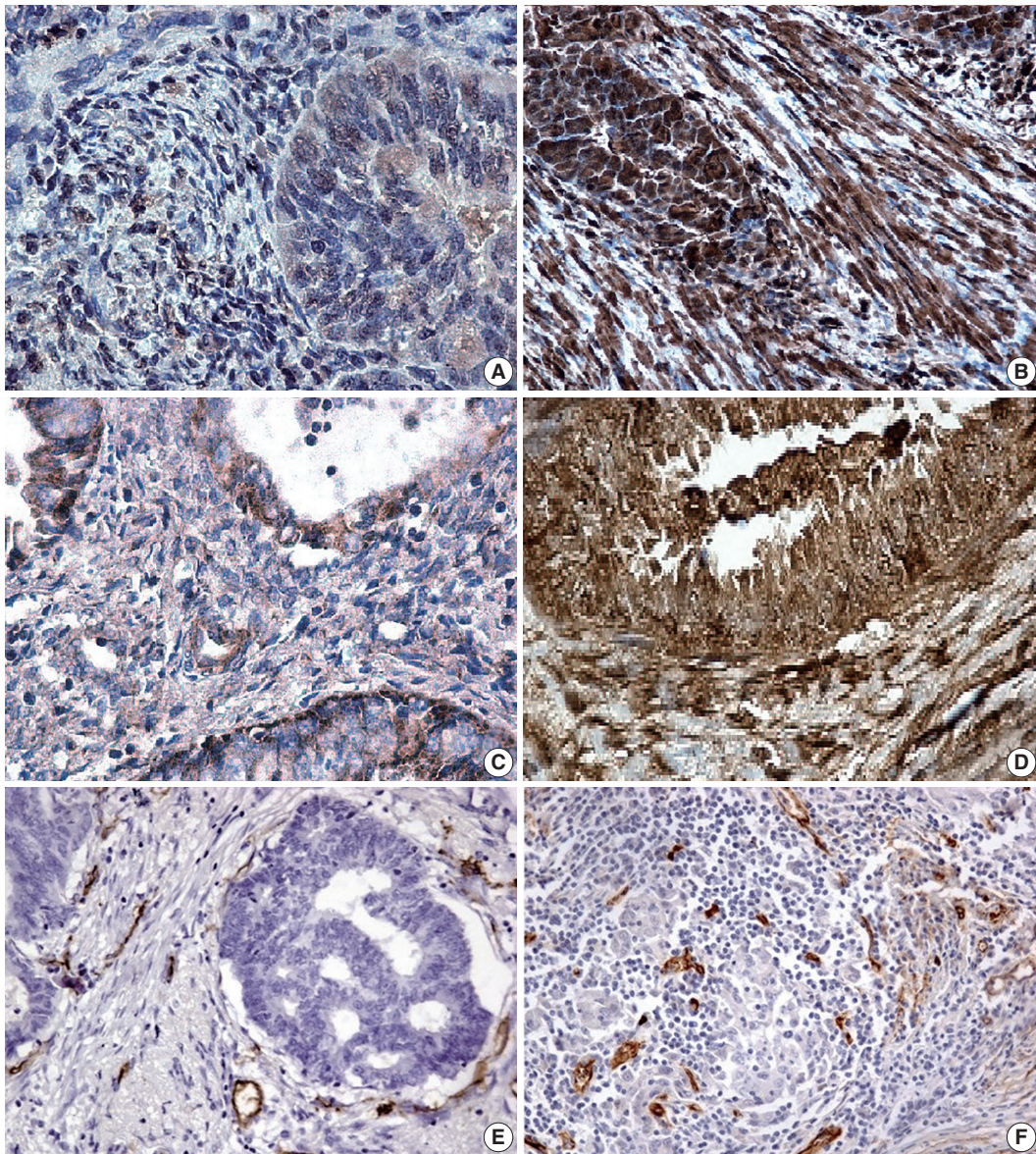


Fig. 2. (A) A few positive glandular cells (microcystic, elongated and fragmented [MELF]-negative group). (B) All glandular cells positive for galectin-1 expression (MELF-positive group) in endometrioid carcinoma. (C) Positive local areas of cytoplasmic expression of vascular endothelial growth factor (VEGF; MELF-negative group). (D) Intense glandular and cytoplasmic (MELF-positive group) expression of VEGF in glands of the endometrioid carcinoma. Low (normal stroma) (E) and increased number of vessels (F) in fibromyxoid stroma situated around cancer cells forming gland without lumens.

90.1 to 127.9 vessels/mm²) and 134.5 vessels/mm² (range, 98.5 to 156.7 vessels/mm²), respectively, where the latter group showed significantly higher presence than the former ($p < .010$).

The area of vessels per mm² was also significantly higher ($p < 0.001$) in the stromal changes of the MELF-positive group (4,788.3 $\mu\text{m}^2/\text{mm}^2$; range, 3,087.3 to 5,130.4 $\mu\text{m}^2/\text{mm}^2$) compared to the group without such specific stromal changes (3,037.3 $\mu\text{m}^2/\text{mm}^2$; range, 2,508.3 to 5,130.4 $\mu\text{m}^2/\text{mm}^2$).

Correlation analyses

We also analyzed the associations among expressions of the MELF pattern, galectin-1, VEGF, area and number of vessels per mm², the outcome of EA (survival or death), and the number of days of survival (Fig. 3). For instance, galectin-1 demonstrated a moderate positive correlation with the area of vessels per mm² ($p < .001$, $r = 0.69$) and VEGF expression ($p < .001$, $r = 0.67$). Furthermore, galectin-1 expression had a highly positive correlation with the outcome of EA ($p < .001$, $r = 0.78$) and a high-

ly negative one with the number of days of survival ($p < .001$, $r = -0.84$).

The expression of VEGF had a highly positive correlation with the outcome of EA ($p < .001$, $r = 0.85$) and a highly negative correlation with the number of days of survival ($p < .001$, $r = -0.78$). The number of vessels per mm^2 revealed moderately positive correlations with galectin-1 ($p < .001$, $r = 0.54$), area of vessels per mm^2 ($p < .001$, $r = 0.61$), and VEGF ($p < .001$, $r = 0.56$); a highly

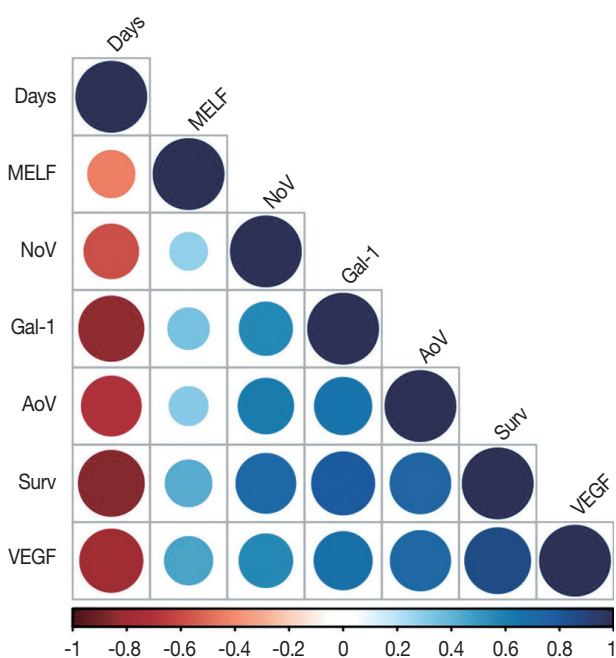


Fig. 3. A correlation plot. Days, number of days of survival from surgical treatment to death or end of observation; MELF, microcystic, elongated and fragmented pattern; NoV, number of vessels per mm^2 ; Gal-1, galectin-1 expression; AoV, area of vessels per mm^2 ; Surv, survival (survival or death); VEGF, vascular endothelial growth factor expression.

positive correlation with the outcome of EA ($p < .001$, $r = 0.71$); and a moderately negative correlation with the number of days of survival ($p < .001$, $r = -0.59$).

A highly positive correlation was observed between the area of vessels per mm^2 and the outcome of EA ($p < .001$, $r = 0.73$) and VEGF expression ($p < .001$, $r = 0.72$). A highly negative correlation was found between the area of vessels per mm^2 and the number of days of survival ($p < .001$, $r = -0.71$).

MELF pattern had a slightly negative correlation with the number of days of survival ($p < .001$, $r = -0.47$) and slightly positive correlation with galectin-1 expression ($p < .001$, $r = 0.39$), the area of vessels per mm^2 ($p < .001$, $r = 0.36$), the outcome of EA ($p < .001$, $r = 0.42$), and VEGF expression ($p < .001$, $r = 0.39$).

Survival analysis

An OS univariate survival analysis was performed, indicating that all parameters except age play a role in the survival of patients with EA (Table 2). However, a multivariate Cox proportional hazard regression analysis of OS revealed that only the area of vessels per mm^2 (HR, 1.018; 95% CI, 1.002 to 1.033), galectin-1 (HR, 1.049; 95% CI, 1.025 to 1.074) and VEGF (HR, 1.049; 95% CI, 1.022 to 1.077) play key roles in survival irrespective of MELF pattern (Table 2).

A univariate analysis was performed, revealing that all parameters except age and tumor grade play a role in DFS of patients with EA (Table 3). However, our multivariate Cox proportional hazard regression analysis demonstrated that only MELF pattern (HR, 1.018; 95% CI, 1.002 to 1.033) and galectin-1 expression (HR, 1.049; 95% CI, 1.025 to 1.074) were significant predictors of DFS (Table 3).

Table 2. The univariate and multivariate Cox regression analysis results for overall survival

Parameter	Univariable analysis			Multivariable analysis		
	Hazard ratio	95% CI	p-value	Hazard ratio	95% CI	p-value
Age	1.012	0.983–1.041	.435	0.992	0.959–1.027	.668
FIGO	1.993	1.361–2.918	<.001	1.304	0.774–2.292	.332
Grade	2.201	1.469–3.297	<.001	1.332	0.776–2.251	.304
Lymphovascular invasion	1.084	1.052–1.118	<.001	1.010	0.942–1.049	.624
Myometrial invasion	1.032	1.011–1.048	<.001	1.028	0.911–1.037	.698
MELF pattern	4.115	2.240–7.558	<.001	1.748	0.870–3.513	.117
No. of vessels	1.036	1.026–1.045	<.001	1.000	0.999–1.000	.623
Area of vessels	1.001	1.001–1.001	<.001	1.018	1.002–1.033	.025
VEGF	1.078	1.058–1.098	<.001	1.049	1.022–1.077	<.001
Galectin-1	1.071	1.054–1.089	<.001	1.049	1.025–1.074	<.001

CI, confidence interval; FIGO, International Federation of Gynecology and Obstetrics; MELF, microcystic, elongated and fragmented; VEGF, vascular endothelial growth factor.

Table 3. The univariate and multivariate Cox regression analysis results for disease-free survival

Parameter	Univariable analysis			Multivariable analysis		
	Hazard ratio	95% CI	p-value	Hazard ratio	95% CI	p-value
Age	1.013	0.977–1.049	.495	0.984	0.930–1.042	.584
FIGO	2.330	1.456–3.728	<.001	0.960	0.473–1.948	.910
Grade	1.512	0.928–2.463	.097	0.886	0.409–1.846	.714
Lymphovascular invasion	1.083	1.043–1.124	<.001	0.986	0.940–1.032	.544
Myometrial invasion	1.014	1.012–1.052	<.001	0.978	0.937–1.048	.587
MELF pattern	4.510	1.938–6.342	<.001	3.472	3.109–3.877	<.001
No. of vessels	1.026	1.014–1.038	<.001	1.007	0.989–1.025	.441
Area of vessels	1.002	1.001–1.004	<.001	1.000	0.999–1.000	.431
VEGF	1.049	1.029–1.068	<.001	1.004	0.968–1.043	.813
Galectin-1	1.037	1.023–1.057	<.001	1.050	1.016–1.084	.003

CI, confidence interval; FIGO, International Federation of Gynecology and Obstetrics; MELF, microcystic, elongated and fragmented; VEGF, vascular endothelial growth factor.

DISCUSSION

In this study, we investigated the associations between galectin-1, VEGF, MVD, area of vessels, and survival outcome of EA patients with and without a MELF pattern. We identified 49 patients out of 100 with a MELF pattern and 51 patients without this stromal change who were observed throughout 36 months from admission to the hospital. In this immunohistochemical study, we demonstrated differential expressions of galectin-1, VEGF and measurement of MVD in cases with and without MELF pattern.

In the last two decades, several galectin family members have emerged as versatile modulators of tumor progression. Galectin-1 expression is also frequently reported to be increased in the reproductive system as well as the placenta. There is ample evidence that malignant transformation is accompanied by elevated galectin-1 levels.¹² Jeschke et al.¹³ reported a statistically significant increase of galectin-1 expression in EA with grade 3 and stages III/VI (FIGO) compared to grades 1 and 2 and FIGO I/II. However, no data are available on the expression of galectin-1 in EA with different types of stromal changes and survival. In our study, we found that galectin-1 expression is higher in EA with a MELF pattern compared to cases without a MELF pattern. Our observation of positive correlations between galectin-1 expression and MELF pattern (fibromyxoid changes) and EA outcome agrees with our previous report and with a report by Sandberg et al.,¹⁴ in which a correlation was shown between an increased galectin-1 expression and fibrotic reaction in tumor progression in the stroma in colon cancer. This was accompanied by decreased immune cell infiltration, indicating a pro-cancerous role of galectin-1.^{14,15}

VEGF was originally identified as a multifunctional cytokine

in angiogenesis and lymphangiogenesis.¹⁶ In cancer angiogenesis, VEGF promotes the mobilization of inflammatory cells to the tumor site, maintaining the local inflammatory process and inducing the synthesis of proangiogenic factors by endothelial cells, platelets, smooth muscle cells, inflammatory cells, fibroblasts, and tumor cells.¹⁷ This interaction between tumor and stromal cells may result in an increased VEGF expression with cancer-associated fibroblasts being the primary source of VEGF.¹⁸ Immature cells of the tumor microenvironment have higher secretion of VEGF than mature cells.¹⁹ We suggest that this is the reason that in our study, MELF pattern stroma had higher expression of VEGF than normal stroma in EA.

Angiogenesis is also known to play crucial roles in the malignant behavior of tumors by increasing oxygen and nutrient supply to cancer cells where the neo-vasculatures form an irregular network of capillaries. In addition, such abnormal vasculatures are important as a pathway for cancer cell metastasis.²⁰ Accumulated evidence indicates that tumor angiogenesis assessed by blood MVD is associated with advanced clinicopathological parameters and poor prognostic outcomes in different types of cancers.²¹ MVD analysis demonstrates high prognostic value in cancers of different locations, such as renal, cervical, colorectal and others.^{22,23} In MELF pattern positive EA, an increased number and area of vessels were observed, which agrees with the previously reported study by Joehlin-Price et al.²⁴ on the high frequency of lymph node metastasis.

A moderate correlation between the area of vessels per mm² and galectin-1 may be due to the cross-talk between galectin-glycan interactions and vascular compartments.²⁵ The correlation between galectin-1 and VEGF may be associated with the mirroring effects of these proangiogenic factors.²⁶ Galectin-1 expression in EA may be a prognostic factor in OS of patients, an

observation that was reported by Wu et al.²⁷ That study reported predictive values of this parameter for cholangiocarcinoma, hepatocellular carcinoma, gingival squamous cell carcinoma, head and neck squamous cell carcinoma, renal cell carcinoma, non-small cell lung cancer, gastric carcinoma and glioblastoma multiforme.²⁷

VEGF as the main proangiogenic factor and immune suppressive factor of the tumor microenvironment correlates with the survival of patients suffering from EA. Goel and Mercurio²⁸ reported a strong expression of VEGF in endothelial cells in the stromal microvessels adjacent to malignant glands, which has been reported to be significantly associated with tumor progression and metastasis.

A positive correlation between MVD and galectin-1/VEGF expression suggested that these parameters play a role in angiogenesis. Additionally, a highly positive correlation between galectin-1 expression and poor survival, as well as MVD and poor survival, suggested that these factors may have a considerable predictive role in survival.²⁹

The presence of a MELF pattern revealed low correlations with the above parameters of proangiogenic response in EA. However, a low negative correlation of MELF pattern with the number of days of survival and a moderate positive correlation with the outcome of the disease may show that MELF pattern may be an independent prognostic criterion of patients' OS.

The results of multivariate survival analyses showed that MELF pattern plays a role in DFS of patients with EA, but not in OS. However, our univariate analysis demonstrated a significant effect of MELF pattern on both OS and DFS. Previous reports have been contradictory on the role of MELF pattern. Sanci et al.⁶ and our previous work reported a positive association, but other authors showed that the presence of a MELF pattern plays no role in OS. Our study also demonstrated MELF pattern as a predictive factor of DFS that may be associated with more frequent lymph node involvement in cases of MELF pattern presence. The absence of influence of FIGO and tumor grade on DFS and OS in our study could be associated with homogeneity of the comparison groups for these parameters. However, our inclusion and exclusion criteria eliminated any potential bias. The systematic review of Prodromidou et al.³⁰ revealed that most of the published literature describing the role of MELF patterns in patients' survival did not study large cohorts of patients, which may be a factor in the inconclusive observations.

Potential limitations of this study are its case-control nature with a relatively small volume of cases due to the rare incidence of MELF patterns in EA. Despite these limitations, a number of

study population characteristics mitigated the weaknesses and increased the validity of our results. One characteristic was the availability of excellent follow-up data. Another was that histopathological analyses made by experienced pathologists. Others included that uniform surgical and radiological treatment was provided by the same surgical teams in two oncological dispensaries and followed protocols of diagnostics and treatment of oncological diseases of the Republic of Belarus.

In conclusion, this study presented an increase of MVD in areas of "hot spots" and angiogenic factors such as VEGF and galectin-1 in cases of EA with MELF presence. Hence, these biomarkers may be used as potential targets for therapy of EA, especially in the implementation of personalized medicine in cases with such specific stromal changes. Our univariate survival analysis revealed MELF pattern presence to be an independent predictor in overall EA survival, but the multivariate analysis did not show that its combination with previously described parameters plays a role in survival. Thus, a large case-control study should be conducted to confirm our findings.

ORCID

Dmitry Aleksandrovich Zinovkin:

<https://orcid.org/0000-0002-3808-8832>

Sergey Leonidovich Achinovich:

<https://orcid.org/0000-0002-0172-0320>

Mikhail Grigoryevich Zubritskiy:

<https://orcid.org/0000-0001-5355-9076>

Jacqueline Linda Whatmore:

<https://orcid.org/0000-0002-8753-1116>

Md Zahidul Islam Pranjol:

<https://orcid.org/0000-0002-6164-6281>

Author Contributions

Conceptualization: DAZ, MZIP.

Data curation: SLA, MGZ.

Formal analysis: SLA, MGZ.

Funding acquisition: JLW (partial).

Investigation: DAZ, MZIP.

Methodology: DAZ.

Project administration: DAZ, MZIP.

Resources: SLA, MGZ.

Software: DAZ.

Supervision: JLW, MZIP.

Validation: SLA, MGZ.

Visualization: SLA, MGZ.

Writing—original draft: DAZ, MZIP.

Writing—review & editing: DAZ, JLW, MZIP.

Conflicts of Interest

The authors declare that they have no potential conflicts of interest.

Funding

This research was partially supported by FORCE Cancer Charity, Devon, UK and initial grant of the Gomel State Medical University “Development and implementation of a prognostic model of the endometrioid adenocarcinoma of the uterine body based on pathological parameters of the tumor microenvironment,” registration number 20190038, registration date 24.01.2019, Gomel, Belarus.

REFERENCES

1. Horn LC, Meinel A, Handzel R, Eienkel J. Histopathology of endometrial hyperplasia and endometrial carcinoma: an update. *Ann Diagn Pathol* 2007; 11: 297-311.
2. Banas T, Pitynski K, Okon K, Winiarska A. Non-endometrioid and high-grade endometrioid endometrial cancers show DNA fragmentation factor 40 (DFF40) and B-cell lymphoma 2 protein (BCL2) underexpression, which predicts disease-free and overall survival, but not DNA fragmentation factor 45 (DFF45) underexpression. *BMC Cancer* 2018; 18: 418.
3. Reeves KW, Carter GC, Rodabough RJ, et al. Obesity in relation to endometrial cancer risk and disease characteristics in the Women’s Health Initiative. *Gynecol Oncol* 2011; 121: 376-82.
4. SGO Clinical Practice Endometrial Cancer Working Group, Burke WM, Orr J, et al. Endometrial cancer: a review and current management strategies: part II. *Gynecol Oncol* 2014; 134: 393-402.
5. Murray SK, Young RH, Scully RE. Unusual epithelial and stromal changes in myoinvasive endometrioid adenocarcinoma: a study of their frequency, associated diagnostic problems, and prognostic significance. *Int J Gynecol Pathol* 2003; 22: 324-33.
6. Sancı M, Güngördük K, Gülseren V, et al. MELF pattern for predicting lymph node involvement and survival in grade I-II endometrioid-type endometrial cancer. *Int J Gynecol Pathol* 2018; 37: 17-21.
7. Kihara A, Yoshida H, Watanabe R, et al. Clinicopathologic association and prognostic value of microcystic, elongated, and fragmented (MELF) pattern in endometrial endometrioid carcinoma. *Am J Surg Pathol* 2017; 41: 896-905.
8. Pelletier MP, Trinh VQ, Stephenson P, et al. Microcystic, elongated, and fragmented pattern invasion is mainly associated with isolated tumor cell pattern metastases in International Federation of Gynecology and Obstetrics grade I endometrioid endometrial cancer. *Hum Pathol* 2017; 62: 33-9.
9. Stewart CJ, Brennan BA, Leung YC, Little L. MELF pattern invasion in endometrial carcinoma: association with low grade, myoinvasive endometrioid tumours, focal mucinous differentiation and vascular invasion. *Pathology* 2009; 41: 454-9.
10. Zinovkin DA, Pranjol MZI, Petrenyov DR, Nadyrov EA, Savchenko OG. The potential roles of MELF-pattern, microvessel density, and VEGF expression in survival of patients with endometrioid endometrial carcinoma: a morphometrical and immunohistochemical analysis of 100 cases. *J Pathol Transl Med* 2017; 51: 456-62.
11. Zinovkin D, Pranjol MZ. Tumor-infiltrated lymphocytes, macrophages, and dendritic cells in endometrioid adenocarcinoma of corpus uteri as potential prognostic factors: an immunohistochemical study. *Int J Gynecol Cancer* 2016; 26: 1207-12.
12. Zhu X, Wang K, Zhang K, et al. Galectin-1 knockdown in carcinoma-associated fibroblasts inhibits migration and invasion of human MDA-MB-231 breast cancer cells by modulating MMP-9 expression. *Acta Biochim Biophys Sin (Shanghai)* 2016; 48: 462-7.
13. Jeschke U, Walzel H, Mylonas I, et al. The human endometrium expresses the glycoprotein mucin-1 and shows positive correlation for Thomsen-Friedenreich epitope expression and galectin-1 binding. *J Histochem Cytochem* 2009; 57: 871-81.
14. Sandberg TP, Oosting J, van Pelt GW, Mesker WE, Tollenaar R, Morreau H. Molecular profiling of colorectal tumors stratified by the histological tumor-stroma ratio: increased expression of galectin-1 in tumors with high stromal content. *Oncotarget* 2018; 9: 31502-15.
15. Zinovkin DA, Pranjol MZ, Bilsky IA, Zmushko VA. Tumor-associated T-lymphocytes and macrophages are decreased in endometrioid endometrial carcinoma with MELF-pattern stromal changes. *Cancer Microenviron* 2018; 11: 107-14.
16. Albini A, Bruno A, Noonan DM, Mortara L. Contribution to tumor angiogenesis from innate immune cells within the tumor microenvironment: implications for immunotherapy. *Front Immunol* 2018; 9: 527.
17. Melincovici CS, Boşca AB, Şuşman S, et al. Vascular endothelial growth factor (VEGF): key factor in normal and pathological angiogenesis. *Rom J Morphol Embryol* 2018; 59: 455-67.
18. Tao L, Huang G, Song H, Chen Y, Chen L. Cancer associated fibroblasts: an essential role in the tumor microenvironment. *Oncol Lett* 2017; 14: 2611-20.
19. Li YL, Zhao H, Ren XB. Relationship of VEGF/VEGFR with immune and cancer cells: staggering or forward? *Cancer Biol Med* 2016; 13: 206-14.
20. Miyata Y, Sakai H. Reconsideration of the clinical and histopatho-

- logical significance of angiogenesis in prostate cancer: Usefulness and limitations of microvessel density measurement. *Int J Urol* 2015; 22: 806-15.
21. Jilaveanu LB, Puligandla M, Weiss SA, et al. Tumor microvessel density as a prognostic marker in high-risk renal cell carcinoma patients treated on ECOG-ACRIN E2805. *Clin Cancer Res* 2018; 24: 217-23.
 22. Hu X, Liu H, Ye M, Zhu X. Prognostic value of microvessel density in cervical cancer. *Cancer Cell Int* 2018; 18: 152.
 23. Mezheyeuski A, Nerovnya A, Bich T, Tur G, Ostman A, Portyanko A. Inter- and intra-tumoral relationships between vasculature characteristics, GLUT1 and budding in colorectal carcinoma. *Histol Histopathol* 2015; 30: 1203-11.
 24. Joehlin-Price AS, McHugh KE, Stephens JA, et al. The microcystic, elongated, and fragmented (MELF) pattern of invasion: a single institution report of 464 consecutive FIGO grade 1 endometrial endometrioid adenocarcinomas. *Am J Surg Pathol* 2017; 41: 49-55.
 25. Kamili NA, Arthur CM, Gerner-Smidt C, et al. Key regulators of galectin-glycan interactions. *Proteomics* 2016; 16: 3111-25.
 26. Chen J, Tang D, Wang S, et al. High expressions of galectin-1 and VEGF are associated with poor prognosis in gastric cancer patients. *Tumour Biol* 2014; 35: 2513-9.
 27. Wu R, Wu T, Wang K, et al. Prognostic significance of galectin-1 expression in patients with cancer: a meta-analysis. *Cancer Cell Int* 2018; 18: 108.
 28. Goel HL, Mercurio AM. VEGF targets the tumour cell. *Nat Rev Cancer* 2013; 13: 871-82.
 29. Wang JZ, Xiong YJ, Man GC, Chen XY, Kwong J, Wang CC. Clinicopathological and prognostic significance of blood microvessel density in endometrial cancer: a meta-analysis and subgroup analysis. *Arch Gynecol Obstet* 2018; 297: 731-40.
 30. Prodromidou A, Vorgias G, Bakogiannis K, Kalinoglou N, Iavazzo C. MELF pattern of myometrial invasion and role in possible endometrial cancer diagnostic pathway: a systematic review of the literature. *Eur J Obstet Gynecol Reprod Biol* 2018; 230: 147-52.

Clinicopathological Characterization and Prognostic Implication of SMAD4 Expression in Colorectal Carcinoma

Seung-Yeon Yoo^{1,2}, Ji-Ae Lee^{1,2}, Yunjoo Shin², Nam-Yun Cho², Jeong Mo Bae^{1,2}, Gyeong Hoon Kang^{1,2}

¹Department of Pathology, Seoul National University Hospital, Seoul;

²Laboratory of Epigenetics, Cancer Research Institute, Seoul National University College of Medicine, Seoul, Korea

Background: SMAD family member 4 (SMAD4) has gained attention as a promising prognostic factor of colorectal cancer (CRC) as well as a key molecule to understand the tumorigenesis and progression of CRC. **Methods:** We retrospectively analyzed 1,281 CRC cases immunohistochemically for their expression status of SMAD4, and correlated this status with clinicopathologic and molecular features of CRCs. **Results:** A loss of nuclear SMAD4 was significantly associated with frequent lymphovascular and perineural invasion, tumor budding, fewer tumor-infiltrating lymphocytes, higher pT and pN category, and frequent distant metastasis. In contrast, tumors overexpressing SMAD4 showed a significant association with sporadic microsatellite instability. After adjustment for TNM stage, tumor differentiation, adjuvant chemotherapy, and lymphovascular invasion, the loss of SMAD4 was found to be an independent prognostic factor for worse 5-year progression-free survival (hazard ratio [HR], 1.27; 95% confidence interval [CI], 1.01 to 1.60; $p = .042$) and 7-year cancer-specific survival (HR, 1.45; 95% CI, 1.06 to 1.99; $p = .022$). **Conclusions:** We confirmed the value of determining the loss of SMAD4 immunohistochemically as an independent prognostic factor for CRC in general. In addition, we identified some histologic and molecular features that might be clues to elucidate the role of SMAD4 in colorectal tumorigenesis and progression.

Key Words: Biomarker; SMAD4; Colorectal neoplasms; Prognosis

Received: May 7, 2019 Revised: May 29, 2019 Accepted: June 7, 2019

Corresponding Author: Jeong Mo Bae, MD, Department of Pathology, Seoul National University College of Medicine, 103 Daehak-ro, Jongno-gu, Seoul 03080, Korea
Tel: +82-2-2072-3374, Fax: +82-2-743-5530, E-mail: jeongmobae@gmail.com

Corresponding Author: Gyeong Hoon Kang, MD, Department of Pathology, Seoul National University College of Medicine, 103 Daehak-ro, Jongno-gu, Seoul 03080, Korea
Tel: +82-2-740-8263, Fax: +82-2-765-5600, E-mail: ghkang@snu.ac.kr

Ranked third in terms of incidence and second in terms of mortality in the latest global cancer report,¹ colorectal cancer (CRC) is a major health burden worldwide. Notably, this report mentioned South Korea as one of the countries where the highest colon cancer incidence rates were observed. Moreover, the report specifically stated that the highest incidence rates of rectal cancer were seen in South Korean males. In this regard, the importance of understanding the biology of Korean CRC cannot be emphasized enough.

SMAD family member 4 (SMAD4) is a transcription factor that acts as the central mediator of the transforming growth factor β (TGF- β) pathway.² Also known as deleted pancreatic cancer locus-4, heterozygous or homozygous deletion of SMAD4 was first discovered in pancreatic ductal adenocarcinoma,³ and later detected in other types of cancer, including CRC. Meta-analyses have revealed that the loss of SMAD4 is a negative predictor of

overall survival, cancer-specific survival (CSS), and relapse-free survival.^{4,5} In CRC, the loss of SMAD4 is associated with poor differentiation,^{6,7} higher stage,⁸⁻¹² frequent lymph node metastasis,¹³⁻¹⁷ loss of immune infiltrates,¹⁷ and poor response to 5-fluorouracil.¹⁷⁻¹⁹ Accordingly, numerous studies have reported the value of determining SMAD4 loss as a negative prognostic factor.^{9-12,17,20-25} Although some studies failed to identify a significant association,^{6,8,26-28} a meta-analysis reported pooled hazard ratios over 1 with statistical significance for overall survival, disease-free survival, and CSS.²⁹ Mechanistically, the loss of SMAD4 has been implicated with activation of the Akt pathway³⁰ and Wnt pathways.³¹ Moreover, germline mutations of *SMAD4* and *BMPRIA* (a gene upstream from *SMAD4* in the TGF- β pathway), cause juvenile polyposis syndrome, a genetic cancer predisposition syndrome with increased risk of gastrointestinal cancers.³² Collectively, these data suggest that SMAD4 is a key

molecule to decipher the pathophysiology of CRC while acting as a feasible prognostic marker for optimal surveillance of patients. However, only a handful of studies have explored the expression of SMAD4 and its prognostic significance in a limited number of Korean CRC patients.^{15,28,33} Moreover, comprehensive clinicopathologic and molecular characterization of CRCs with respect to SMAD4 expression was rarely performed.

In this study, we analyzed 1,281 CRC cases for their expression status of SMAD4 using immunohistochemistry and demonstrated comprehensive clinicopathologic and molecular characteristics of CRCs including *KRAS* and *BRAF* mutation, microsatellite instability (MSI) and CpG island methylator phenotype (CIMP) depending on nuclear SMAD4 expression status. Finally, we evaluated its value as a prognostic factor for CSS and progression-free survival.

MATERIALS AND METHODS

Patients and tissue samples

Under the exclusion criteria described previously,³⁴ 1,370 out of 1,853 CRC cases resected at Seoul National University Hospital, Seoul, Korea, between January 2004 and June 2008 were reviewed. Among them, 1,281 cases with formalin-fixed, paraffin-embedded (FFPE) tumor blocks sufficient for construction of a tissue microarray (TMA) were included in the study. Initial pathologic diagnosis and clinical information, including age, tumor location and radiologic/pathologic evidences of distant metastases were obtained from electronic medical records. Additional histologic parameters including tumor differentiation, tumor budding, representative number of tumor-infiltrating lymphocytes (TILs) per one high power field (400× magnification), were evaluated by two pathologists as described previously.³⁴ FFPE tissues were used for molecular analysis and immunohistochemistry.

Immunohistochemistry

For each CRC case, a pair of 2-mm cores of representative tumor areas in the FFPE tissue were extracted to construct the TMA. To evaluate SMAD4 expression in CRCs, TMAs were sectioned at a thickness of 4-μm and stained using a rabbit monoclonal anti-SMAD4 antibody (1:200 dilution, clone EP618Y, Abcam, Cambridge, UK). Stained slides were scanned by an Aperio AT2 slide scanner (Sausalito, CA, USA) at 40× magnification with a resolution of 0.25 μm per pixel. The proportion and the intensity of SMAD4 staining in nuclear compartment were evaluated using TMA Assistant protocol of QuPath,³⁵ open-source soft-

ware for digital pathology image analysis. In detail, the intensity of SMAD4 staining in nuclear compartment was graded using intensity feature of nuclear diaminobenzidine (DAB) optical densities (OD). Because nuclear DAB ODs of entrapped non-neoplastic epithelium range from 0.2 to 0.6, intensity of nuclear SMAD4 staining of tumor cells were evaluated using following cut-offs: intensity 0, DAB OD < 0.2; intensity 1, DAB OD ≥ 0.2 and < 0.6; and intensity 2, DAB OD ≥ 0.6. Finally, each case was classified to SMAD4-loss (≥95% of tumor cells showed intensity 0), SMAD4-low (≥5% of tumor cells showed intensity 1, and < 30% of tumor cells showed intensity 2), and SMAD4-high (≥30% of tumor cells showed intensity 2). For survival analysis, CRC cases were dichotomized to CRCs with SMAD4 loss and CRCs with retained SMAD4 (SMAD4-low and SMAD4-high). The evaluation method and cut-offs for the expression of cytokeratin 7 (CK7) (clone OV-TL, 12/30, Dako, Carpinteria, CA, USA), cytokeratin 20 (CK20) (clone Ks20.8, Dako), and nuclear protein CDX2 (clone EPR2764Y, ready-to-use, Cell Marque, Rocklin, CA, USA) were described previously.³⁶ All immunohistochemical procedures in this study were conducted with an automated immunostainer (BenchMark XT, Ventana Medical Systems, Tucson, AZ, USA).

Molecular analyses

Through histological examination, representative tumor portions were marked and then subjected to manual microdissection. The dissected tissues were collected into microtubes containing lysis buffer and proteinase K and were incubated at 55°C for 2 days. DNA from paraffin-embedded tissues was extracted, and the polymerase chain reaction (PCR) was performed. Direct sequencing of *KRAS* codons 12 and 13 and allele-specific PCR for *BRAF* codon 600 were performed as described previously.³⁴ The MSI status of each tumor was determined by evaluating five microsatellite markers (BAT25, BAT26, D2S123, D5S346, and D17S250) as standardized by the National Cancer Institute.³⁷ A fluorescent label was added to either the forward or reverse primer for each marker, and the PCR products were electrophoresed and analyzed. We classified MSI status as MSI-positive (instability at two or more microsatellite marker), and MSI-negative (no instability or instability at one marker). The CIMP status was evaluated by the MethyLight assay of eight markers (CACNA1G, CDKN2A [p16], CRABP1, IGF2, MLH1, NEUROG1, RUNX3, and SOCS1).³⁸ We classified CRCs into CIMP-negative (0–4 methylated markers), CIMP-positive 1 (5–6 methylated markers), and CIMP-positive 2 (CIMP-P2) (7–8 methylated markers), as previously described.³⁴

Statistical analyses

SAS ver. 9.4 (SAS Institute Inc., Cary, NC, USA) and R software (<http://www.r-project.org>) were used for statistical analyses. Clinicopathological characteristics were compared between the three SMAD4 expression groups by use of chi-square test or Fisher exact test, as appropriate. Chi-square test for trend was used to compute p for trend. Survival curves after surgery were estimated with the Kaplan-Meier method, and differences in survival curves were tested with the log-rank test. All statistical tests were two-sided, and statistical significance was defined as $p < .05$.

Ethics statement

This study was approved by the Institutional Review Board which waived the requirement to obtain informed consent (IRB No. C-1502-029-647).

RESULTS

Clinicopathological and molecular correlation of nuclear SMAD4 expression in CRCs

Out of 1,281 CRC cases, 210 (16.4%) showed a loss of nuclear expression of SMAD4 (Fig. 1A). Among the remaining cases with retained SMAD4 expression, 942 cases (73.5%) showed low-level expression (Fig. 1B), while high-level expression was observed in 129 cases (10.1%) (Fig. 1C).

We then sought to identify clinicopathologic features showing gradual changes according to the loss or overexpression of SMAD4 (Table 1). With decreasing expression of SMAD4, tumors tended to show an infiltrative gross type, more frequent lymphovascular and perineural invasion, tumor budding, and lower TILs

(all $p < .001$). Consequently, CRC cases showed significant associations with higher pT ($p < .001$) and pN ($p < .001$) category, and frequent distant metastasis ($p = .001$) as nuclear SMAD4 expression decreased. Notably, statistically significant increase of SMAD4 loss and concomitant decrease of SMAD4 expression was noted as TNM stage increased ($p < .001$) (Supplementary Fig. S1).

To identify molecular phenotypical correlates of such linear trends, we evaluated MSI, CIMP status, *KRAS* exon 2, *BRAF* codon 600, and immunohistochemical expression of CK7, CK20, and CDX2 (Table 2). With increasing expression of SMAD4, tumors tended to be more associated with MSI ($p < .001$), CIMP-P2 ($p = .001$), and *MLH1* promoter methylation ($p < .001$). Interestingly, the expression of CK20 and CDX2 showed opposite trends with increasing SMAD2 expression; CDX2 expression was lost as nuclear SMAD4 expression increased ($p = .001$), while the expression of CK20 increased ($p < .001$).

Prognostic implication of SMAD4 loss in CRCs

A univariate survival analysis revealed that CRCs with a loss of nuclear SMAD4 expression exhibited a significantly worse 5-year progression-free survival (PFS) ($p < .001$) (Fig. 2A), and 7-year CSS ($p = .001$) (Fig. 2B). To explore whether there exists a differential prognostic effect of SMAD4 according to TNM stage, we performed the Kaplan-Meier analysis for each TNM stage subgroups (Supplementary Figs. S2, S3). In a stage-specific analysis, SMAD4 loss was associated with worse 5-year PFS ($p = .019$) in stage II CRCs, worse 5-year PFS ($p = .055$) and 7-year CSS ($p = .011$) in stage IV CRCs. In the multivariate Cox proportional hazard analysis, a loss of SMAD4 expression proved to be an independent prognostic factor for 5-year PFS

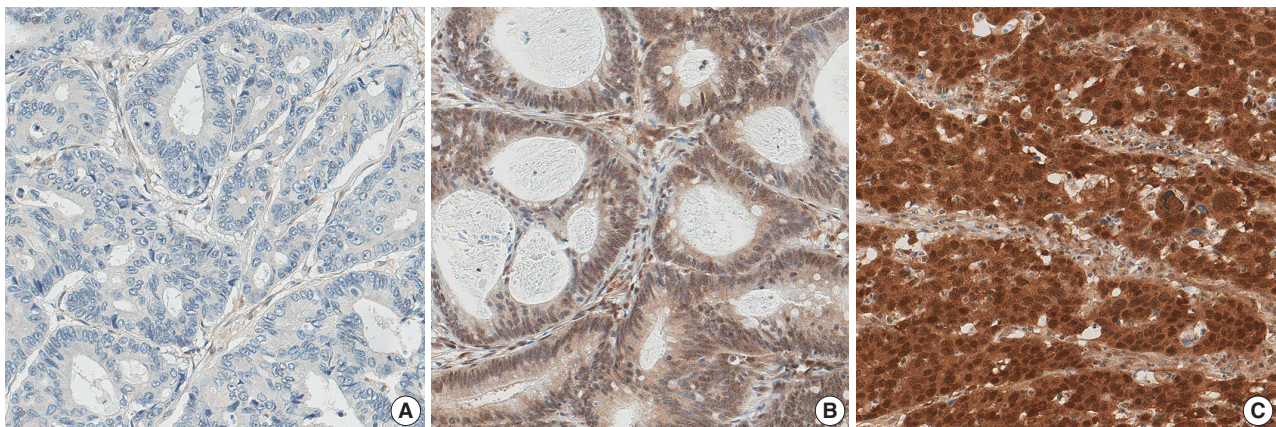


Fig. 1. Nuclear expression of SMAD4 in colorectal cancers. Representative examples for the loss of expression (A), low-level expression (B), and high-level expression (C).

Table 1. Clinicopathologic characteristics of colorectal cancers according to SMAD4 expression

	SMAD4-loss (n=210, 16.4%)	SMAD4-low (n=942, 73.5%)	SMAD4-high (n=129, 10.1%)	p for difference	p for trend
Age (yr)	64 (27–83)	63 (20–90)	61 (25–93)	.222	
Sex				.225	.105
Male	132 (62.9)	566 (60.1)	69 (53.5)		
Female	78 (37.1)	376 (39.9)	60 (46.5)		
Location				<.001	.222
Proximal	61 (29.1)	216 (22.9)	50 (38.8)		
Distal/Rectum	149 (70.9)	726 (77.1)	79 (61.2)		
Gross type				.002	<.001
Fungating	122 (58.1)	624 (66.2)	99 (76.7)		
Infiltrative	88 (41.9)	318 (33.8)	30 (23.3)		
pT category				<.001	<.001
pT1-2	20 (9.5)	176 (18.7)	37 (28.7)		
pT3-4	190 (90.5)	766 (81.3)	92 (71.3)		
pN category				<.001	<.001
pN0	85 (40.5)	471 (50.0)	89 (69.0)		
pN1-2	125 (59.5)	471 (50.0)	40 (31.0)		
Distant metastasis				.001	.001
M0	167 (79.5)	775 (82.3)	122 (94.6)		
M1	43 (20.5)	167 (17.7)	7 (5.4)		
TNM stage				<.001	<.001
I, II	76 (36.2)	448 (47.6)	87 (67.4)		
III, IV	134 (63.8)	494 (52.4)	42 (32.6)		
Lymphovascular invasion				<.001	<.001
Absent	97 (46.2)	543 (57.6)	96 (74.4)		
Present	113 (53.8)	399 (42.4)	33 (26.6)		
Perineural invasion				<.001	<.001
Absent	133 (63.3)	730 (77.5)	113 (87.6)		
Present	77 (36.7)	212 (22.5)	16 (12.4)		
Differentiation (grade)				.612	.923
Differentiated (G1/2)	200 (95.2)	906 (94.2)	122 (94.6)		
Undifferentiated (G3/4)	10 (4.8)	36 (3.8)	7 (5.4)		
Tumor budding				<.001	<.001
Absent	48 (22.9)	256 (27.2)	57 (44.2)		
Present	162 (77.1)	686 (72.8)	72 (55.8)		
Tumor-infiltrating lymphocytes (400× magnification)				<.001	<.001
Low (<8)	164 (78.1)	739 (78.4)	72 (55.8)		
High (≥8)	46 (21.9)	203 (21.6)	57 (44.2)		
Mucin production				.002	.581
Absent	176 (83.8)	839 (89.1)	102 (79.1)		
Present	34 (16.2)	103 (10.9)	27 (20.9)		

Values are presented as median (range) or number (%).

(hazard ratio [HR], 1.27; 95% confidence interval [CI], 1.01 to 1.60; $p = .042$) (Table 3), and for 7-year CSS (HR, 1.45; 95% CI, 1.06 to 1.99; $p = .022$), after adjustment for TNM stage, tumor differentiation, adjuvant chemotherapy, and lymphovascular invasion.

DISCUSSION

To the best of our knowledge, this is the second largest study

focusing on the clinicopathologic and prognostic implications of SMAD4 expression in CRC, and the largest in an Asian population. While the largest previous study was performed on 1,381 stage II or III CRC patients enrolled at a pan-European clinical trial for adjuvant chemotherapy,¹² our cohort consisted of 1,281 retrospectively collected patients ranging from stage I to IV. By combining CIMP analysis with additional histologic features such as tumor budding and TILs, we identified the general expression status of SMAD4 and its association with

Table 2. Molecular characteristics of colorectal cancers according to SMAD4 expression

	SMAD4-loss (n=210, 16.4%)	SMAD4-low (n=942, 73.5%)	SMAD4-high (n=129, 10.1%)	p for difference	p for trend
<i>KRAS</i> mutation				.866	.606
Absent	143 (68.1)	657 (69.7)	91 (70.5)		
Present	67 (31.9)	285 (30.3)	38 (29.5)		
<i>BRAF</i> mutation (n=1,278)				.094	.330
Absent	196 (93.3)	906 (96.5)	122 (94.6)		
Present	14 (6.7)	33 (3.5)	7 (5.4)		
MSI				<.001	<.001
MSS	204 (97.1)	889 (94.4)	93 (72.1)		
MSI	6 (2.9)	53 (5.6)	36 (27.9)		
CIMP				.229 ^a	.001
CIMP-N, P1	209 (99.5)	930 (98.7)	122 (94.6)		
CIMP-P2	1 (0.5)	12 (1.3)	7 (5.4)		
<i>MLH1</i> promoter methylation				<.001	<.001
Unmethylated	205 (97.6)	921 (97.8)	112 (86.8)		
Methylated	5 (2.4)	21 (2.2)	17 (13.2)		
CK7 expression (n=1,277)				.273	.120
Absent	186 (89.4)	868 (92.3)	121 (93.8)		
Present	22 (10.6)	72 (7.7)	8 (6.2)		
CK20 expression (n=1,271)				<.001	<.001
Retained	183 (88.8)	780 (83.3)	90 (69.8)		
Loss	23 (11.2)	156 (16.7)	39 (30.2)		
CDX2 expression (n=1,262)				.001	.001
Retained	166 (80.6)	831 (89.4)	116 (91.3)		
Loss	40 (19.4)	98 (10.6)	11 (8.7)		

Values are presented as median (range) or number (%).

MSI, microsatellite instability; MSS, microsatellite stable; CIMP, CpG island methylator phenotype; CIMP-N, CIMP-negative; CIMP-P1, CIMP-positive 1; CIMP-P2, CIMP-positive 2; CK, cytokeratin.

^ap-value with Fisher exact test.

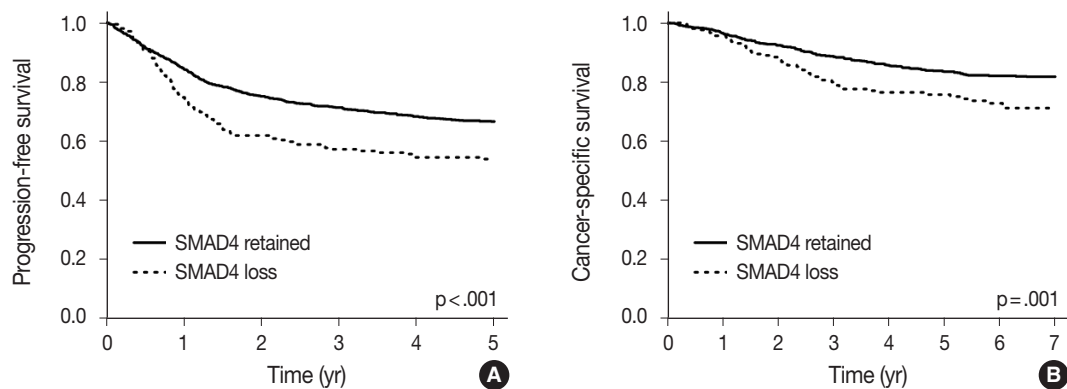


Fig. 2. Kaplan-Meier survival curves according to the nuclear SMAD4 expression. (A) 5-Year progression-free survival. (B) 7-Year cancer-specific survival.

clinicopathologic and molecular features of CRC.

Most previous studies evaluated SMAD4 expression based on two-tier classification: loss versus no loss, or low versus high expression.^{7,8,10,11,13-15,17,18,20} Because of ambiguities in the definition of low expression, the reported prevalence of low-level SMAD4 expression varied significantly from 2.34% to 75.2%. On the other hand, studies that adopted a multi-tier classifica-

tion reported relatively homogeneous results, with the prevalence of low-level SMAD4 expression ranging from 9.3% to 37.7%.^{6,9,12,16} Considering the presence of an apparent loss, overexpression, and intermediate expression of SMAD4, we felt it more appropriate to use a three-tier classification (loss, low-level, and high-level) of SMAD4 expression. As a result, 16.4% of our cases were identified as SMAD4 loss, which falls within

Table 3. Multivariate Cox proportional hazard analysis with respect to 5-year PFS and 7-year CSS

	5-Year PFS		7-Year CSS	
	HR (95% CI)	p-value	HR (95% CI)	p-value
Stage (III, IV vs I, II)	4.57 (3.47–6.00)	<.001	4.99 (3.38–7.37)	<.001
Grade (G3/4 vs G1/2)	1.80 (1.27–2.56)	.001	1.62 (0.95–2.75)	.077
Post-operative chemotherapy (yes vs no)	0.63 (0.49–0.81)	<.001	0.34 (0.25–0.47)	<.001
Lymphovascular invasion (yes vs no)	1.83 (1.48–2.26)	<.001	2.22 (1.63–3.03)	<.001
SMAD4 expression (loss vs retained)	1.27 (1.01–1.60)	.042	1.45 (1.06–1.99)	.022

PFS, progression-free survival; CSS, cancer-specific survival; HR, hazard ratio; CI, confidence interval.

the range of previous reports.

Consistent with the previous studies,⁸⁻¹⁷ we observed a significant association between SMAD4 loss and higher pT and pN category, and frequent distant metastasis. Consequently, we confirmed the value of SMAD4 loss as a prognostic factor for poor CSS and PFS of CRC. In colonic epithelial cells, TGF- β signaling reduces proliferation and promotes apoptosis and differentiation.³⁹ Because SMAD4 translocates to the nucleus by forming a heterodimeric complex with SMAD2/3 that is phosphorylated by the activated TGF- β receptor,² it is intuitive that the immunohistochemical loss of nuclear SMAD4 expression suggests a concomitant loss of TGF- β signaling, which leads to uncontrolled proliferative behavior.

Interestingly, we observed that some tumors overexpressed SMAD4 and those tumors tend to be MSI, CIMP-P2, and have their *MLH1* promoter methylated. Along with the association between fungating gross type, these data collectively suggested an association between the sporadic MSI-high (MSI-H)/CIMP-high phenotype and overexpression of nuclear SMAD4. Although the meaning of SMAD4 overexpression is not straightforward, such a trend has been reported previously.^{9,12,40} One possibility is that overexpression of SMAD4 in MSI-H tumors might be the consequence of a compensatory mechanism for mutational inactivation of the TGF- β signaling pathway; i.e., some machineries in the pathway, such as transforming growth factor β receptor II (*TGFBR2*) or activin type II receptor (*ACVR2*), are prone to mutations when mismatch repair is impaired.³⁹ At the same time, there are reports suggesting various bypass mechanisms to overcome such mutations.⁴¹⁻⁴⁴ Further mechanistic studies are needed to confirm this hypothesis.

A novel finding in our study was the gradual increase of CDX2 expression as nuclear SMAD4 increased, while CK20 showed the opposite trend. Although this is in contrast with our previous report that expression of both CK20 and CDX2 got lost according to CpG island methylation,³⁴ the proportional relationship of CDX2 and SMAD4 is consistent with some previous reports. In stomach, it has been reported that SMAD4 can

activate the promoter of CDX2, and knockdown of SMAD4 led to the decreased expression of CDX2.⁴⁵ Concomitant loss of SMAD4 and CDX2 was also observed in colorectal juvenile polyps obtained from juvenile polyposis syndrome patients.⁴⁶ The loss of CK20 expression could be explained as a consequence of epithelial mesenchymal transition (EMT). It is known that switch of intermediate filaments from cytokeratin to vimentin occurs during EMT.⁴⁷ It has been reported that the immunohistochemical expression of SMAD4 was positively correlated with that of EMT-related transcription factors such as Snail-1 and Twist-1,⁴⁸ and silencing of SMAD4 inhibited EMT.⁴⁹ Consequently, an intriguing hypothesis emerges that overexpression of SMAD4 accompanied loss of CK20 by promoting EMT.

Consistent with a previous study,¹⁷ we observed a significant association between low TIL infiltration and SMAD4 loss. Although this could be a secondary effect of the MSI status, there are a series of reports on the correlation between SMAD4 loss and CCL15 expression.⁵⁰⁻⁵² These researchers demonstrated that the loss of SMAD4 upregulated CCL15, which resulted in recruitment of CCR1+ cells at the invasive front. CCR1+ cells are phenotypically myeloid-derived suppressor cells (MDSC) and express immunosuppressive molecules such as indoleamine 2,3-dioxygenase. Using mouse models, these researchers demonstrated that the loss of SMAD4 promoted pulmonary and hepatic metastasis through the CCL15-CCR1 axis. It is plausible that the MDSCs are also responsible for the lower TIL infiltration we observed for tumors with SMAD4 loss.

In conclusion, we confirmed the value of determining expression of SMAD4 immunohistochemically as an independent prognostic factor for CRC in general. Furthermore, we identified some histologic and molecular features that might be clues to elucidate the role of SMAD4 in colorectal tumorigenesis and progression. Further studies are needed to validate these findings with an independent large-scale series of CRC cases.

Electronic Supplementary Material

Supplementary materials are available at Journal of Pathology and Translational Medicine (<https://jpatholtm.org>).

ORCID

Seung-Yeon Yoo: <https://orcid.org/0000-0002-7881-9038>

Ji-Aee Lee: <https://orcid.org/0000-0003-1493-6208>

Yunjoo Shin: <https://orcid.org/0000-0002-7375-9048>

Nam-Yun Cho: <https://orcid.org/0000-0002-5736-2956>

Jeong Mo Bae: <https://orcid.org/0000-0003-0462-3072>

Gyeong Hoon Kang: <https://orcid.org/0000-0003-2380-6675>

Author Contributions

Conceptualization: JMB, GHK.

Data curation: SYY, JMB.

Formal analysis: SYY, JMB.

Funding acquisition: JMB, GHK.

Investigation: SYY, JAL, JMB.

Methodology: SYY, JAL, YS, NYC, JMB.

Project administration: JMB, GHK.

Resources: JMB, GHK.

Supervision: JMB, GHK.

Validation: JMB, GHK.

Visualization: SYY, JMB.

Writing—original draft: SYY, JMB.

Writing—review & editing: JMB, GHK.

Conflicts of Interest

The authors declare that they have no potential conflicts of interest.

Funding

This study was supported by grants from the National Research Foundation (NRF) funded by the Korean Ministry of Science, ICT and Future Planning (2011-0030049, 2016M3A9B6026921), Korean Health Technology R&D Project, Ministry of Health and Welfare (HI14C1277), and a grant from the SNUH Research Fund (04-2018-0620).

REFERENCES

- Bray F, Ferlay J, Soerjomataram I, Siegel RL, Torre LA, Jemal A. Global cancer statistics 2018: GLOBOCAN estimates of incidence and mortality worldwide for 36 cancers in 185 countries. *CA Cancer J Clin* 2018; 68: 394-424.
- Zhao M, Mishra L, Deng CX. The role of TGF-beta/SMAD4 signaling in cancer. *Int J Biol Sci* 2018; 14: 111-23.
- Schutte M. DPC4/SMAD4 gene alterations in human cancer, and their functional implications. *Ann Oncol* 1999; 10 Suppl 4: 56-9.
- Du Y, Zhou X, Huang Z, et al. Meta-analysis of the prognostic value of smad4 immunohistochemistry in various cancers. *PLoS One* 2014; 9: e110182.
- Wang JD, Jin K, Chen XY, Lv JQ, Ji KW. Clinicopathological significance of SMAD4 loss in pancreatic ductal adenocarcinomas: a systematic review and meta-analysis. *Oncotarget* 2017; 8: 16704-11.
- Kouvidou C, Latoufis C, Lianou E, et al. Expression of Smad4 and TGF-beta2 in colorectal carcinoma. *Anticancer Res* 2006; 26: 2901-7.
- Xu WQ, Jiang XC, Zheng L, Yu YY, Tang JM. Expression of TGF-beta1, TbetaRII and Smad4 in colorectal carcinoma. *Exp Mol Pathol* 2007; 82: 284-91.
- Bacman D, Merkel S, Croner R, Papadopoulos T, Brueckl W, Dimmler A. TGF-beta receptor 2 downregulation in tumour-associated stroma worsens prognosis and high-grade tumours show more tumour-associated macrophages and lower TGF-beta1 expression in colon carcinoma: a retrospective study. *BMC Cancer* 2007; 7: 156.
- Isaksson-Mettavainio M, Palmqvist R, Dahlin AM, et al. High SMAD4 levels appear in microsatellite instability and hypermethylated colon cancers, and indicate a better prognosis. *Int J Cancer* 2012; 131: 779-88.
- Voorneveld PW, Jacobs RJ, De Miranda NF, et al. Evaluation of the prognostic value of pSMAD immunohistochemistry in colorectal cancer. *Eur J Cancer Prev* 2013; 22: 420-4.
- Kozak MM, von Eyben R, Pai J, et al. Smad4 inactivation predicts for worse prognosis and response to fluorouracil-based treatment in colorectal cancer. *J Clin Pathol* 2015; 68: 341-5.
- Yan P, Klingbiel D, Saridaki Z, et al. Reduced expression of SMAD4 is associated with poor survival in colon cancer. *Clin Cancer Res* 2016; 22: 3037-47.
- Jain S, Singhal S, Francis F, et al. Association of overexpression of TIF1gamma with colorectal carcinogenesis and advanced colorectal adenocarcinoma. *World J Gastroenterol* 2011; 17: 3994-4000.
- Handra-Luca A, Olschwang S, Fléjou JF. SMAD4 protein expression and cell proliferation in colorectal adenocarcinomas. *Virchows Arch* 2011; 459: 511-9.
- Chung Y, Wi YC, Kim Y, et al. The Smad4/PTEN expression pattern predicts clinical outcomes in colorectal adenocarcinoma. *J Pathol Transl Med* 2018; 52: 37-44.
- Oyanagi H, Shimada Y, Nagahashi M, et al. SMAD4 alteration associates with invasive-front pathological markers and poor prognosis in colorectal cancer. *Histopathology* 2019; 74: 873-82.
- Wasserman I, Lee LH, Ogino S, et al. SMAD4 loss in colorectal cancer patients correlates with recurrence, loss of immune infiltrate, and

- chemoresistance. *Clin Cancer Res* 2019; 25: 1948-56.
18. Alhopuro P, Alazzouzi H, Sammalkorpi H, et al. SMAD4 levels and response to 5-fluorouracil in colorectal cancer. *Clin Cancer Res* 2005; 11: 6311-6.
 19. Boulay JL, Mild G, Lowy A, et al. SMAD4 is a predictive marker for 5-fluorouracil-based chemotherapy in patients with colorectal cancer. *Br J Cancer* 2002; 87: 630-4.
 20. Alazzouzi H, Alhopuro P, Salovaara R, et al. SMAD4 as a prognostic marker in colorectal cancer. *Clin Cancer Res* 2005; 11: 2606-11.
 21. Isaksson-Mettavainio M, Palmqvist R, Forssell J, Stenling R, Oberg A. SMAD4/DPC4 expression and prognosis in human colorectal cancer. *Anticancer Res* 2006; 26: 507-10.
 22. Mesker WE, Liefers GJ, Junggeburst JM, et al. Presence of a high amount of stroma and downregulation of SMAD4 predict for worse survival for stage I-II colon cancer patients. *Cell Oncol* 2009; 31: 169-78.
 23. Baraniskin A, Munding J, Schulmann K, et al. Prognostic value of reduced SMAD4 expression in patients with metastatic colorectal cancer under oxaliplatin-containing chemotherapy: a translational study of the AIO colorectal study group. *Clin Colorectal Cancer* 2011; 10: 24-9.
 24. Wang C, Zhou Y, Ruan R, Zheng M, Han W, Liao L. High expression of COUP-TF II cooperated with negative Smad4 expression predicts poor prognosis in patients with colorectal cancer. *Int J Clin Exp Pathol* 2015; 8: 7112-21.
 25. Coates RF, Gardner JA, Gao Y, et al. Significance of positive and inhibitory regulators in the TGF-beta signaling pathway in colorectal cancers. *Hum Pathol* 2017; 66: 34-9.
 26. Xie W, Rimm DL, Lin Y, Shih WJ, Reiss M. Loss of Smad signaling in human colorectal cancer is associated with advanced disease and poor prognosis. *Cancer J* 2003; 9: 302-12.
 27. Gulubova M, Manolova I, Ananiev J, Julianov A, Yovchev Y, Peeva K. Role of TGF-beta1, its receptor TGFbetaRII, and Smad proteins in the progression of colorectal cancer. *Int J Colorectal Dis* 2010; 25: 591-9.
 28. Chun HK, Jung KU, Choi YL, et al. Low expression of transforming growth factor beta-1 in cancer tissue predicts a poor prognosis for patients with stage III rectal cancers. *Oncology* 2014; 86: 159-69.
 29. Voorneveld PW, Jacobs RJ, Kodach LL, Hardwick JC. A Meta-analysis of SMAD4 immunohistochemistry as a prognostic marker in colorectal cancer. *Transl Oncol* 2015; 8: 18-24.
 30. Zhang B, Zhang B, Chen X, et al. Loss of Smad4 in colorectal cancer induces resistance to 5-fluorouracil through activating Akt pathway. *Br J Cancer* 2014; 110: 946-57.
 31. Voorneveld PW, Kodach LL, Jacobs RJ, et al. The BMP pathway either enhances or inhibits the Wnt pathway depending on the SMAD4 and p53 status in CRC. *Br J Cancer* 2015; 112: 122-30.
 32. Chow E, Macrae F. A review of juvenile polyposis syndrome. *J Gastroenterol Hepatol* 2005; 20: 1634-40.
 33. Ahn BK, Jang SH, Paik SS, Lee KH. Smad4 may help to identify a subset of colorectal cancer patients with early recurrence after curative therapy. *Hepatogastroenterology* 2011; 58: 1933-6.
 34. Bae JM, Kim JH, Kwak Y, et al. Distinct clinical outcomes of two CIMP-positive colorectal cancer subtypes based on a revised CIMP classification system. *Br J Cancer* 2017; 116: 1012-20.
 35. Bankhead P, Loughrey MB, Fernández JA, et al. QuPath: open source software for digital pathology image analysis. *Sci Rep* 2017; 7: 16878.
 36. Bae JM, Lee TH, Cho NY, Kim TY, Kang GH. Loss of CDX2 expression is associated with poor prognosis in colorectal cancer patients. *World J Gastroenterol* 2015; 21: 1457-67.
 37. Boland CR, Thibodeau SN, Hamilton SR, et al. A National Cancer Institute Workshop on Microsatellite Instability for cancer detection and familial predisposition: development of international criteria for the determination of microsatellite instability in colorectal cancer. *Cancer Res* 1998; 58: 5248-57.
 38. Weisenberger DJ, Siegmund KD, Campan M, et al. CpG island methylator phenotype underlies sporadic microsatellite instability and is tightly associated with BRAF mutation in colorectal cancer. *Nat Genet* 2006; 38: 787-93.
 39. Jung B, Staudacher JJ, Beauchamp D. Transforming growth factor beta superfamily signaling in development of colorectal cancer. *Gastroenterology* 2017; 152: 36-52.
 40. Salovaara R, Roth S, Loukola A, et al. Frequent loss of SMAD4/DPC4 protein in colorectal cancers. *Gut* 2002; 51: 56-9.
 41. Ilyas M, Efstathiou JA, Straub J, Kim HC, Bodmer WF. Transforming growth factor beta stimulation of colorectal cancer cell lines: type II receptor bypass and changes in adhesion molecule expression. *Proc Natl Acad Sci U S A* 1999; 96: 3087-91.
 42. Deacu E, Mori Y, Sato F, et al. Activin type II receptor restoration in ACVR2-deficient colon cancer cells induces transforming growth factor-beta response pathway genes. *Cancer Res* 2004; 64: 7690-6.
 43. Baker K, Raut P, Jass JR. Microsatellite unstable colorectal cancer cell lines with truncating TGFbetaRII mutations remain sensitive to endogenous TGFbeta. *J Pathol* 2007; 213: 257-65.
 44. de Miranda NF, van Dinther M, van den Akker BE, van Wezel T, ten Dijke P, Morreau H. Transforming growth factor beta signaling in colorectal cancer cells with microsatellite instability despite biallelic mutations in TGFBR2. *Gastroenterology* 2015; 148: 1427-37.e8.
 45. Barros R, Pereira B, Duluc I, et al. Key elements of the BMP/SMAD pathway co-localize with CDX2 in intestinal metaplasia and regulate CDX2 expression in human gastric cell lines. *J Pathol* 2008; 215:

- 411-20.
46. Barros R, Mendes N, Howe JR, et al. Juvenile polyps have gastric differentiation with MUC5AC expression and downregulation of CDX2 and SMAD4. *Histochem Cell Biol* 2009; 131: 765-72.
 47. Savagner P. The epithelial-mesenchymal transition (EMT) phenomenon. *Ann Oncol* 2010; 21 Suppl 7: vii89-92.
 48. Ioannou M, Kouvaras E, Papamichali R, Samara M, Chiotoglou I, Koukoulis G. Smad4 and epithelial-mesenchymal transition proteins in colorectal carcinoma: an immunohistochemical study. *J Mol Histol* 2018; 49: 235-44.
 49. Deckers M, van Dinther M, Buijs J, et al. The tumor suppressor Smad4 is required for transforming growth factor beta-induced epithelial to mesenchymal transition and bone metastasis of breast cancer cells. *Cancer Res* 2006; 66: 2202-9.
 50. Itatani Y, Kawada K, Fujishita T, et al. Loss of SMAD4 from colorectal cancer cells promotes CCL15 expression to recruit CCR1+ myeloid cells and facilitate liver metastasis. *Gastroenterology* 2013; 145: 1064-75.e11.
 51. Inamoto S, Itatani Y, Yamamoto T, et al. Loss of SMAD4 promotes colorectal cancer progression by accumulation of myeloid-derived suppressor cells through the CCL15-CCR1 chemokine axis. *Clin Cancer Res* 2016; 22: 492-501.
 52. Yamamoto T, Kawada K, Itatani Y, et al. Loss of SMAD4 promotes lung metastasis of colorectal cancer by accumulation of CCR1+ tumor-associated neutrophils through CCL15-CCR1 axis. *Clin Cancer Res* 2017; 23: 833-44.

Reclassification of Mongolian Diffuse Gliomas According to the Revised 2016 World Health Organization Central Nervous System Tumor Classification

Enkhee Ochirjav, Bayarmaa Enkhbat, Tuul Baldandorj, Gheeyoung Choe¹

Department of Pathology, School of Biomedicine, Mongolian National University of Medical Sciences, Ulaanbaatar, Mongolia;

¹Department of Pathology, Seoul National University Bundang Hospital, Seoul National University College of Medicine, Seongnam, Korea

Background: The 2016 World Health Organization (WHO) classification of central nervous system (CNS) tumors has been modified to incorporate the IDH mutation and 1p/19q co-deletion in the diagnosis of diffuse gliomas. In this study, we aimed to evaluate the feasibility and prognostic significance of the revised 2016 WHO classification of CNS tumors in Mongolian patients with diffuse gliomas. **Methods:** A total of 124 cases of diffuse gliomas were collected, and tissue microarray blocks were made. *IDH1* mutation was tested using immunohistochemistry, and 1p/19q co-deletion status was examined using fluorescence in situ hybridization analysis. **Results:** According to the 2016 WHO classification, 124 cases of diffuse brain glioma were reclassified as follows: 10 oligodendroglioma, IDH^{mut} and 1p/19q co-deleted; three anaplastic oligodendroglioma, IDH^{mut} and 1p/19q co-deleted; 35 diffuse astrocytoma, IDH^{mut}, 11 diffuse astrocytoma, IDH^{wt}, not otherwise specified (NOS); 22 anaplastic astrocytoma, IDH^{mut}, eight anaplastic astrocytoma, IDH^{wt}, NOS; and 35 glioblastoma, IDH^{wt}, NOS, respectively. The 2016 WHO classification presented better prognostic value for overall survival in patients with grade II tumors than traditional histological classification. Among patients with grade II tumors, those with oligodendroglioma IDH^{mut} and 1p/19q co-deleted and diffuse astrocytoma IDH^{mut} showed significantly higher survival than those with diffuse astrocytoma IDH^{wt}, NOS ($p < .01$). **Conclusions:** Mongolian diffuse gliomas could be reclassified according to the new 2016 WHO classification. Reclassification revealed substantial changes in diagnosis of both oligodendroglial and astrocytic entities. We have confirmed that the revised 2016 WHO CNS tumor classification has prognostic significance in Mongolian patients with diffuse gliomas, especially those with grade II tumors.

Key Words: World Health Organization; Classification; Glioma; Isocitrate dehydrogenase; Chromosome deletion

Received: May 3, 2019 Revised: July 12, 2019 Accepted: July 15, 2019

Corresponding Author: Gheeyoung Choe, MD, Department of Pathology, Seoul National University Bundang Hospital, Seoul National University College of Medicine, 82 Gumi-ro 173beon-gil, Bundang-gu, Seongnam 13620, Korea

Tel: +82-31-787-7711, Fax: +82-31-787-4012, E-mail: gychoe@snuh.org

Gliomas are the primary tumors that develop in the central nervous system (CNS). Diffuse glioma is defined by indefinite border of tumor mass and is considered as a more aggressive form of gliomas.^{1,2} Diagnosis of glioma was mainly based on the 2007 World Health Organization (WHO) classification, which considered increased cellularity, nuclear atypia, mitotic activity, microvascular proliferation, and necrosis for malignant criteria (histologic grade of gliomas).³ Histological evaluation for grading is important for the treatment of diffuse gliomas; however, histologic grade is not the only prognostic determinant in diffuse gliomas. The chromosomal aberrations such as deletion and mutation are common in gliomas,⁴ and oligodendroglial phenotype gliomas with 1p/19q co-deletion tend to have a better

prognosis and respond well to chemotherapy and concurrent chemoradiation therapy.⁵ Moreover, gliomas with IDH mutation have more favorable prognosis than IDH-wildtype gliomas.² Therefore, at the Haarlem meeting in 2014, multidisciplinary specialists concluded that molecular information should be incorporated into the diagnosis of gliomas to make more integrated diagnosis.⁶

The updated 2016 WHO classification of CNS tumors incorporated molecular features such as IDH mutation and chromosome 1p/19q co-deletion into the diagnosis of gliomas.⁷ Previous classification published in 2007 was mainly based on the histological and immunohistochemical features of the tumor.^{3,8} The new 2016 WHO CNS tumor classification led to substantial

changes in the diagnosis of diffuse gliomas depending on the presence or absence of IDH mutation and 1p/19q co-deletion.^{5,9} Diffuse glioma with both IDH mutation and 1p/19q co-deletion is referred to as oligodendroglioma, IDH-mutant, and 1p/19q co-deleted, which has a better prognosis compared with intact cases.¹⁰ Although a glioma shows oligodendroglioma-like histologic feature, it is no longer classified as an oligodendroglial tumor if neither IDH mutation nor 1p/19q co-deletion is present. Diffuse astrocytic gliomas are classified as an IDH-mutant or IDH-wildtype according to the IDH mutation status. IDH-wildtype gliomas with epidermal growth factor receptor (*EGFR*) amplification are considered to have more aggressive behavior like glioblastoma.¹¹ Diffuse astrocytoma or oligodendroglioma, which has been diagnosed based on histologic features only without molecular testing, is classified into the “NOS (not otherwise specified)” category.^{11,12} cIMPACT-NOW (the Consortium to Inform Molecular and Practical Approaches to CNS Tumor Taxonomy) was established to provide a forum to evaluate and recommend proposed changes to future CNS tumor classifications. Recently, cIMPACT clarified the use of the term NOS and proposed the use of an additional term “NEC (not elsewhere classified)” as well.¹³ For an NOS designation, diagnostic information (histological or molecular) necessary to assign more specific WHO diagnosis is not available. For an NEC designation, necessary diagnostic testing has been successfully performed, but the results do not readily allow for a WHO 2016 diagnosis. In some instances, this will be caused by a mismatch between clinical, histological, immunohistological and/or genetic features; in others, the results may support a new or emerging entity that is not yet included in the WHO classification.¹³

In this study, we aimed to reclassify diffuse brain gliomas according to the revised 2016 WHO classification of CNS tumors in Mongolian patients with brain gliomas and to evaluate the prognostic significance of the revised 2016 WHO classification of CNS tumors.

MATERIALS AND METHODS

Tumor samples

Data of 124 patients who have been diagnosed with diffuse gliomas according to the WHO 2007 criteria in the National Center for Pathology of Mongolia between January 2006 and December 2017 were obtained in this study. We marked the representative tumor areas on hematoxylin and eosin (H&E)-stained sections. Tumor areas containing viable tumor cell infiltration over 60% without necrosis or hemorrhage were selected.

Corresponding areas were identified on the formalin-fixed, paraffin-embedded archival blocks, and we constructed tissue microarray (TMA) blocks using 3-mm cores. Each TMA block was verified by H&E staining to determine whether each core has intact glioma tissue.

IDH mutation status

In immunohistochemistry, 4- μ m-thick tissue sections were deparaffinized in xylene and hydrated by immersing them in a series of graded ethanol. Antigen retrieval was performed in the microwave by placing the sections in epitope retrieval solution (0.01 M citrate buffer, pH 6.0) for 20 minutes; endogenous peroxidase was inhibited by immersing the sections in 0.3% hydrogen peroxide for 10 minutes. Sections were then incubated with IDH1 (1:100, Dianova, Hamburg, Germany) antibody. Then, an OptiView DAB IHC Detection Kit (Ventana Medical Systems, Tucson, AZ, USA) was used following the manufacturer's recommendations in conjunction with an automated staining procedure using Benchmark XT (Ventana Medical Systems). Finally, the samples were counterstained with hematoxylin, dehydrated, mounted, and evaluated under a light microscope equipped with an Olympus CX21 camera (Tokyo, Japan) (Fig. 1).

Fluorescence in situ hybridization

Fluorescence in situ hybridization (FISH) with Vysis probes was used to assess 1p/19q status. TMA sections were deparaffinized with xylene, incubated with 0.3% pepsin in 10 mM HCl at 37°C for 10 minutes, and then denatured at 85°C for 10 minutes. FISH analyses were performed on deparaffinized sections with a dual-color approach for chromosomes 1 and 19, respectively. Target probes were hybridized to subtelomeric 1p36 and 19q13 in combination with control probes on 1q25 and 19p13, respectively. For evaluation, the signal ratio in 50–100 adjacent, non-overlapping interphase nuclei was assessed, and the results were expressed as percentage (Fig. 2).

Statistical analysis

Continuous data were presented as the mean \pm standard deviation, while categorical data were presented as frequencies and percentages. Continuous variables that were not normally distributed (as evaluated by Kolmogorov-Smirnov tests) were presented as medians and 25th and 75th percentiles. Differences in baseline characteristics were estimated using the chi-square test.

Overall survival (OS) was defined as the time from the date of surgery to death from any cause. The discriminative value of the 2007 and 2016 WHO classifications were estimated using Cox

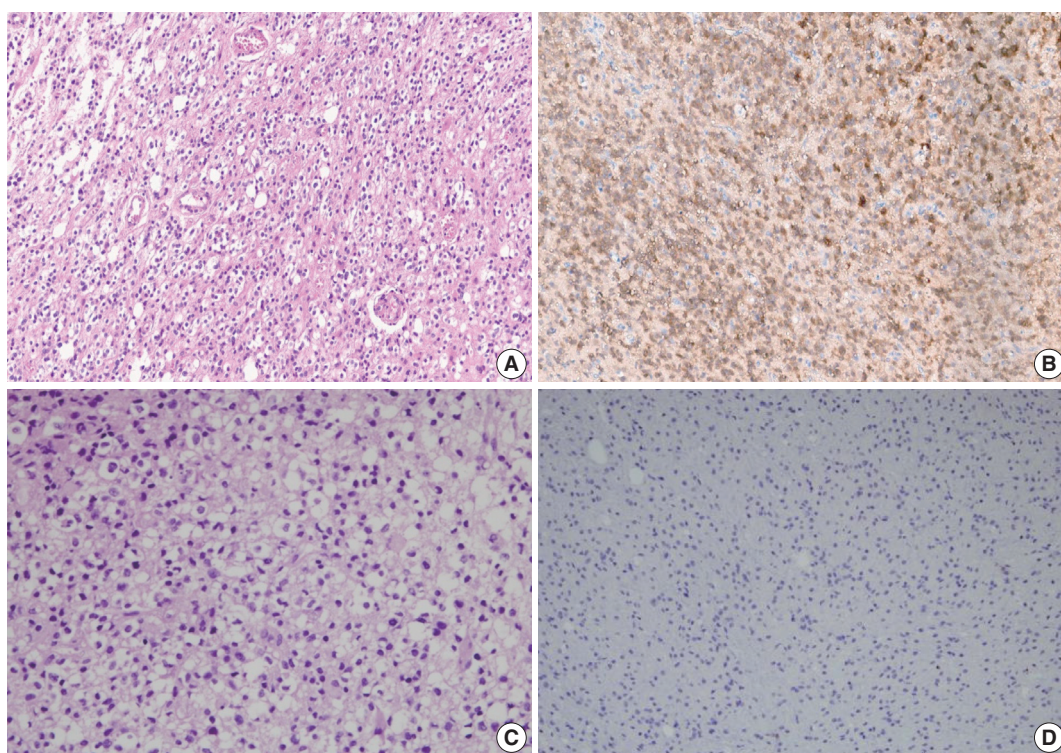


Fig. 1. IDH1 immunohistochemical staining of diffuse brain glioma. (A) Definite fried egg appearance (perinuclear halo) of oligodendrogloma in hematoxylin and eosin (H&E) staining $\times 100$. (B) The tumor cells express IDH1 in the cytoplasm by immunohistochemistry. The unstained cells in the brain parenchyma represent non-neoplastic cells. (C) H&E staining of anaplastic astrocytoma with pleomorphic nucleus $\times 100$. (D) The tumor cells are negative for IDH1 immunostaining.

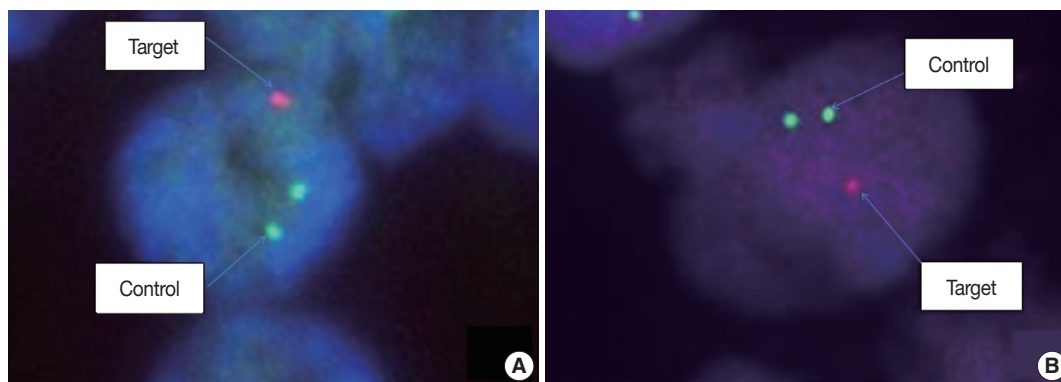


Fig. 2. Fluorescence in situ hybridization (FISH) analysis of 1p/19q co-deletion on formalin-fixed paraffin-embedded specimen: (A) FISH preparation showing 1p deletion in an oligodendrogloma. A tumor cell in 1p deletion status is clearly seen, with a 2:1 ratio of control (green) signals and target (red) signal. (B) FISH preparation showing 19q deletion in the same oligodendrogloma case. One cell is labeled showing one red signal for the 19q test probe and two green signals for the 19q control probe, indicating loss of one copy of 19q.

proportional hazard regression model for all-cause mortality. The Kaplan-Meier method was used to estimate survival distributions.

All statistical tests were two-sided, and a p-value of $< .05$ was considered significant. All statistical analyses were conducted using SPSS ver. 22.0 (IBM Corp., Armonk, NY, USA).

Ethics statement

All procedures performed in the current study were approved by the Institutional Review Board of Seoul National University Bundang Hospital (B-1703/385-302) and Research Ethics Committee of the Mongolian National University of Medical Sciences (MNUMS) (2017/3-201702) in accordance with the 1964 Helsinki declaration and its later amendments. Formal

written informed consent was not required with a waiver by the Institutional Review Board of Seoul National University Bundang Hospital and Research Ethics Committee of the MNUMS.

RESULTS

Patient characteristics

Data of 124 patients diagnosed with diffuse brain glioma between January 2006 and December 2017 were collected (men, 48.4% and women, 51.6%). The median age at diagnosis was 41 years (interquartile range [IQR], 29 to 52), and the median follow-up period was 8 months (IQR, 4 to 15). Grade II, III, and IV tumors developed in 45.2% (n = 56), 26.6% (n = 33), and 28.2% (n = 35) of patients, respectively. Approximately 46.8% (n = 58) of patients underwent complete tumor resection, while 53.2% (n = 66) underwent partial tumor resection. According to the 2007 WHO classification, 23.4% (n = 29) of patients developed diffuse astrocytoma; 21% (n = 26), oligodendroglioma; 0.8% (n = 1), oligoastrocytoma; 13.7% (n = 17), anaplastic astro-

cytoma; 12.9% (n = 16), anaplastic oligodendroglioma; and 28.2% (n = 35), glioblastoma. Patients' baseline characteristics are summarized in Table 1.

Molecular data and tumor reclassification according to the 2016 WHO classification

A total of 124 patients underwent FISH test; however, 32 patients, whose tissue samples were archived before 2012, showed no signal on FISH test. Therefore, 92 patients were analyzed for 1p/19q co-deletion by FISH. About 32 patients, with absence of signal on FISH test, were reclassified based on histological pattern and *IDH1* mutation status only without 1p/19q co-deletion information. Immunohistochemical staining of IDH1 was performed on all 124 patients. 1p/19q co-deletion was detected in 13 of 92 patients (10.5%) who underwent FISH test, and IDH1 mutation was detected in 70 of 124 IDH1 immunostained patients (56.5%).

The molecular studies performed for reclassification have limitations in this study. The updated 2016 WHO classification of CNS tumors recommends full assessment of IDH mutation status (sequence analysis for *IDH1* codon 132 and *IDH2* codon 172) in cases of diffuse gliomas that are immunohistochemically negative for *IDH1* R132H mutation. In the present study, IDH mutation status has been investigated only by immunohistochemistry, and no further molecular analysis for IDH mutation was performed. Therefore, we reclassified IDH1 immunonegative diffuse gliomas as diffuse gliomas, IDH-wildtype, NOS. Among 32 cases which showed technical failure for FISH test, neither immunohistochemical expression of IDH1 nor morphological phenotype of oligodendroglioma was detected. Therefore, there was no case of oligodendroglioma/anaplastic oligodendroglioma, IDH-mutant, NOS.

According to the updated 2016 WHO classification, diffuse astrocytomas (n = 29) were reclassified into 18 diffuse astrocytomas IDH^{mut} (IDH-mutant), nine diffuse astrocytomas IDH^{wt} (IDH-wildtype), NOS, and two oligodendrogliomas IDH^{mut} and 1p/19q co-deleted. Anaplastic astrocytomas (n = 17) were reclassified into eight anaplastic astrocytomas IDH^{mut}, eight anaplastic astrocytomas IDH^{wt}, NOS, and one anaplastic oligodendroglioma IDH^{mut} and 1p/19q co-deleted. Glioblastomas (n = 35) were all reclassified into glioblastoma IDH^{wt}, NOS. Oligodendrogliomas (n = 26) were reclassified into 16 diffuse astrocytomas IDH^{mut}, eight oligodendrogliomas IDH^{mut} and 1p/19q co-deleted, and two diffuse astrocytomas IDH^{wt}, NOS. Anaplastic oligodendrogliomas (n = 16) were reclassified into 14 anaplastic astrocytomas IDH^{mut} and two anaplastic oligodendrogli-

Table 1. Patient characteristics

Variable	No. (%)
Age, median (IQR, yr)	41 (29–52)
Sex	
Male	60 (48.4)
Female	64 (51.6)
WHO tumor grade	
Grade II	56 (45.2)
Grade III	33 (26.6)
Grade IV	35 (28.2)
Type of surgery	
Complete resection	58 (46.8)
Partial resection	66 (53.2)
Immunohistochemical and molecular changes	
p53 expression > 10%	53 (42.7)
PTEN loss	73 (54.9)
EGFR amplification	43 (32.8)
WT1 high expression	39 (29.3)
IDH1 ^{mut}	70 (56.5)
1p/19q co-deletion	13 (10.5)
Histological diagnosis according to the 2007 WHO classification	
Astrocytic tumors	
Diffuse astrocytoma (grade II)	29 (23.4)
Anaplastic astrocytoma (grade III)	17 (13.7)
Glioblastoma (grade IV)	35 (28.2)
Oligodendroglial tumors	
Oligodendroglioma (grade II)	26 (21.0)
Anaplastic oligodendroglioma (grade III)	16 (12.9)
Mixed oligoastrocytoma (grade II)	1 (0.8)

IQR, interquartile range; WHO, World Health Organization; PTEN, phosphatase and tensin homolog; EGFR, endothelial growth factor receptor; WT1, Wilms tumor 1; IDH1^{mut}, isocitrate dehydrogenase 1-mutant.

Table 2. Summary of subgroups of diffuse gliomas according to updated 2016 WHO classification

Histological diagnosis (WHO 2007)	Integrated diagnoses (WHO 2016)	No.
Diffuse astrocytoma (n=29)	Diffuse astrocytoma IDH ^{mut}	18
	Diffuse astrocytoma IDH ^{wt} , NOS	9
	Oligodendroglioma IDH ^{mut} , 1p/19q co-deleted	2
Anaplastic astrocytoma (n=17)	Anaplastic astrocytoma IDH ^{mut}	8
	Anaplastic astrocytoma IDH ^{wt} , NOS	8
	Anaplastic oligodendroglioma IDH ^{mut} , 1p/19q co-deleted	1
Glioblastoma (n=35)	Glioblastoma IDH ^{wt} , NOS	35
Oligodendroglioma (n=26)	Diffuse astrocytoma IDH ^{mut}	16
	Oligodendroglioma IDH ^{mut} , 1p/19q co-deleted	8
	Diffuse astrocytoma IDH ^{wt} , NOS	2
Anaplastic oligodendroglioma (n=16)	Anaplastic astrocytoma IDH ^{mut}	14
	Anaplastic oligodendroglioma IDH ^{mut} , 1p/19q co-deleted	2
Mixed oligoastrocytoma (n=1)	Diffuse astrocytoma IDH ^{mut}	1
Total		124

WHO, World Health Organization; IDH^{mut}, isocitrate dehydrogenase mutant; IDH^{wt}, NOS, isocitrate dehydrogenase wildtype, not otherwise specified.

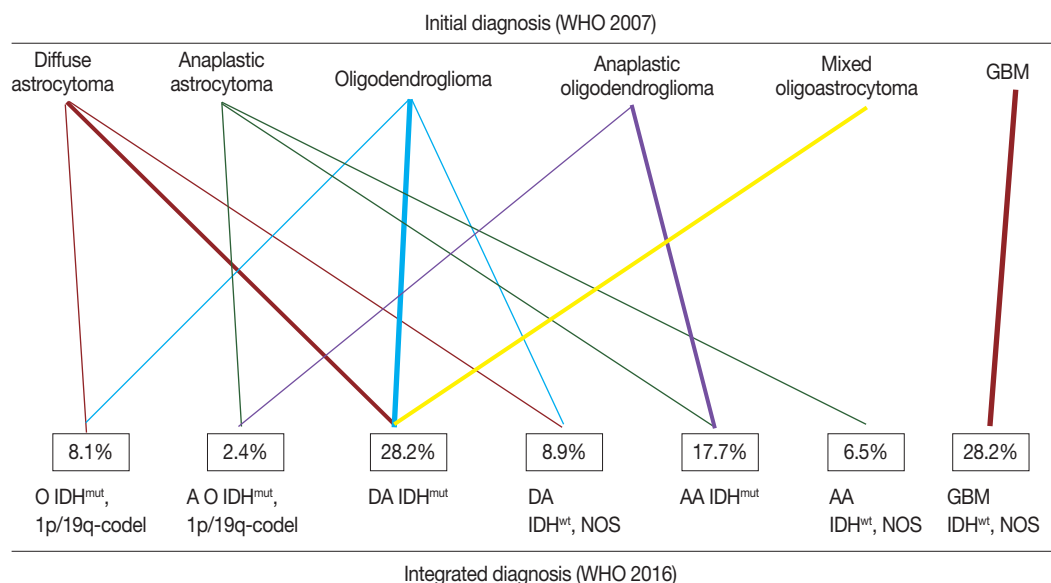


Fig. 3. Change in diagnosis after applying molecular genetics integrated diagnostic criteria according to the updated 2016 WHO classification. WHO, World Health Organization; IDH^{mut}, isocitrate dehydrogenase mutant; IDH^{wt}, NOS, isocitrate dehydrogenase wildtype, not otherwise specified; 1p/19q codel, 1p/19q co-deleted.

omas IDH^{mut} and 1p/19q co-deleted. One case of mixed oligoastrocytoma was reclassified as diffuse astrocytoma IDH^{mut}. The summary of integrated diagnosis is shown in Table 2 and Fig. 3.

In this study, 124 patients were reclassified as diffuse astrocytoma IDH^{mut}, 28.2% (n = 35); diffuse astrocytoma IDH^{wt}, NOS, 8.9% (n = 11); anaplastic astrocytoma IDH^{mut}, 17.7% (n = 22); anaplastic astrocytoma IDH^{wt}, NOS, 6.5% (n = 8); oligodendroglioma IDH^{mut} and 1p/19q co-deleted, 8.1% (n = 10); anaplastic oligodendroglioma IDH^{mut} and 1p/19q co-deleted, 2.4% (n = 3); and glioblastoma IDH^{wt}, NOS, 28.2% (n = 35). None of the patients developed glioblastoma IDH^{mut} (Table 3).

There was a significant change in frequency of both oligodendroglial (34.7% to 10.5%) and astrocytic (37.1% to 60.7%) entities after reclassification according to the new 2016 WHO classification. The frequencies of 1p/19q co-deletion and IDH1 mutation were significantly higher in patients with low-grade tumors (grade II) than in patients with high-grade tumors (grades III and IV) (17.9% vs 4.4%, p < .05 for 1p/19q co-deletion and 80.4% vs 36.8%, p < .001 for IDH1 mutation). Notably, neither 1p/19q co-deletion nor IDH1 mutation was observed in patients with grade IV glioblastoma (Table 3).

Table 3. Comparison between 2007 and 2016 WHO classification of diffuse gliomas

Original histological diagnosis according to WHO 2007	WHO grade	No. (%)
Astrocytic tumors		
Diffuse astrocytoma	II	29 (23.4)
Anaplastic astrocytoma	III	17 (13.7)
Glioblastoma	IV	35 (28.2)
Oligodendroglial tumors		
Oligodendroglioma	II	26 (21.0)
Anaplastic oligodendroglioma	III	16 (12.9)
Mixed oligoastrocytoma	II	1 (0.8)
Integrated diagnosis according to updated WHO 2016		
Diffuse astrocytoma IDH ^{mut}	II	35 (28.2)
Diffuse astrocytoma IDH ^{wt} , NOS	II	11 (8.9)
Anaplastic astrocytoma IDH ^{mut}	III	22 (17.7)
Anaplastic astrocytoma IDH ^{wt} , NOS	III	8 (6.5)
Oligodendroglioma IDH ^{mut} , 1p/19q co-deleted	II	10 (8.1)
Anaplastic oligodendroglioma IDH ^{mut} , 1p/19q co-deleted	III	3 (2.4)
Glioblastoma IDH ^{wt} , NOS	IV	35 (28.2)

WHO, World Health Organization; IDH^{mut}, isocitrate dehydrogenase mutant; IDH^{wt}, NOS, isocitrate dehydrogenase wildtype, not otherwise specified.

Prognostic value of 2016 WHO classifications

During follow-up, all-cause mortality occurred in 61.3% (n = 76) of patients, and 38.7% (n = 48) of patients survived. Median OS was 13 months (95% confidence interval, 10.2 to 15.7). The discriminative value of the 2007 and 2016 WHO classifications was tested using Cox proportional hazard regression model for all-cause mortality and summarized in Table 4. Oligodendroglioma and oligodendroglioma IDH^{mut} and 1p/19q co-deleted were selected as the reference diagnoses for 2007 and 2016 WHO classifications, respectively. The prognostic significance of the 2007 WHO classifications was compared with that of the new 2016 WHO classifications using Kaplan-Meier estimation. Both the 2007 and 2016 WHO classifications had significantly discriminative information for all-cause mortality (p < .001) (Fig. 4A, B). However, the new 2016 WHO classification had higher hazard ratio than the 2007 WHO classification (Table 4).

The new 2016 WHO classification showed a statistically significant survival advantage for grade II tumors compared with the 2007 WHO classification (Fig. 4C, D). Based on the 2007 WHO classification, no survival difference was found between patients with grade II tumors including those with oligodendroglioma, diffuse astrocytoma, and oligoastrocytoma (p = .437). However, the new 2016 WHO classification showed that oligodendroglioma IDH^{mut} and 1p/19q co-deleted and diffuse astrocytoma IDH^{mut} had better survival compared with diffuse astrocytoma IDH^{wt}, NOS in grade II tumors (p < .01). Both

Table 4. Discriminative value of 2007 and 2016 WHO classification based on Cox proportional hazard regression for all-cause mortality

	HR	95% CI	p-value
2007 WHO classification			
Oligodendroglioma	RF		
Diffuse astrocytoma	0.60	0.27–1.37	.227
Mixed oligoastrocytoma	1.30	0.17–9.96	.802
Anaplastic astrocytoma	2.16	1.01–4.65	.048
Anaplastic oligodendroglioma	2.42	1.12–5.22	.025
Glioblastoma	2.67	1.36–5.24	.004
2016 WHO classification			
Oligodendroglioma IDH ^{mut} , 1p/19q co-deleted	RF		
Diffuse astrocytoma IDH ^{mut}	1.07	0.31–3.72	.913
Anaplastic oligodendroglioma IDH ^{mut} , 1p/19q co-deleted	2.94	0.49–17.6	.239
Anaplastic astrocytoma IDH ^{wt} , NOS	3.70	0.87–15.6	.075
Diffuse astrocytoma IDH ^{wt} , NOS	4.13	1.02–16.8	.047
Anaplastic astrocytoma IDH ^{mut}	3.95	1.16–13.4	.028
Glioblastoma IDH ^{wt} , NOS	4.50	1.34–15.0	.015

WHO, World Health Organization; HR, hazard ratio; CI, confidence interval; IDH^{mut}, isocitrate dehydrogenase mutant; IDH^{wt}, NOS, isocitrate dehydrogenase wildtype, not otherwise specified.

2007 and 2016 WHO classifications did not show any survival difference in patients with grade III and grade IV tumors (p = .777 and p = .936, respectively) (Fig. 4E, F).

DISCUSSION

Our study results were summarized as follows: (1) the new 2016 WHO classification led to substantial changes in the diagnosis of diffuse gliomas, and (2) the new integrated histomolecular classification, based on molecular data, provided more valuable prognostic information.

Studies over the last two decades clearly demonstrated that the genetic basis of oncogenesis is important for the development of brain tumor entities and clarified their role in patients' prognosis. Boulay et al.¹⁴ and Hata et al.¹⁵ reported chromosomal changes in human gliomas. Notably, Mizoguchi et al.¹⁶ investigated the role of 1p/19q co-deletion in patients with glioblastoma and its prognostic relation. Furthermore, several studies revealed the frequency of IDH mutation and its prognostic value in human gliomas.^{17–20} Based on these results, new integrated WHO CNS tumor classification was introduced to clinical practice in 2016⁷; conceptual and practical advances were made over previous version.³ First, 2016 WHO classification is based on not only histological features but also genetic alterations of gliomas, such as 1p/19q co-deletion and IDH mutation, for diffuse brain glioma classification. Second, molecular pathologic tests are essen-

tial for the diagnosis of diffuse gliomas. The 2016 WHO classification of CNS tumors requires at least IDH1 immunohistochemistry and 1p/19q co-deletion status for the diagnosis of diffuse gliomas in addition to histologic evaluation. With regard

to IDH mutation, mutation analyses of both IDH-1 and IDH-2 are recommended more than immunohistochemistry for detection of *IDH1* hotspot mutation (p.R132H).

Mellai et al.²¹ reported that *IDH1* mutations consisted 98.5%

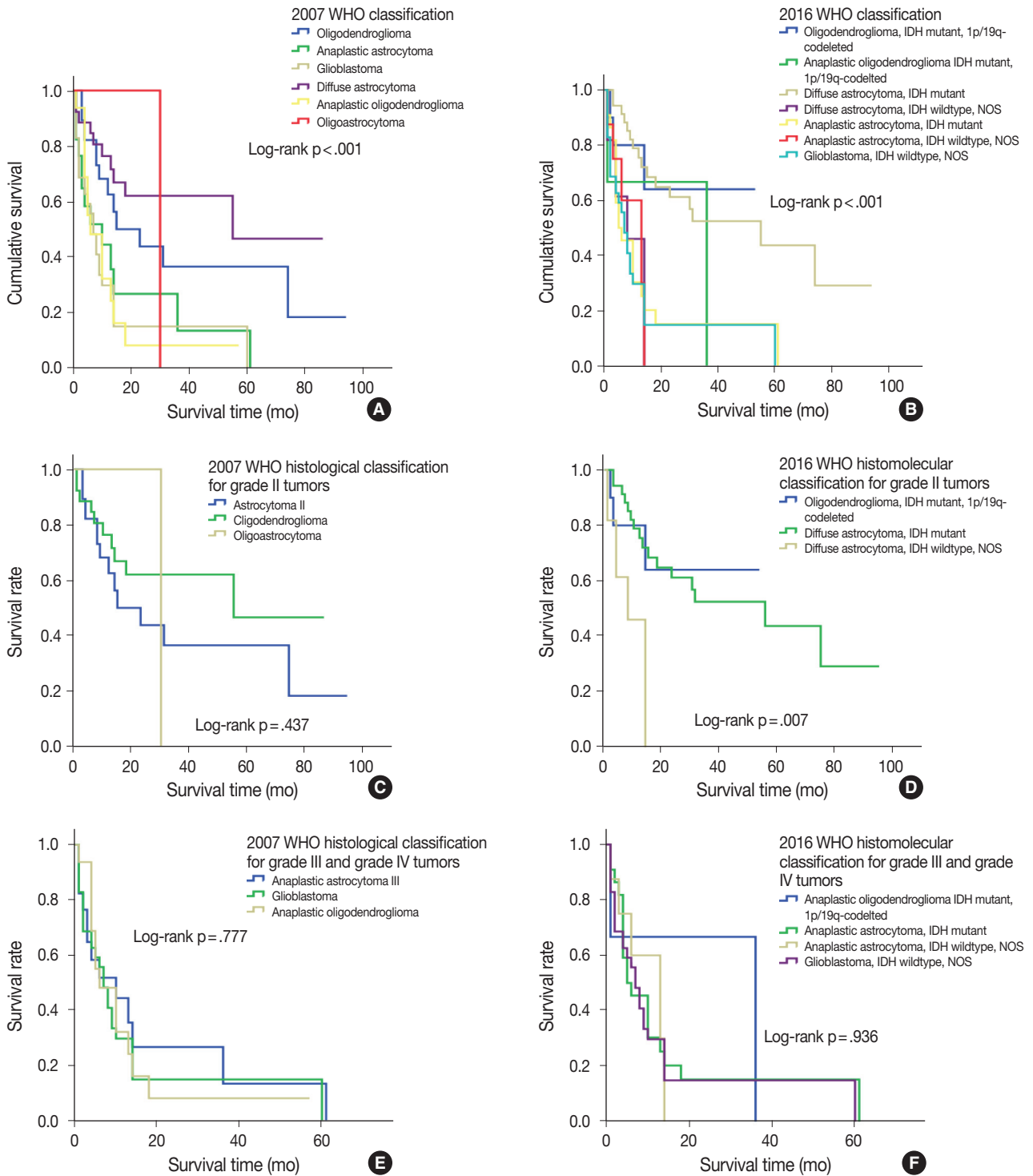


Fig. 4. Kaplan-Meier curves for overall survival according to the 2007 WHO classification (A, C, E) and 2016 WHO classification (B, D, F), respectively. (A, B) For all tumors. (C, D) For grade II tumors. (E, F) For grades III and IV tumors. WHO, World Health Organization.

of all IDH mutations in gliomas. Among *IDH1* mutations, 93.7% were c.395G > A (p.R132H) which can be detected by mIDH1^{R132H} antibody immunostaining. There was a statistically significant correlation between mIDH1^{R132H} antibody immunostaining and the relevant mutation c.395G > A (p.R132H) ($p = .0001$).²¹ Different types of *IDH1* gene mutations at codon R132 have been identified, of which c.395G > A (p.R132H) mutation accounts for about 93%, c.394C > T (p.R132C) for 4%, c.394C > A (p.R132S) for 1.5% in the different types of gliomas.^{17,22}

The 2016 WHO classification of CNS tumors is a global standard, and it has better prognostic significance than traditional histological classification. To perform the molecular diagnosis of gliomas according to the 2016 WHO classification of CNS tumors, full assessment of IDH mutation status and 1p/19q analyses are mandatory. Operating a well-equipped molecular laboratory is a challenging situation in the developing countries including Mongolia. Expansion of facilities for molecular pathology is required to avoid the diagnosis of diffuse glioma, NOS. Nowadays pathology laboratories in developing countries struggle to provide specialized molecular tests, and it requires increase of medical costs.

In this study, we could reclassify Mongolian diffuse gliomas according to the new 2016 WHO classification. Reclassification revealed substantial changes in diagnosis of both oligodendroglial and astrocytic entities. For example, histologically astrocytic entities, which had both IDH mutation and 1p/19q co-deletion, were reclassified into oligodendroglial entities (3 of 46 patients), and oligodendroglial entities, without 1p/19q co-deletion, were reclassified into astrocytic entities (30 of 42 patients). Furthermore, molecular subgroups, such as IDH^{mut} and IDH^{wc}, NOS, were added to the diagnosis of diffuse glioma based on the results of immunohistochemical staining of IDH1. Similar results were observed in the French POLA cohort study by Tabouret et al.⁵

The previous studies suggest that 1p/19q co-deletion or IDH mutation is a relatively early event during the development of glioma.^{23,24} As a result, the frequency of 1p/19q co-deletion or IDH mutation could be higher in low-grade gliomas. In our study, the frequency of 1p/19q co-deletion and *IDH1* mutation were significantly higher in patients with low-grade gliomas than in those with high-grade gliomas (17.9% vs 4.4%, $p < .05$ and 80.4% vs 36.8% $p < .001$, respectively).

Reclassification of diffuse gliomas not only categorizes molecular subgroups of diffuse gliomas but it also has important prognostic value. Yan et al.²⁵ revealed that tumors with IDH mutation are distinctive genetically and clinically, and had better

outcomes than those with wildtype IDH gene. Akagi et al.¹⁰ and Tabouret et al.⁵ demonstrated that the new 2016 WHO classification has better prognostic value in terms of OS. In particular, IDH^{mut} is a strong prognostic marker and is associated with better survival compared with IDH^{wc}.^{5,10} However, the prognostic advantage of IDH1^{mut} was only evident for low-grade gliomas in this study.

In our study, the 2016 WHO classification showed higher hazard ratio for OS than the 2007 WHO classification and reinforced the prognostic value of integrated histomolecular classification. The 2007 WHO classification did not show survival difference in grade II tumors, whereas 2016 WHO classification showed that oligodendroglioma, IDH^{mut} and 1p/19q co-deleted and diffuse astrocytoma IDH^{mut} had better survival compared with diffuse astrocytoma IDH^{wc}, NOS in grade II tumors.

Finally, our study has several limitations. First, the total study population was relatively small compared with those in other similar studies. Therefore, further studies with a large sample size are required to confirm these findings. Second, there were some technical difficulties associated with FISH testing. In our study, 32 patients who were diagnosed before 2012 had no signal on FISH test. It could be caused by laboratory suboptimal conditions such as poor fixation of tissue and storage duration of tissue blocks. Therefore, we reclassified those cases based on histological pattern and *IDH1* mutation status only without 1p/19q co-deletion information. Third, IDH mutation status has been investigated only by immunohistochemistry, and no further molecular analysis for IDH mutation was performed in cases of diffuse gliomas that are immunohistochemically negative for *IDH1* R132H mutation. Therefore, we could not avoid the diagnosis of diffuse gliomas, IDH-wildtype, NOS.

This is the first study to report the reclassification of Mongolian diffuse gliomas according to the revised 2016 WHO CNS tumor classification. There has been no study regarding pathological classification of brain gliomas according to the 2007 WHO classification as well as survival analysis of gliomas in Mongolia. In spite of several technical limitations, our results were still similar to those of previous publications. Additionally, we have confirmed that the revised 2016 WHO CNS tumor classification is also feasible for Mongolian diffuse gliomas and that it has prognostic significance in Mongolian patients with diffuse gliomas.

ORCID

Enkhee Ochirjav: <https://orcid.org/0000-0003-4525-2378>

Bayarmaa Enkhbat: <https://orcid.org/0000-0003-3163-4316>

Tuul Baldandorj: <https://orcid.org/0000-0001-5932-1114>
Gheeyoung Choe: <https://orcid.org/0000-0001-6547-5603>

Author Contributions

Conceptualization: EO, GC.
Data curation: EO.
Formal analysis: EO.
Investigation: EO.
Methodology: EO, GC.
Project administration: BE.
Resources: EO, TB, BE.
Supervision: GC.
Validation: EO, TB.
Visualization: EO.
Writing—original draft: EO, TB.
Writing—review & editing: BE, GC.

Conflicts of Interest

The authors declare that they have no potential conflicts of interest.

Acknowledgments

This study was conducted in the National Center for Pathology; Department of Pathology, MNUMS; Department of Neurosurgery, State Third Central Hospital; and Department of Pathology, Seoul National University Bundang Hospital. We gratefully acknowledge their support.

REFERENCES

1. Cancer Genome Atlas Research Network, Brat DJ, Verhaak RG, et al. Comprehensive, integrative genomic analysis of diffuse lower-grade gliomas. *N Engl J Med* 2015; 372: 2481-98.
2. Reuss DE, Kratz A, Sahm F, et al. Adult IDH wild type astrocytomas biologically and clinically resolve into other tumor entities. *Acta Neuropathol* 2015; 130: 407-17.
3. Louis DN, Ohgaki H, Wiestler OD, et al. The 2007 WHO classification of tumours of the central nervous system. *Acta Neuropathol* 2007; 114: 97-109.
4. Hirose Y, Sasaki H, Abe M, et al. Subgrouping of gliomas on the basis of genetic profiles. *Brain Tumor Pathol* 2013; 30: 203-8.
5. Tabouret E, Nguyen AT, Dehais C, et al. Prognostic impact of the 2016 WHO classification of diffuse gliomas in the French POLA cohort. *Acta Neuropathol* 2016; 132: 625-34.
6. Hainfellner J, Louis DN, Perry A, Wesseling P. Letter in response to David N. Louis et al, International Society of Neuropathology-Haarlem Consensus Guidelines for Nervous System Tumor Classification and Grading, *Brain Pathology*, doi: 10.1111/bpa.12171. *Brain Pathol* 2014; 24: 671-2.
7. Louis DN, Perry A, Reifenberger G, et al. The 2016 World Health Organization classification of tumors of the central nervous system: a summary. *Acta Neuropathol* 2016; 131: 803-20.
8. Gupta A, Dwivedi T. A simplified overview of World Health Organization classification update of central nervous system tumors 2016. *J Neurosci Rural Pract* 2017; 8: 629-41.
9. Wesseling P, Capper D. WHO 2016 classification of gliomas. *Neuropathol Appl Neurobiol* 2018; 44: 139-50.
10. Akagi Y, Yoshimoto K, Hata N, et al. Reclassification of 400 consecutive glioma cases based on the revised 2016WHO classification. *Brain Tumor Pathol* 2018; 35: 81-9.
11. Iuchi T, Sugiyama T, Ohira M, et al. Clinical significance of the 2016 WHO classification in Japanese patients with gliomas. *Brain Tumor Pathol* 2018; 35: 71-80.
12. Pisapia DJ. The updated World Health Organization glioma classification: cellular and molecular origins of adult infiltrating gliomas. *Arch Pathol Lab Med* 2017; 141: 1633-45.
13. Louis DN, Ellison DW, Brat DJ, et al. cIMPACT-NOW: a practical summary of diagnostic points from Round 1 updates. *Brain Pathol* 2019; 29: 469-72.
14. Boulay JL, Stiefel U, Taylor E, Dolder B, Merlo A, Hirth F. Loss of heterozygosity of TRIM3 in malignant gliomas. *BMC Cancer* 2009; 9: 71.
15. Hata N, Yoshimoto K, Yokoyama N, et al. Allelic losses of chromosome 10 in glioma tissues detected by quantitative single-strand conformation polymorphism analysis. *Clin Chem* 2006; 52: 370-8.
16. Mizoguchi M, Yoshimoto K, Ma X, et al. Molecular characteristics of glioblastoma with 1p/19q co-deletion. *Brain Tumor Pathol* 2012; 29: 148-53.
17. Bals J, Meyer J, Mueller W, Korshunov A, Hartmann C, von Deimling A. Analysis of the *IDH1* codon 132 mutation in brain tumors. *Acta Neuropathol* 2008; 116: 597-602.
18. Hartmann C, Meyer J, Bals J, et al. Type and frequency of *IDH1* and *IDH2* mutations are related to astrocytic and oligodendroglial differentiation and age: a study of 1,010 diffuse gliomas. *Acta Neuropathol* 2009; 118: 469-74.
19. Ichimura K, Pearson DM, Kocalkowski S, et al. *IDH1* mutations are present in the majority of common adult gliomas but rare in primary glioblastomas. *Neuro Oncol* 2009; 11: 341-7.
20. Sanson M, Marie Y, Paris S, et al. Isocitrate dehydrogenase 1 codon 132 mutation is an important prognostic biomarker in gliomas. *J Clin Oncol* 2009; 27: 4150-4.
21. Mellai M, Piazzini A, Caldera V, et al. *IDH1* and *IDH2* mutations, im-

- munohistochemistry and associations in a series of brain tumors. *J Neurooncol* 2011; 105: 345-57.
22. von Deimling A, Korshunov A, Hartmann C. The next generation of glioma biomarkers: MGMT methylation, *BRAF* fusions and *IDH1* mutations. *Brain Pathol* 2011; 21: 74-87.
 23. Bigner SH, Matthews MR, Rasheed BK, et al. Molecular genetic aspects of oligodendrogliomas including analysis by comparative genomic hybridization. *Am J Pathol* 1999; 155: 375-86.
 24. Cohen AL, Holmen SL, Colman H. *IDH1* and *IDH2* mutations in gliomas. *Curr Neurol Neurosci Rep* 2013; 13: 345.
 25. Yan H, Parsons DW, Jin G, et al. *IDH1* and *IDH2* mutations in gliomas. *N Engl J Med* 2009; 360: 765-73.

Primary Rhabdomyosarcoma of the Breast: Study of Three Cases at One Institution with a Review of Primary Breast Sarcomas

Junyoung Shin, Hee Jeong Kim¹, Dae-Yeon Kim², Gyungyub Gong, Kyung-Ja Cho

Departments of Pathology, ¹Surgery, and ²Pediatric Surgery, Asan Medical Center, University of Ulsan College of Medicine, Seoul, Korea

Background: Primary breast sarcoma (PBS) is rare, comprising approximately 1% of breast malignancies. Rhabdomyosarcoma (RMS) accounts for an extremely small proportion of PBSs, often leading to delayed histologic confirmation. **Methods:** Upon reviewing Asan Medical Center's pathology database between 2000 and 2018, 41 PBS cases were retrieved, including three cases of primary RMS of the breast. Their clinicopathological features were analyzed, and the literature related to PBS and primary RMS of the breast was reviewed. **Results:** We identified three primary breast RMS cases from our institution database, comprising 7.3% of PBS: one case each of spindle cell/sclerosing RMS (ssRMS), alveolar RMS (aRMS), and embryonal RMS (eRMS). All cases involved adolescents or young adults (14, 16, and 25 years, respectively) who underwent mastectomy or radiotherapy and were confirmed using immunohistochemical testing for myogenin, desmin, and myogenic differentiation. The ssRMS patient experienced recurrence at the operation site 4 months post-surgery despite undergoing concurrent chemoradiotherapy. The aRMS patient had multiple metastases at diagnosis and showed *FAX3-FOXO1* fusion transcripts; she died 22 months after the diagnosis. The eRMS patient had enlarged axillary lymph nodes; post-radiotherapy, the lesion recurred as multiple metastases to the bone and lung. She died 18 months post-diagnosis. **Conclusions:** Our experience on RMS cases suggests that spindle cell or small round cell malignancy in breasts of young female should raise suspicion for the possibility of primary or secondary RMS. To our knowledge, this is the second report of primary breast ssRMS and it may help clinicians who encounter this rare disease in the future.

Key Words: Spindle cell rhabdomyosarcoma; Sclerosing rhabdomyosarcoma; Primary sarcoma of the breast

Received: March 11, 2019 **Revised:** July 11, 2019 **Accepted:** July 22, 2019

Corresponding Author: Kyung-Ja Cho, MD, PhD, Department of Pathology, Asan Medical Center, University of Ulsan College of Medicine, 88 Olympic-ro 43-gil, Songpa-gu, Seoul 05505, Korea

Tel: +82-2-3010-4545, Fax: +82-2-472-7898, E-mail: kjc@amc.seoul.kr

Primary breast sarcoma (PBS) is a rare heterogeneous group of tumors, which comprises approximately 1% of breast malignancies.¹ Distribution of histologic subtypes varies among studies; however, angiosarcoma is the most prevalent while liposarcoma, fibrosarcoma, and malignant fibrous histiocytoma have also been reported.²⁻⁴

Rhabdomyosarcoma (RMS) is one of the most common sarcomas in young patients; however, RMS of the breast origin is very rare, with only 26 cases reported in international journals.⁵⁻⁷ Among the reported cases, alveolar subtype was most common, followed by embryonal, spindle cell/sclerosing, and pleomorphic subtypes. Spindle cell/sclerosing RMS (ssRMS) is a new subtype of RMS included in the World Health Organization Classification of Tumors of Soft Tissue and Bone in 2013,⁸ and only one primary breast ssRMS has been reported in an international

journal.⁹

We recently encountered a case of ssRMS of the breast that could have been misdiagnosed as some other spindle cell sarcoma. To better understand the clinicopathological characteristics of these rare conditions, we searched and reviewed data from Asan Medical Center databases and reviewed the literature related to this disease.

MATERIALS AND METHODS

Case selection

Upon reviewing Asan Medical Center pathology database between January 1, 2000 and November 30, 2018, 41 PBS cases including three cases of primary RMS of the breast were retrieved. Cases of metastatic sarcoma and radiation-induced

sarcoma were excluded. The clinicopathological features of primary RMS were analyzed, and literature related to PBS and primary RMS of the breast was reviewed.

Immunohistochemical study

For immunohistochemical (IHC) staining, 4- μ m thick tissue sections were deparaffinized and hydrated by immersion in xylene and a graded ethanol series. Endogenous peroxidase was blocked by incubation in 3% H₂O₂ for 10 minutes, and then heat-induced antigen retrieval was performed. Primary antibody staining was performed using a Benchmark autostainer (Ventana Medical Systems, Tucson, AZ, USA) following the manufacturer's protocol. Sections were incubated at room temperature for 24 or 32 minutes in primary antibodies for desmin (1:200, D33, Dako, Glostrup, Denmark), myogenic differentiation 1 (1:50, MyoD1, EP212, Cell Marque, Rocklin, CA, USA), myogenin (1:200, Neomarkers, Fremont, CA, USA), smooth muscle actin (SMA; 1:4,000, 1A4, Dako), nestin (1:1,000, 10C2, Cell Marque), CD34 (1:500, QBEND10, Immunotech, Marseille, France), CD56 (1:100, 504, Leica, Chicago, IL, USA), pancytokeratin AE1/AE3 (CK AE1/AE3, 1:400, Leica), and pancytokeratin MNF-116 (1:100, MNF 116, Dako), and then labeled with an iView detection kit using the automated immunostaining system (Benchmark XT, Ventana Medical Systems). Immunostained sections were lightly counterstained with hematoxylin, dehydrated in ethanol, and cleared in xylene.

Nested real time polymerase chain reaction (nested reverse transcription polymerase chain reaction)

An alveolar RMS (aRMS) case was examined for nested reverse transcription polymerase chain reaction (RT-PCR) of *FAX3/TKHR (FOXO1)* fusion and *FAX7/TKFR (FOXO1)* fusion gene transcript. After the histologic and IHC examinations, formalin-fixed paraffin-embedded block were used for the test. DNA was extracted using the RecoverAll Total Nucleic Acid Isolation Kit (Life Technologies, Carlsbad, CA, USA) according to the manufacturer's instructions. The DNA quality was assessed by amplification of the housekeeping gene β -globulin.

The nested RT-PCR was carried out with ABI 7500 RT-PCR system (Applied Biosystems, Foster City, CA, USA) using 2 μ L of genomic DNA as the template, 1 μ L of each primer, 1 μ L of each probe, 2 μ L of dNTP, 2.5 μ L of buffer, 0.1 μ L of Taq polymerase, and 16.4 μ L of distilled water, in a total volume of 25 μ L. The synthesized primer PAX3/PAX7 (5'-CCGACAGCAGCTC-TACCTAC-3'), PAX3 (5'-CTACTGCCTCCCCAGCAGC-3'), PAX7 (5'-CACAGCTTCTCCAGCTACTCTG-3' and 5'-CA-

CAGCTTCTCCAGCT-3'), and FKHR (5'-GCACACGAAT-GAACTTGCTG-3' and reverse transcript 3'-CCAAGAACTTTTCCAGTTCC-5') was used. The thermal cycling conditions of the first cycle of nested RT-PCR were 5 minutes at 94°C, followed by 35 cycles of 40 seconds at 94°C, 40 seconds at 55°C and 1 minute at 72°C. After 1 cycle of 10 minutes at 72°C, second RT-PCR was performed with the same thermal cycling condition. A positive result for PAX3/PAX7-TKHR (FOXO1) was defined as a threshold cycle (CT) value < 40, and the internal control was defined as a CT value < 36.

Ethics statement

The study plan was reviewed by the institutional review board of Asan Medical Center and it was exempted from delib-eration (exemption number: 2018-0883); informed consent was obtained from the only living patient.

RESULTS

Case descriptions

Patient A

Patient A was a 14-year-old Korean girl who had a painful 10-cm mass in her left breast. Magnetic resonance imaging (MRI) revealed a huge, heterogeneously enhancing mass measuring 12×9.5×8.3 cm that involved her whole left breast. No other abnormalities were identified on MRI and computed tomography (Fig. 1A).

A skin-sparing mastectomy was performed. The surgical specimen included fragmented tumor tissue measuring 16.7×10.2×3.5 cm in an aggregate, weighing 711 g. The cut surface of the mass showed creamy white-colored trabecular features with firm texture (Fig. 1B). Microscopic examination revealed a mesenchymal tumor composed of spindle cells, with a fascicular growth pattern and varying amount of myxoid matrix (Fig. 1C). The nuclei were elongated and highly pleomorphic; the cytoplasm was pale to eosinophilic (Fig. 1D). The mitotic rate was extremely high (up to 94/10 high-power fields). No epithelial component was identified in the tumor. On IHC staining, the tumor cells tested positive for desmin, MyoD1, myogenin, and nestin but not for CK AE1/AE3, MNF-116, SMA, CD34, and S100 (Fig. 1E–H). ssRMS of the breast was diagnosed based on histological and IHC findings. Resection margin could not be assessed because of the disruption caused during mastectomy. She was postoperatively treated with combination chemotherapy (vincristine, actinomycin, and cyclophosphamide).

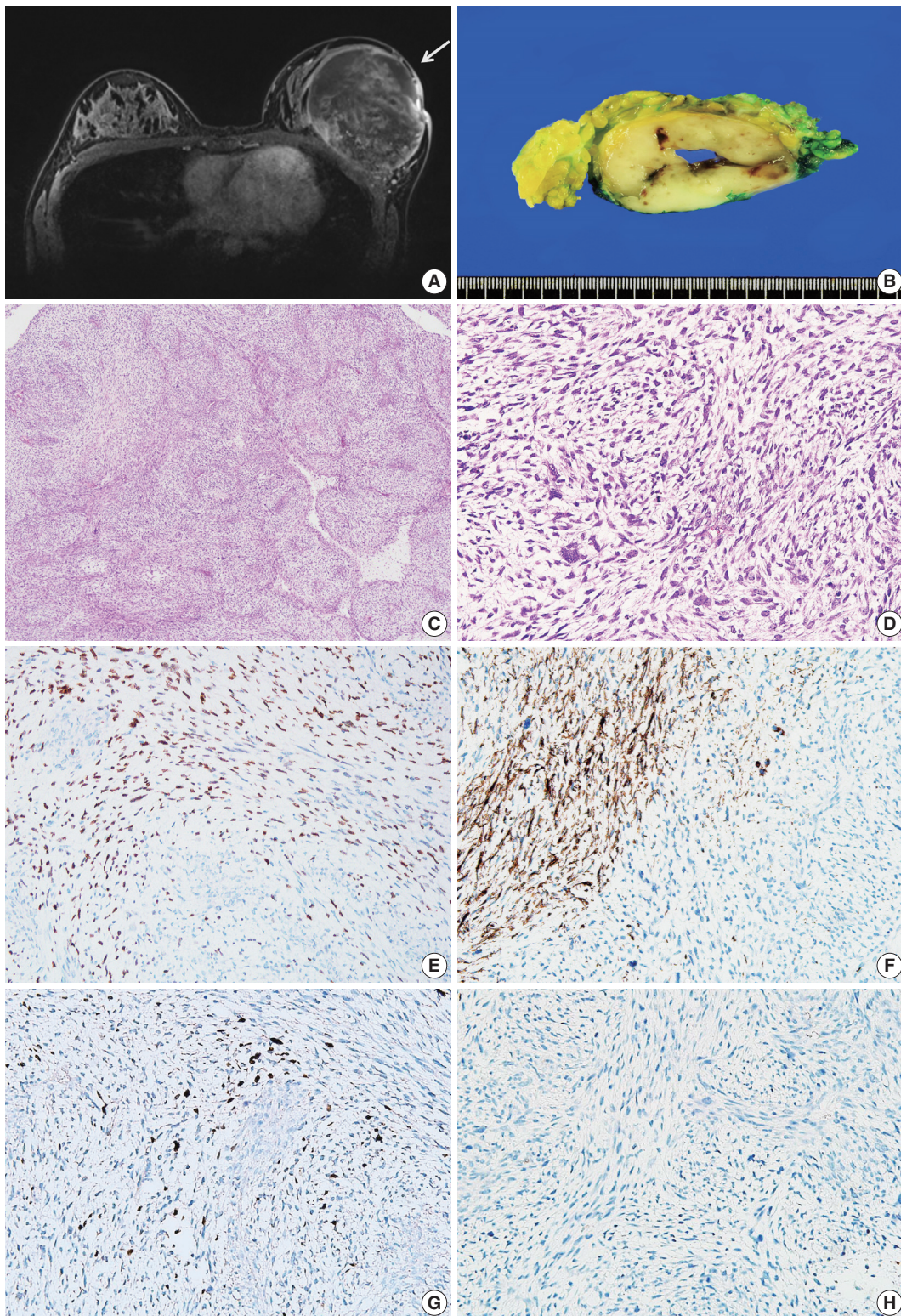


Fig. 1. Primary breast sarcoma of patient A. (A) A 12×9.5×8.3-cm-sized heterogeneously enhancing mass in the left breast (yellow arrow). (B) Grayish-yellow cut surface of the mass with multifocal hemorrhagic spots and central cavity formation. (C, D) Spindle cells exhibiting a fascicular or storiform growth pattern with a small amount of myxoid matrix. The image showing highly pleomorphic elongated nuclei and pale to eosinophilic cytoplasm, with high mitotic rates (up to 94/10 high power fields). (E–H) Immunohistochemical staining showing positivity of tumor cells for MyoD1 (E), desmin (F), and myogenin (G) and negativity for MNF-116 (H).

Four-month post-mastectomy, a mass was identified at the operation site and diagnosed as a recurrent ssRMS. The patient continued chemotherapy (cyclophosphamide, doxorubicin, and ifosfamide) and radiation therapy.

Patient B

Patient B was a 16-year-old Korean girl who had a 10-cm mass in her left breast. Imaging examination at an outside hospital revealed a breast mass and multiple metastatic lesions in the lumbar spine and left axillary lymph nodes. She underwent core needle biopsy of the breast mass; the tumor was diagnosed as aRMS.

After receiving the first neoadjuvant chemotherapy cycle, she was referred to our center and continued to receive the treatment for 8 cycles. However, MRI showed no change in the status of the left breast and metastatic masses.

The patient underwent palliative mastectomy. The surgical specimen consisted of a lump of breast tissue that measured $9.5 \times 8.5 \times 4$ cm and weighed 114 g. A well-demarcated lobulating soft mass measuring $4 \times 2.5 \times 2$ cm was identified in the breast

parenchyma; the resection margins were clear. The mass was composed of nests and sheets of primitive round cells separated by fibrous septa. These nests exhibited a central loss of cellular cohesion (Fig. 2A). IHC staining of the tumor cells yielded positive results for desmin (Fig. 2B), CD56, and myogenin (Fig. 2C) and negative results for CK AE/AE3 and SMA.

PAX3-FKHR (FOXO1) fusion transcripts [t(2;13)(q35;q14)] were identified using nested RT-PCR, supporting the diagnosis of aRMS (Fig. 2D). Post-surgery, she received eight chemotherapy cycles (carboplatin, VP-16, and ifosfamide), which was interrupted by fungal infection and low platelet counts. Follow-up imaging examination revealed recurrence of the chest wall mass and exacerbation of the multifocal bone metastasis with bone marrow involvement. The patient died due to respiratory suppression 22-month post-diagnosis.

Patient C

Patient C was a previously healthy 25-year-old Korean woman who had palpable masses on her left breast. Ultrasonography and MRI revealed multiple infiltrative masses in her left breast

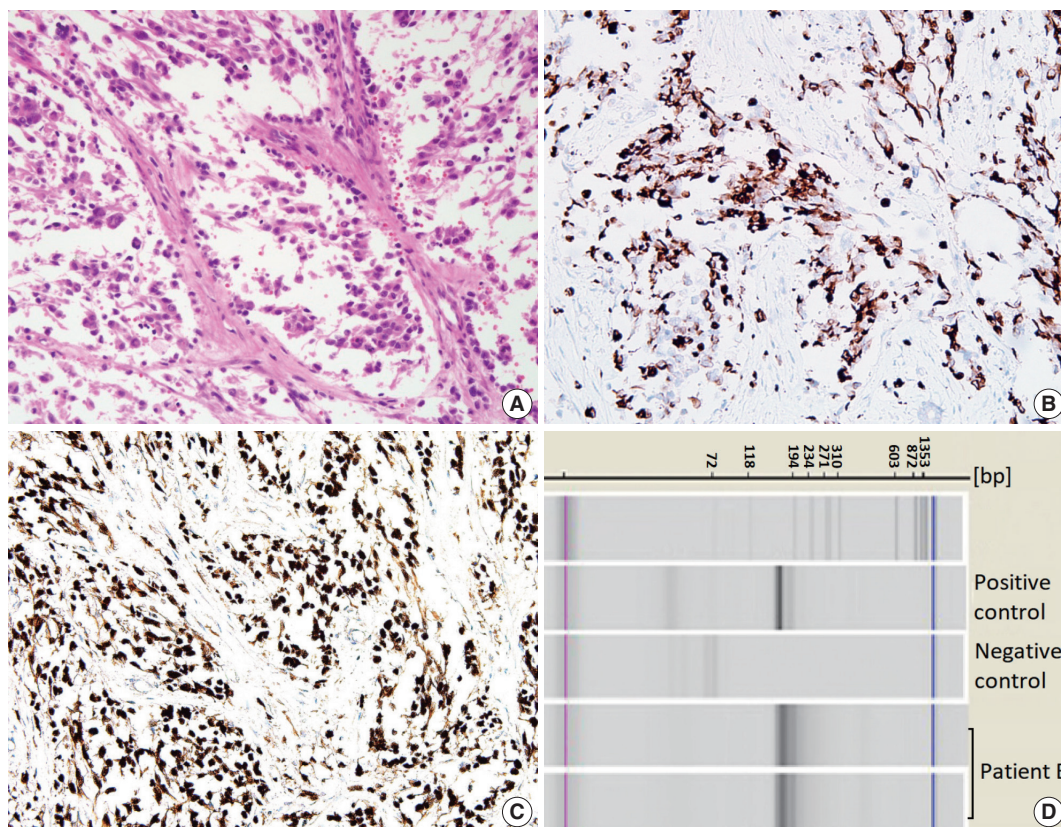


Fig. 2. Primary breast sarcoma of patient B. (A) Primitive round-to-polygonal cells comprising the nests separated by fibrous septa and showing a loss of cellular cohesion. (B, C) Immunohistochemical staining for desmin (B) and myogenin (C). (D) *PAX3-FKHR (FOXO1)* fusion identified by *PAX3/PAX-7-FKHR (FOXO1)* nested reverse transcription polymerase chain reaction analysis.

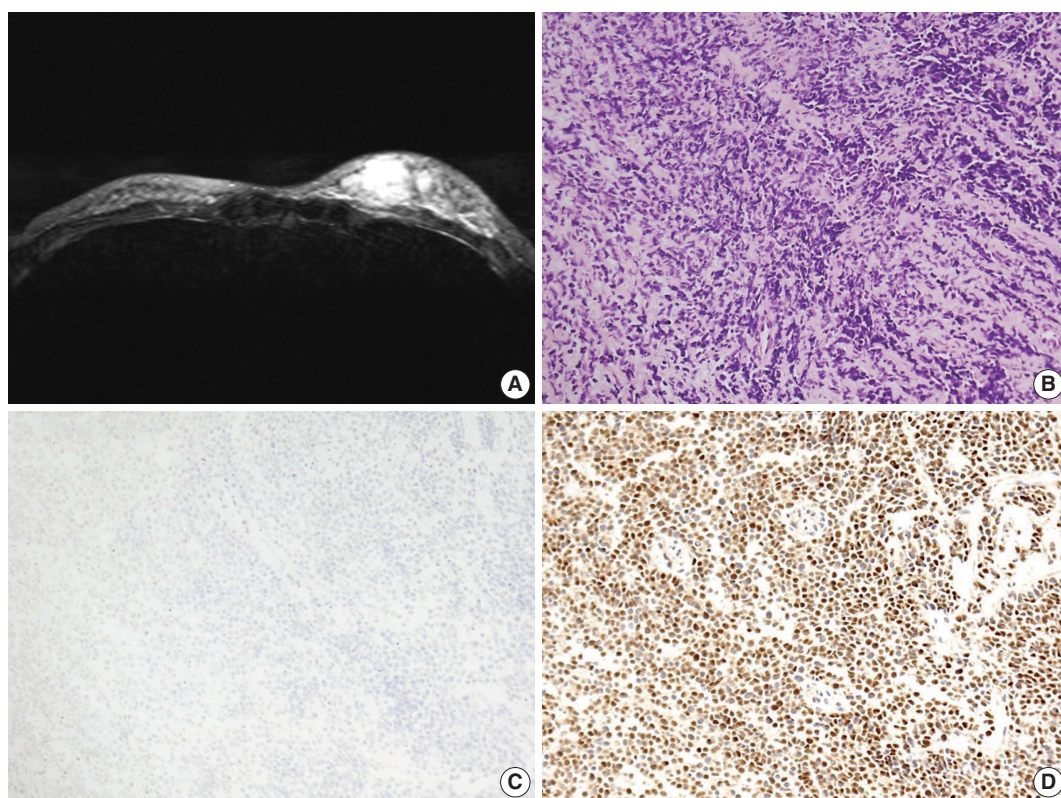


Fig. 3. Primary breast sarcoma of patient C. (A) Magnetic resonance imaging of the breast showing multifocal, infiltrating, ill-defined, enhancing masses in the left lower inner, upper inner, and lower outer quadrants. (B) Hyperchromatic small round cells with scanty cytoplasm exhibiting solid-sheet and cord-like growth patterns. (C, D) Immunohistochemical staining showing negativity for desmin (C) and positivity for myogenin (D).

that measured up to 3 cm (Fig. 3A). Positron emission tomography revealed multiple hypermetabolic lesions in the left breast and axillary lymph nodes.

Ultrasonography-guided needle biopsy of the breast mass was performed. The lesion consisted of loosely cohesive small round cells showing solid sheet or cord-like growth patterns. The cells had scant amounts of cytoplasm and round-to-polygonal shaped hyperchromatic nuclei (Fig. 3B). On IHC examination, these cells showed nuclear positivity for myogenin and negativity for desmin (Fig. 3C, D). The tumors were diagnosed as embryonal RMS (eRMS) based on histological and IHC findings.

The patient received 5 cycles of neoadjuvant chemotherapy (vincristine, adriamycin, cyclophosphamide, ifosfamide, and etoposide) and radiation therapy; however, 8 months post-diagnosis, multiple metastatic lesions were found in bone and left upper lobe of the lung. She received additional chemotherapy but died due to adriamycin cardiotoxicity 18 months post-diagnosis.

Other PBSs

A total of 41 patients were diagnosed with PBS from 2000 to 2018 at Asan Medical Center (Table 1). Among these, two cases were males (5%); one case each of dermatofibrosarcoma protuberans (DFSP) and fibrosarcoma. Mean age of the 41 patients was 44.1 years (range, 14 to 75 years); the most common age group was 50–60 years old (15 cases, 37%) (Table 1).

Angiosarcoma was the most common type of PBS (13 cases, 32%), followed by extra-skeletal osteosarcoma (5 cases, 12%), liposarcoma, and DFSP (4 cases, 10%, respectively); other PBS types occurred with a similar frequency as each other (Table 1, Fig. 4). Among patients aged less than 30 years (7/41 cases), angiosarcoma was not the dominant subtype; instead, we identified three cases of RMS and one case each of undifferentiated spindle cell sarcoma, DFSP, angiosarcoma, and leiomyosarcoma (Table 1, Fig. 4).

Two cases were consultation cases for which only hematoxylin and eosin slides were available for review, and thus it was difficult to confirm the subtype. These were categorized as indeterminate type.

Table 1. Distribution of primary breast sarcoma according to age (review of single institution)

Parameter	No. of cases (%)	Subtypes (number of cases)
Total	41 (100)	-
Male sex	2 (4)	DFSP (1), fibrosarcoma (1)
Mean age (range, yr)	44.1 (14–75)	-
Age group (yr)		
<20	3 (7)	RMS (2), undifferentiated spindle cell sarcoma (1)
20–30	4 (10)	RMS (1), DFSP (1), angiosarcoma (1), leiomyosarcoma (1)
30–40	6 (15)	Angiosarcoma (1), liposarcoma (2), osteosarcoma (2), DFSP (1)
40–50	10 (24)	Angiosarcoma (5), fibrosarcoma (2), leiomyosarcoma (1), DFSP (1), liposarcoma (1)
50–60	15 (37)	Angiosarcoma (5), indeterminate-type (2), osteosarcoma (2), UPS (1), myeloid sarcoma (1), liposarcoma (1), undifferentiated spindle cell sarcoma (1), MPNST (1), DFSP (1)
≥60	3 (7)	Angiosarcoma (1), osteosarcoma (1), myxofibrosarcoma (1)

DFSP, dermatofibrosarcoma protuberans; RMS, rhabdomyosarcoma; UPS, undifferentiated pleomorphic sarcoma; MPNST, malignant peripheral nerve sheath tumor.

DISCUSSION

PBSs are a group of mesenchymal-derived de novo malignancies, accounting for less than 1% of breast cancer.^{4,10} Due to their rarity, large scale analyses have been limited, and PBS has no known etiology.^{4,11} Some breast sarcomas are related with previous treatment (radiation therapy, therapy-associated chronic lymphedema and variable chemicals), and they are categorized as secondary breast sarcoma.^{4,11,12}

Thus far, angiosarcoma is the most commonly reported PBS; virtually any type of sarcoma can occur in the breast as a PBS.¹³ Based on our 18-year institutional experience, angiosarcoma is the most common type of PBS, followed by extra-skeletal osteosarcoma and liposarcoma. However, the distribution of PBS subtypes is not consistent across age groups; angiosarcomas were mostly found in middle-aged women (age, 40 to 60 years). Among young females (age, 10 to 30 years), angiosarcoma was rare. RMS was the most common subtype of PBS in this age group (Table 1, Fig. 4).

Only 26 cases of RMS of breast origin have been reported in English literature, almost exclusively in the young females.⁷ Demographic features, treatments, outcomes, and associated genetic findings of the 29 RMS cases (including our 3 cases) are given in Table 2.

Among the 29 cases, aRMS was the most common type (n = 17, 59%), followed by eRMS (n = 6, 21%), ssRMS (n = 2, 7%), and pleomorphic RMS (n = 1, 3%). Subtype-related information was not available for three cases (n = 3, 10%). All cases involved female patients; median age was 16.4 years (range, 11 to 60 years). Majority of the cases involved adolescents and young adults (range, 10 to 30 years; 24 cases, 83%); five cases (19.2%) involved middle-aged patients. All but one aRMS cases involved teenage girls; contrastingly, eRMS cases were almost equally

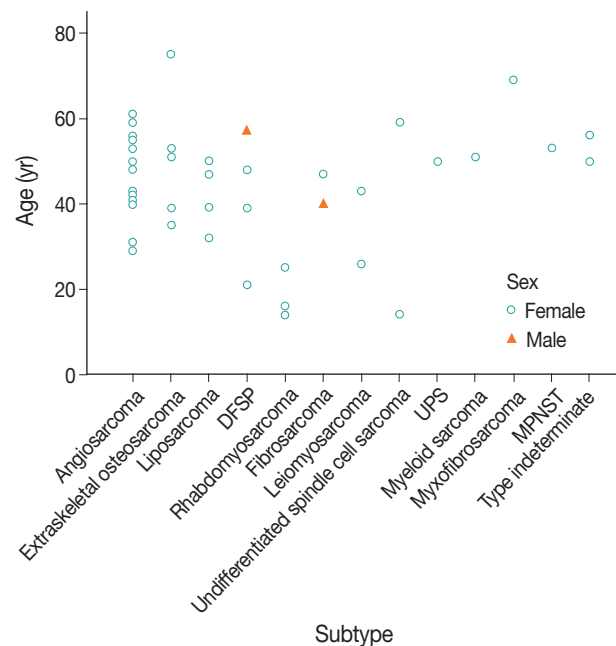


Fig. 4. Age distribution of primary breast sarcoma (PBS) according to subtype. Angiosarcoma was the most common sarcoma, followed by extra-skeletal osteosarcoma, liposarcoma, and dermatofibrosarcoma protuberans (DFSP). The most prevalent age-group was 50–60 years. PBS was rare in people aged less than 30, and rhabdomyosarcoma was the most common subtype in this age-group. UPS, undifferentiated pleomorphic sarcoma; MPNST, malignant peripheral nerve sheath tumor.

distributed between adolescents and middle-aged women; the other RMS types mostly involved middle-aged patients. Interestingly, aRMS cases frequently presented with axillary lymphadenopathy, mimicking mammary carcinomas.

To the best of our knowledge, the ssRMS case in this series is the second to be reported in the literature. ssRMS is a newly classified subtype that accounts for 5%–10% of all RMS cases; it mostly involves paratesticular lesions in pediatric populations

Table 2. Cases of primary rhabdomyosarcoma of the breast (review of literature)

Study	Age (yr)	Subtype	Size (cm)	LN	Meta	Surgical procedure	Other treatment	Prognosis
Hays et al. (1997) ¹⁸	13.6	Alveolar	3	+	+	NI	RTx	DOD 79 wk
	16.9	Alveolar	15	+	+	Excision	CTx, RTx	DOD 42 wk
	15.5	Alveolar	21	+	–	Radical mastectomy	CTx	NED 252 wk
	16.9	Alveolar	8	–	–	Radical mastectomy	RTx	NED 365 wk
	15.2	Alveolar	6.5	–	–	Mastectomy	RTx	NED 150 wk
	15	Alveolar	NI	–	+	NI	NI	DOD 124 wk
	14.9	Embryonal	10	–	–	Excision	RTx	NED 362 wk
Hererra and Lugo-Vicente (1998) ¹⁹	13	Embryonal	6	–	–	NI	CTx	NED 1 yr
Binokay et al. (2003) ²⁰	16	Alveolar	10	+	–	MRM	NI	NI
Vishnevskaja et al. (2004) ²¹	14	Alveolar	NI	+	+	NI	NI	DOD 3 yr 1 mo
Italiano et al. (2005) ^{14,a}	46	Embryonal	3.5	NI	NI	Quadrantectomy	CTx, RTx	NED 18 mo
Nogi et al. (2007) ²³	13	Alveolar	13	+	–	Total mastectomy	CTx	DOD 8 mo
Attili et al. (2007) ⁵	40	Embryonal	4	+	–	MRM	CTx	NED 1 yr
Rasinariu et al. (2011) ⁹	58	Spindle cell/sclerosing	11	NI	NI	Mastectomy	NI	NI
Li et al. (2012) ¹²	30	Alveolar	2.5	+	–	MRM	neoCTx	DOD 29 mo
	17	Embryonal	10	–	–	Simple mastectomy	NI	NED 34 mo
Valera et al. (2013) ²⁴	17	Alveolar	3.1	NI	+	None	CCRT	NI
Bhosale et al. (2013) ²⁵	60	NI	8	+	–	MRM	CTx	NED 6 mo
Mondal et al. (2014) ²⁶	49	Pleomorphic	7	–	–	MRM	None	NED 12 mo
Kallianpur et al. (2015) ²⁷	19	NI	30	–	–	Mastectomy	CTx, RTx	NED 2 mo
Pareekutty et al. (2016) ²⁸	12	Alveolar	9	+	–	MRM	CTx, RTx	NED 35 mo
Audino et al. (2017) ⁷	16	Alveolar	12.5	+	+	MRM	CTx, RTx	Recur 19 mo
Kim et al. (2017) ¹⁰	17	Alveolar	3.1	–	+	Mastectomy	CTx	Recur 5 mo
Yuan et al. (2017) ²⁹	34	NI	3.5	NI	NI	Mastectomy	CTx	NED 23 mo
Bayramoglu et al. (2018) ³⁰	12	Alveolar	NI	+	–	NI	NI	NI
Jean-Louis (2018) ³¹	16	Alveolar	8.1	+	–	Excision	NI	NI
Current study	14	Spindle cell/sclerosing	16.7	–	+	Mastectomy	CTx, RTx	Recur 4 mo
	16	Alveolar	9.5	+	+	Mastectomy	CTx	DOD 22 mo
	25	Embryonal	3	+	–	-	CTx, RTx	DOD 18 mo

LN, lymph node status; Meta, metastasis; NI, not identified; RTx, radiotherapy; DOD, dead of disease; CTx, chemotherapy; NED, no evidence of disease; MRM, modified radical mastectomy; neoCTx, neoadjuvant chemotherapy; CCRT, concurrent chemoradiation therapy.

^aThis was an identical case of Dausse et al. (2005)²².

and head and neck and genitourinary lesions in adults.⁸ As ss-RMS was defined as a variant of eRMS, we reviewed all reports of eRMS for reclassification; however, none of the eRMS cases had the histological characteristics that indicated ssRMS.

Differential diagnoses vary according to RMS subtype, however, differentiation of malignant phyllodes tumor (MPT) with sarcomatous overgrowth is always important regardless of subtypes.² Age can be used to differentiate these malignancies; most MPTs occur in the fifth or sixth decade of life, whereas primary RMS of the breast mainly affects young patients.^{3,14,15} Extensive tissue sampling is necessary, especially in middle-aged patients, as the epithelial component of the MPT can be very small.²

IHC results are critical after excluding MPT with sarcomatous overgrowth; single staining or a combination of desmin, MyoD1, and myogenin staining have been used to diagnose RMS. However, Parham et al.¹⁶ suggested that desmin should always be

used as part of a panel and never as a sole diagnostic marker, as it can non-specifically stain other small round cells and smooth muscle cells. However, despite positive IHC results, the possibility of other myogenic neoplasms cannot be excluded in some cases; therefore, genetic analysis is useful for both histological typing and diagnosis.⁸ Two characteristic cytogenetic changes— $t(2;13)(q35;q14)$ resulting in *PAX3-FKHR (FOXO1)* fusion and $t(1;13)(p13;q14)$ resulting in *PAX7-FKHR (FOXO1)* fusion—are identified in about 80% of aRMS cases, which allow aRMS to be distinguished from other types of round cell neoplasms and RMS.⁸ These fusions are known to be associated with the activation of transcription from *PAX3/PAX7*-binding sites and to contribute to tumorigenesis.¹⁷ In the D9803 COG study, failure-free survival of fusion-positive aRMS patients was lower than that of fusion-negative patients, and *PAX3-FKHR (FOXO1)* fusion-positive patients showed higher overall survival than *PAX7-*

FKHR (FOXO1) fusion–positive patients.¹⁷

Due to its rarity, definite treatment has not been established for RMS of the breast. Generally, axillary dissection of PBS is not recommended as sarcoma usually does not metastasize to lymph nodes; axillary dissection is only required in cases involving palpable lymphadenopathy. However, more than 50% of breast aRMS cases (12/17 cases, 71%) showed axillary node metastasis; moreover, 58% of these cases had no disseminated metastases (7/12 cases). These findings might suggest that axillary node metastasis of aRMS is not only incidental findings of disseminated metastasis, but also early event of disease spreading. Therefore, axillary node dissection or sentinel node sampling of aRMS needs to be considered in cases that require surgery.

RMS of the breast is a rare malignancy that mainly occurs in young females. Our experience regarding RMS cases suggests that spindle cell or small round cell malignancies in the breasts of young females should be suspected of being primary or secondary RMSs. This is the second report that describes a case of ssRMS of the breast, and it may help clinicians who encounter this rare disease in the future.^{5,7,9,10,12,14,18-31}

ORCID

Junyoung Shin: <https://orcid.org/0000-0002-4833-9738>

Hee Jeong Kim: <https://orcid.org/0000-0002-4509-953X>

Dae-Yeon Kim: <https://orcid.org/0000-0001-8852-6389>

Gyungyub Gong: <https://orcid.org/0000-0001-5743-0712>

Kyung-Ja Cho: <https://orcid.org/0000-0002-4911-7774>

Author Contributions

Conceptualization: JS, KJC.

Data curation: JS, KJC.

Formal analysis: JS.

Investigation: HJK, DYK.

Methodology: JS, KJC.

Project administration: GG, KJC.

Supervision: KJC.

Validation: GG, KJC.

Visualization: JS.

Writing—original draft: JS.

Writing—review & editing: JS, KJC.

Conflicts of Interest

The authors declare that they have no potential conflicts of interest.

REFERENCES

1. Lim SZ, Ong KW, Tan BK, Selvarajan S, Tan PH. Sarcoma of the breast: an update on a rare entity. *J Clin Pathol* 2016; 69: 373-81.
2. Hicks DG, Lester SC. *Diagnostic pathology: breast*. 2nd ed. Salt Lake City: Saunders-Elsevier, 2016; 496-577.
3. Chugh R, Baker L. *Nonepithelial malignancies of the breast*. *Oncology (Williston Park)* 2004; 18: 665-73.
4. Yin M, Mackley HB, Drabick JJ, Harvey HA. Primary female breast sarcoma: clinicopathological features, treatment and prognosis. *Sci Rep* 2016; 6: 31497.
5. Attili VS, Dadhich HK, Ramarao C, Bapsy PP, Ramachandra C, Anupama G. A case of primary rhabdomyosarcoma of the breast. *Indian J Surg* 2007; 69: 201-2.
6. Kebudi R, Koc BS, Gorgun O, Celik A, Kebudi A, Darendeliler E. Breast metastases in children and adolescents with rhabdomyosarcoma: a large single-institution experience and literature review. *J Pediatr Hematol Oncol* 2017; 39: 67-71.
7. Audino AN, Setty BA, Yeager ND. Rhabdomyosarcoma of the breast in adolescent and young adult (AYA) women. *J Pediatr Hematol Oncol* 2017; 39: 62-6.
8. Fletcher CD, Bridge JA, Hogendoorn P, Mertens F. *WHO classification of tumors of soft tissue and bone*. 4th ed. Lyon: International Agency for Research on Cancer, 2013; 127-36.
9. Rasinariu A, Andreiuolo F, Terrier P, Balleyguier C, Delaloue S, Vielh P. Primary spindle rhabdomyosarcoma of the breast in an adult female. *Cytopathology* 2011; 22: 137-9.
10. Kim DY, Seol YM, Kim H, Kim A, Choi YJ. Primary rhabdomyosarcoma of the breast in a 17-year-old girl: case report. *Medicine (Baltimore)* 2017; 96: e9076.
11. Bland KI, Klimberg VS, Copeland E, Gradishar WJ. *The breast: comprehensive management of benign and malignant disease*. 5th ed. Philadelphia: Saunders-Elsevier, 2018; 156-68.
12. Li N, Cusido MT, Navarro B, et al. Breast sarcoma: a case report and review of literature. *Int J Surg Case Rep* 2016; 24: 203-5.
13. Schnitt SJ, Collins LC. *Biopsy interpretation of the breast*. 2nd ed. Philadelphia: Lippincott Williams & Wilkins, 2013; 416-7.
14. Italiano A, Largillier R, Peyrottes I, Hannoun-Levy JM, Lallement M, Thyss A. Primary embryonal rhabdomyosarcoma of the breast in an adult female. *Breast J* 2005; 11: 214.
15. Guerrero MA, Ballard BR, Grau AM. Malignant phyllodes tumor of the breast: review of the literature and case report of stromal overgrowth. *Surg Oncol* 2003; 12: 27-37.
16. Parham DM, Ellison DA. Rhabdomyosarcomas in adults and children: an update. *Arch Pathol Lab Med* 2006; 130: 1454-65.
17. Parham DM, Barr FG. Classification of rhabdomyosarcoma and its

- molecular basis. *Adv Anat Pathol* 2013; 20: 387-97.
18. Hays DM, Donaldson SS, Shimada H, et al. Primary and metastatic rhabdomyosarcoma in the breast: neoplasms of adolescent females, a report from the Intergroup Rhabdomyosarcoma Study. *Med Pediatr Oncol* 1997; 29: 181-9.
 19. Herrera LJ, Lugo-Vicente H. Primary embryonal rhabdomyosarcoma of the breast in an adolescent female: a case report. *J Pediatr Surg* 1998; 33: 1582-4.
 20. Binokay F, Soyupak SK, Inal M, Celiktas M, Akgul E, Aksungur E. Primary and metastatic rhabdomyosarcoma in the breast: report of two pediatric cases. *Eur J Radiol* 2003; 48: 282-4.
 21. Vishnevskaya Ia V, Sharoev TA, Stepanova EV, Osipova LV. Rhabdomyosarcoma of the breast in girls. *Arkh Patol* 2004; 66: 47-51.
 22. Dausse F, Balu-Maestro C, Chapellier C, Leblanc-Talent P. Rhabdomyosarcoma of the breast. *Clin Imaging* 2005; 29: 337-41.
 23. Nogi H, Kobayashi T, Kawase K, et al. Primary rhabdomyosarcoma of the breast in a 13-year-old girl: report of a case. *Surg Today* 2007; 37: 38-42.
 24. Valera ET, Brassesco MS, Muglia VF, Scrideli CA, Tone LG. Alveolar rhabdomyosarcoma with breast involvement. *Chin Med J (Engl)* 2013; 126: 998.
 25. Bhosale SJ, Kshirsagar AY, Sulhyan SR, Sulhyan SR. Rhabdomyosarcoma of the breast: a rare malignancy. *Am J Case Rep* 2013; 14: 250-2.
 26. Mondal SK, Mandal PK, Adhikari A, Basak B. Primary pleomorphic rhabdomyosarcoma of breast: report of a rare neoplasm. *J Res Med Sci* 2014; 19: 1200-2.
 27. Kallianpur AA, Praveen, Shukla NK, Deo SV, Khanna P, Durgapal P. Primary mammary rhabdomyosarcoma in a nineteen year old female: a case report and review of literature. *Indian J Cancer* 2015; 52: 295-6.
 28. Pareekutty NM, Bhagat M, Vora T, Qureshi SS. Rhabdomyosarcoma of the breast: report of two cases with the review of literature. *J Indian Assoc Pediatr Surg* 2016; 21: 81-3.
 29. Yuan Y, Hou J, Pan Y. Rhabdomyosarcoma of the breast: report of a rare malignancy. *Cancer Biol Ther* 2017; 18: 676-80.
 30. Bayramoglu Z, Kebudi R, Yilmaz R, et al. Primary rhabdomyosarcoma of the breast: imaging findings and literature review. *Breast Care (Basel)* 2018; 13: 293-7.
 31. Jean-Louis CJ. Alveolar rhabdomyosarcoma of the breast in adolescent female. *Am Surg* 2018; 84: e352-3.

Multistaining Optimization for Epstein-Barr Virus–Encoded RNA In Situ Hybridization and Immunohistochemistry of Formalin-Fixed Paraffin-Embedded Tissues Using an Automated Immunostainer

Jae Nam Ko, Jin Kyoung Jung, Yun Ik Park, Hwa Jeong Shin¹, Jooryung Huh, Sol Back, Yu Jin Kim¹, Jae Ho Kim, Heounjeong Go

Department of Pathology, Asan Medical Center, University of Ulsan College of Medicine, Seoul;

¹Department of Research Support Team, Asan Medical Center, University of Ulsan College of Medicine, Seoul, Korea

Background: Single staining is commonly performed for practical pathologic diagnoses. However, this method is limited in its ability to specify cellular morphology and immunophenotype and often requires consumption of limited tissue. This study aimed to describe an optimized protocol for multiple in situ hybridization (ISH) and immunohistochemistry (IHC). **Methods:** The quality of multistaining was evaluated by carefully changing each step of ISH and IHC in an angioimmunoblastic T-cell lymphoma (AITL) case on a Ventana BenchMark XT automated immunostainer. The optimized protocols were also performed using another immunostainer and in 15 cases of five Epstein-Barr virus (EBV)–associated malignancies using formalin-fixed paraffin-embedded tissue. **Results:** The quality of various ISH-IHC staining protocols was semi-quantitatively evaluated. The best EBV-encoded RNA (EBER)-ISH/double IHC staining quality, equivalent to single staining, was obtained using the following considerations: initial EBER-ISH application, use of protease and antigen retrieval reagent (cell conditioning 1 [CC1] treatment time was minimized due to impact on tissue quality), additional baking/deparaffinization not needed, and reduced dilution ratio and increased reaction time for primary antibody compared with single immunostaining. Furthermore, shorter second CC1 treatment time yielded better results. Multiple staining was the best quality in another immunostainer and for different types of EBV-associated malignancies when it was performed in the same manner as for the Ventana BenchMark XT as determined for AITL. **Conclusions:** EBER-ISH and double IHC could be easily used in clinical practice with currently available automated immunostainers and adjustment of reagent treatment time, dilution ratio, and antibody reaction time.

Key Words: Protocol optimization of multistaining; In situ hybridization; Immunohistochemistry; Epstein-Barr virus-associated malignancy; Formalin-fixed paraffin-embedded tissue

Received: June 15, 2019 **Revised:** July 30, 2019 **Accepted:** August 6, 2019

Corresponding Author: Heounjeong Go, MD, PhD, Department of Pathology, Asan Medical Center, University of Ulsan College of Medicine, 88 Olympic-ro 43-gil, Seoul 05505, Korea
Tel: +82-2-3010-5888, Fax: +82-2-472-7898, E-mail: damul37@amc.seoul.kr

Pathologic diagnosis is usually based on a comprehensive analysis of biomarker expression along with morphological features of lesions. An integrated analysis of the expression pattern of various biomarkers may be a decisive factor in pathologic diagnosis. For example, in lymphoproliferative lesions of childhood, whether atypical cells express Epstein-Barr virus (EBV)-encoded RNA (EBER), and whether they express CD4, CD8, CD56, and/or CD30 may play a key role in diagnosis.¹ Treatment plans for patients may be determined by the expression of specific biomarkers, such as with CD20 expression for rituximab therapy in diffuse large B-cell lymphoma (DLBCL).² In pathologic practices, *in situ* hybridization (ISH) or immunohistochemistry (IHC)

is usually performed to detect genetic material or the expression of protein antigens because of their effectiveness and efficiency. The number of biomarkers evaluated for diagnosis has increased, increasing the need for minimal tissue consumption for the state-of-the-art ancillary tests, especially in small biopsies.³ However, until recently, ISH and IHC have usually been stained with a single marker per slide.

Multistaining can be presented as a way to both reduce tissue consumption and easily identify the cell type expressing biomarkers and patterns of expression. The benefits of multiple IHC or immunofluorescence staining have already been demonstrated in several cancer diagnostic strategies.⁴⁻⁶ In cases where

multiple ISH and IHC procedures are performed, the possibility of tissue damage and antigen loss becomes high, and it becomes difficult to precisely evaluate biomarker expression and morphology of the tissue at a practical level.⁷ Most automated immunostainers automate all staining steps from deparaffinization to visualization, thereby minimizing errors that can occur during manual work and greatly improving accuracy.⁸ However, there are few studies on well-established staining methods for multistaining with ISH and IHC using automated immunostainers.

This study aimed to devise an optimized protocol for multiple ISH and IHC staining on automated immunostainers. The quality of multistaining was evaluated by carefully changing each step of ISH and IHC with formalin-fixed paraffin-embedded (FFPE) tissues of EBV-associated malignancies.

MATERIALS AND METHODS

Specimens

A case of angioimmunoblastic T-cell lymphoma (AITL) with sufficient resected lymph node tissue and confirmed EBV infection at primary diagnosis was selected as the representative specimen for testing ISH and IHC staining conditions. A total of 15 EBV-associated malignancies were further used to validate the optimal multistaining protocol. These 15 samples included three EBV-positive DLBCL, three extranodal natural killer/T-cell lymphomas, three classical Hodgkin lymphomas (cHL) of mixed cellularity type, three AITLs, and three EBV-positive gastric carcinomas with lymphoid stroma (EBV-GCLS). Four EBV-negative malignancies including peripheral T-cell lymphoma and gastric adenocarcinoma were stained with the optimized protocol as controls. All specimens were FFPE tissues and each was cut to a thickness of 4 μ m.

EBER-ISH and IHC

EBER-ISH and IHC for protein antigens were performed using the Ventana BenchMark XT automatic immunostainer following the manufacturer's recommendations (Ventana Medical Systems, Tucson, AZ, USA). EBER-ISH was done with an ISH iView Blue Detection Kit. Protein removal and nucleic acid exposures used ISH protease 2 (#780-4148) or ISH protease 3 (#780-4149), respectively, and the reaction times were varied. Counterstaining was not performed.

Details of the primary antibodies used in IHC and probes used in ISH are summarized in Supplementary Table S1. Two different coloring agents, 3,3'-diaminobenzidine (DAB) and new fuchsin, were used for double ISH-IHC or triple ISH-IHC

staining either alone or in combination. For color development with DAB, the OptiView DAB Detection Kit (hereafter, OptiView kit) was used. Baking and deparaffinization steps were either performed or omitted. When indicated, baking was carried out at 65°C for 10 minutes. For heat-induced epitope retrieval (HIER), treatment time of cell conditioning 1 (CC1) was varied. The dilution ratio of primary antibody was varied taking into consideration the dilution ratio used in single IHC, and the reaction time was varied at 37°C. Counterstaining was performed or omitted as indicated. For color development with new fuchsin, the UltraView Universal Alkaline Phosphatase Red Detection Kit (hereafter, UltraView kit) was used. CC1 treatment time was varied. Dilution ratio and reaction times of primary antibodies were also varied. Counterstaining was performed or omitted as indicated.

EBER-ISH and IHC were also performed using another immunostainer, the Leica Bond III automated immunostainer (Leica Biosystems, Melbourne, Australia). EBER-ISH was performed with the Bond polymer refine detection kit, fluorescein-conjugated EBER oligonucleotide probe (#PB0589) and a mouse monoclonal anti-fluorescein antibody (#AR0833). Procedures were carried out in the same manner as on the Ventana equipment.

Evaluation of the quality of multistaining protocols

The quality of ISH-IHC staining protocols was semi-quantitatively scored by a pathologist (H.G.) and a medical laboratory scientist (J.K.J.) according to the following criteria relative to the quality of a single stain of EBER-ISH or counterstain (Supplementary Fig. S1A–S1C): score 1, no expression (< 1% of cells for which target antigen expression is expected) and scarce preservation of cell or nucleus shape; score 2, rare expression (1% to < 10%) and poor preservation; score 3, minimal expression (10% to < 50%) and bare preservation; score 4, moderate expression (50% to < 75%) and fair preservation; Score 5, abundant expression (\geq 75%) and good preservation. In the case of IHC, intensity of the staining and suitability of the color development position, i.e., location of expression, were evaluated from 1 to 5 points.

The quality of ISH, IHC, and hematoxylin counterstain was separately evaluated and scored. The scores were weighted based on the comparison between the results of single staining and staining according to the nominal protocol. The greater the change in the state of staining from the previous step to the later step, the greater the weight was assigned to the later step, except for the counterstain. More specifically, ISH, the first procedure of multistaining, was given a weight of 0.15 because it was

minimally affected by various factors that reduce the quality of the staining. The intensity and location of IHC were given a weight of 0.30 and 0.35, respectively, because those parameters were more useful in achieving the purpose of immunostaining to evaluate the expression of a targeted antigen, while counterstaining with hematoxylin was given a weight of 0.20. The total score was added to the score of each item to which weights were applied and the maximum was 5.

Ethics statement

Exemption from informed consent after de-identification of samples was approved by the Institutional Review Board of Asan Medical Center (2017-0522).

RESULTS

Multistaining according to nominal protocol

A simple repeat protocol according to the single staining protocols of ISH and IHC was termed the nominal protocol, P1.

When EBER-ISH and CD20- or CD3-IHC staining was sequentially performed on the same slide tissue section of AITL, EBER expression was maintained at the same level as single staining, but CD20 and CD3 were poorly expressed, denaturation of the tissue was so severe that it was difficult to identify the shape of the cells and the quality of the counterstain was also poor (Supplementary Fig. S1D, S1E). As expected, EBER-ISH was not expressed at all using the reverse P1 protocol, i.e., performing IHC first and then ISH, with the same AITL case (Supplementary Fig. S2A, S2B).

Optimization of double ISH-IHC staining protocol

EBER-ISH and CD20-IHC double staining was performed under various conditions with the same tissue used for P1. Double ISH-IHC staining was conducted to tune optimal conditions for five factors, i.e., ISH-protease, CC1, additional baking/deparaffinization, primary antibody dilution and primary antibody reaction time. These factors were considered to affect the quality of multistaining and each protocol was designated from P2-1 to

Table 1. Nominal and optimization protocols of double staining for EBER-ISH and CD20-IHC on a Ventana BenchMark XT immunostainer

Protocol	First procedure (EBER)		Second procedure (CD20)			
	Protease (min)	Baking (min)	Deparaffinization	CC1 (min)	Ab dilution	Ab incubation (min)
P1	Protease 2: 8	10	Selected	32	1:200	32
Optimization protocol for ISH protease						
P2-1	Protease 3: 12 ^a	ND	ND	32	1:200	32
P2-2	Protease 2: 4 ^a	ND	ND	32	1:200	32
P2-3	Protease 2: 8 ^a	ND	ND	32	1:200	32
P2-4	Protease 2: 12 ^a	ND	ND	32	1:200	32
Optimization protocol for CC1						
P3-1	Protease 2: 4	ND	ND	8 ^a	1:200	32
P3-2	Protease 2: 4	ND	ND	16 ^a	1:200	32
P3-3	Protease 2: 4	ND	ND	32 ^a	1:200	32
P3-4	Protease 2: 4	ND	ND	40 ^a	1:200	32
Optimization protocol for baking and deparaffinization						
P4-1	Protease 2: 4 ^a	10 ^a	Selected ^a	8 ^a	1:200	32
P4-2	Protease 2: 4 ^a	10 ^a	Selected ^a	16 ^a	1:200	32
P4-3	Protease 2: 4 ^a	10 ^a	Selected ^a	32 ^a	1:200	32
P4-4	Protease 2: 8 ^a	10 ^a	Selected ^a	8 ^a	1:200	32
P4-5	Protease 2: 8 ^a	10 ^a	Selected ^a	16 ^a	1:200	32
P4-6	Protease 2: 8 ^a	10 ^a	Selected ^a	32 ^a	1:200	32
P4-7	Protease 2: 12 ^a	10 ^a	Selected ^a	8 ^a	1:200	32
P4-8	Protease 2: 12 ^a	10 ^a	Selected ^a	16 ^a	1:200	32
P4-9	Protease 2: 12 ^a	10 ^a	Selected ^a	32 ^a	1:200	32
Optimization protocol for antibody dilution and incubation time						
DS-1	Protease 2: 4	ND	ND	16 ^a	1:200 ^a	60 ^a
DS-2	Protease 2: 4	ND	ND	16 ^a	1:200 ^a	120 ^a
DS-3	Protease 2: 4	ND	ND	16 ^a	1:100 ^a	60 ^a
DS-4	Protease 2: 4	ND	ND	16 ^a	1:100 ^a	120 ^a

EBER, Epstein-Barr virus-encoded RNA; ISH, in situ hybridization; IHC, immunohistochemistry; CC1, cell conditioning 1; Ab, primary antibody; ND, not done.
^aChanges from nominal protocol P1.

Table 2. Scores of the optimization protocols for multistaining on a Ventana BenchMark XT immunostainer

Protocol	EBER	Protein expression				Hematoxylin	Total score
		CD20		CD3			
		Intensity	Location	Intensity	Location		
P1	0.75	0.3	0.35	ND	ND	0.2	1.6
Optimization protocol of double staining for ISH protease							
P2-1	0.45	0.9	0.7	ND	ND	1	3.05
P2-2	0.75 ^a	0.9 ^a	0.7 ^a	ND	ND	1 ^a	3.35 ^a
P2-3	0.75	0.9	0.7	ND	ND	0.4	2.75
P2-4	0.75	0.6	0.35	ND	ND	0.2	1.9
Optimization protocol of double staining for CC1							
P3-1	0.75	0.6	0.7	ND	ND	1	3.05
P3-2	0.75 ^a	0.9 ^a	0.7 ^a	ND	ND	1 ^a	3.35 ^a
P3-3	0.75	0.9	0.7	ND	ND	0.8	3.15
P3-4	0.75	0.9	1.05	ND	ND	0.6	3.3
Optimization protocol of double staining for baking/deparaffinization							
P4-1	0.75	0.6	0.7	ND	ND	1	3.05
P4-2	0.75 ^a	0.9 ^a	0.7 ^a	ND	ND	1 ^a	3.35 ^a
P4-3	0.75	0.9	0.7	ND	ND	0.8	3.15
P4-4	0.75	0.3	0.35	ND	ND	0.6	2
P4-5	0.75	0.6	0.7	ND	ND	0.6	2.65
P4-6	0.75	0.9	0.7	ND	ND	0.4	2.75
P4-7	0.75	0.3	0.35	ND	ND	0.4	1.8
P4-8	0.75	0.3	0.35	ND	ND	0.4	1.8
P4-9	0.75	0.3	0.35	ND	ND	0.2	1.6
Optimization protocol of double staining for antibody dilution and incubation time							
DS-1	0.75	0.9	1.4	ND	ND	1	4.05
DS-2	0.75	1.2	1.4	ND	ND	1	4.35
DS-3	0.75	0.9	1.4	ND	ND	1	4.05
DS-4	0.75 ^a	1.5 ^a	1.75 ^a	ND	ND	1 ^a	5 ^a
Optimization protocol of triple staining with CD3-IHC ^b							
TS-1	0.75	1.5	1.75	0.9	1.05	1	3.7
TS-2	0.75 ^a	1.5 ^a	1.75 ^a	1.5 ^a	1.75 ^a	1 ^a	5 ^a
TS-3	0.75	1.5	1.75	1.5	1.4	0.8	4.45
TS-4	0.75	1.5	1.75	1.5	1.05	0.6	3.9

EBER, Epstein-Barr virus-encoded RNA; ND, not done; ISH, in situ hybridization; CC1, cell conditioning 1; IHC, immunohistochemistry.

^aScores indicate the best under each protocol; ^bThe CD20 score was excluded from the total score calculation because the effect of antigen retrieval on the CD3 antibody of the third procedure was analyzed based on the DS-4 protocol.

DS-4 as summarized in Tables 1 and 2. The reaction time of ISH-protease 2 was varied to minimize the deterioration of CD20-IHC and counterstain and to maintain the quality of EBER-ISH. ISH-protease 3 was set to 12 minutes and ISH-protease 2 was varied to 4, 8, or 12 minutes under CC1 treatment fixed at 32 minutes. Compared with those of the single stain, quality of CD20-IHC was approximately 60% (score 0.9) and 47% (0.7) improved, respectively, and counterstain quality was the same, but the EBER-ISH quality was deteriorated (0.45) with ISH-Protease 3. Thus, ISH-Protease 3 was discarded. In protocols using ISH-protease 2, protease reaction time did not show any deterioration or enhancement in the quality of EBER-ISH, but longer reaction times of ISH-protease worsened CD20-IHC and

the counterstain. In P2-2 with the shortest ISH-protease treatment, EBER-ISH quality was not deteriorated and counterstaining showed good results. However, the score for CD20 IHC was only about 42.7% (1.6/3.25) of the single stain. The total score was 3.35, the highest among P2 protocols (Fig. 1A).

CC1 reaction time (P3 protocols) was varied to 8, 16, 32, and 40 minutes. The quality of CD20-IHC staining increased with longer CC1 reaction time, but the counterstain quality gradually decreased. Among P3 protocols, the quality of staining was best for P3-2 with a total score of 3.35 (Fig. 1B). Next, the effects of baking and additional deparaffinization on the quality of staining were evaluated. Nine P4 protocols were designed by setting the baking time to 10 minutes and varying ISH-protease 2 and

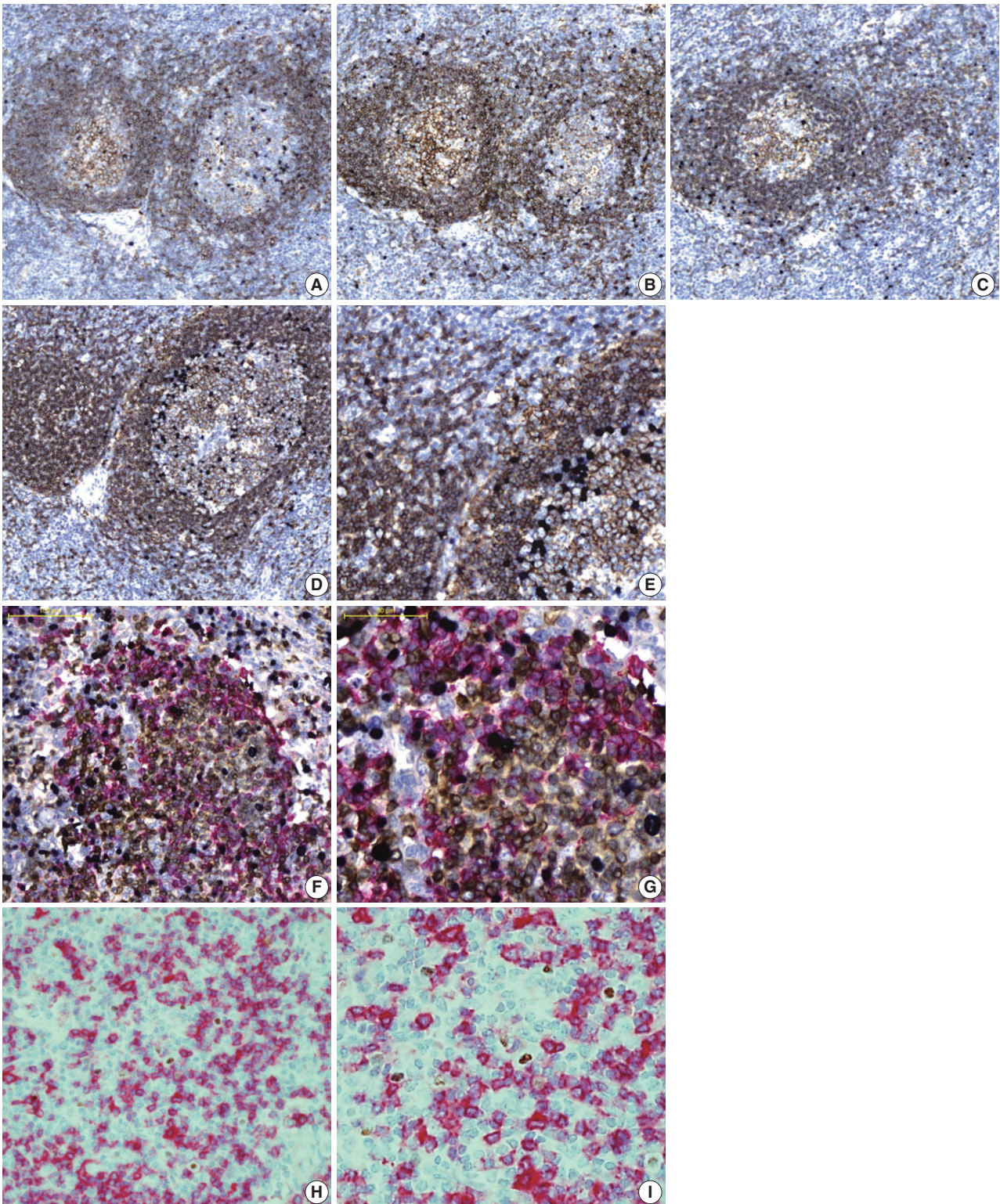


Fig. 1. Multistaining using each protocol for optimization with angioimmunoblastic T-cell lymphoma tissue. (A) P2-2 (Epstein-Barr virus-encoded RNA [EBER], purple; CD20, brown). (B) P3-2 (EBER, purple; CD20, brown). (C) P4-2 (EBER, purple; CD20, brown). (D, E) DS-2 (EBER, purple; CD20, brown). (F, G) TS-4 (EBER, purple; CD20, red; CD3, brown). (H, I) double EBER in situ hybridization and CD20 immunohistochemistry staining on a Leica Bond III immunostainer (EBER, brown; CD20, red).

CC1 reaction times. In all cases, baking and deparaffinization did not deteriorate or improve the quality of staining (Fig. 1C).

Finally, the effects of dilution ratio and timing of primary antibody on the quality of multistaining were evaluated (DS protocols). Based on the optimal dilution ratio and time for CD20 single staining, the dilution ratio of CD20 antibody was halved from 1:200 to 1:100 and/or the reaction time was doubled from 60 to 120 minutes. As a result, the DS-4 protocol with a dilution factor of 1:100 of CD20 primary antibody and a reaction time of 120 minutes resulted in a total score of 5 by summing up the scores of EBER-ISH (0.75), CD20-IHC (3.25), hematoxylin (1) while maintaining a level of quality equivalent to the result of a single stain for each procedure in all evaluation factors (Fig. 1D, E).

Optimization of triple stain of EBER-ISH and double IHC

Based on optimized conditions with EBER and CD20 staining, CD3-IHC triplicate staining was performed under various conditions with the same AITL tissue. The quality of ISH and double IHC staining was evaluated by changing the same five factors as well as the ISH-IHC staining. Among them, CC1 reaction time of CD3-IHC was varied in the same manner as CD20-IHC (Table 3). Consequentially, even when CD3 antibody was added, the best results were obtained when staining was performed in the same manner as ISH-IHC staining, which maintained the same quality of staining as single stains with each probe or primary antibody (Fig. 1F, G).

To further evaluate the applicability of the optimized protocol, ISH-IHC staining was performed on a Leica Bond III automated immunostainer with each case of AITL, cHL, and EBV-GCLS. As with a Ventana immunostainer in all three cases, the best staining quality was obtained when EBER-ISH was first applied and Enzyme I protease treatment time was minimized. In more detail, EBER was fully expressed following treatment with protease K for 10 minutes in both single EBER-ISH and ISH-IHC, and background staining occurred with protease K treatment for 20 minutes or more and when the incubation time of

the EBER probe was increased from 45 minutes in single EBER-ISH to 3 hours in ISH-IHC. Antibody dilution ratio was halved and antibody reaction time was doubled compared with single immunostaining conditions (Fig. 1H, I).

Validation of the optimized protocols in EBV-associated and non-associated malignancies

The optimized multi-EBER-ISH and double IHC staining protocols were validated in 15 EBV-associated (3 cases per cancer type) and four EBV-non-associated (2 cases per cancer type) malignancies. Staining conditions were the same as in the TS-4 protocol, and the dilution ratio of each antibody was concentrated to half the dilution of the single stain while reaction time was doubled (Table 4).

As showed in Fig. 2A and B, in the EBV-positive DLBCL, (1) EBER-ISH and CD20 (red)-/CD3 (DAB)-IHC and (2) EBER-ISH and CD20 (red)-/CD30 (DAB)-IHC staining was performed to evaluate whether EBV-infected cell types were identifiable. CD20-positive cells expressing a red membrane were large with atypical nuclei and diffusely proliferated. These cells were frequently observed with dark blue color nuclei, and the surrounding small lymphocytes were admixed with red- or brown-expressing cells. These colors indicated that EBV-infected cells were not small T or B cells, but rather large atypical B cells. In addition, in EBER-ISH and CD20-/CD30-IHC staining, some EBER- and CD20-positive cells were observed to be reddish brown. When staining results were taken together, EBV-positive DLBCL were found to be neoplastic B cells infected with EBV, and some of these cells expressed CD30. Similarly, it was easy to determine which biomarker was expressed on EBV-infected cells compared to single staining in other types of EBV-associated malignancies (Fig. 2C–J, Supplementary Fig. S3). Furthermore, for all tested EBV-associated malignancies, the staining quality of each biomarker and counterstain was nearly identical to that of a single stain. In contrast, EBER was never expressed but the staining quality was well preserved in all EBV-non-associated malignancies (Supplementary Fig. S4).

Table 3. Optimization of triple staining for EBER-ISH and CD20- and CD3-IHC staining on a Ventana BenchMark XT immunostainer

Protocol	First procedure (EBER-ISH)		Second procedure (CD20-IHC)		Third procedure (CD3-IHC)		
	Protease (min)	CC1 (min)	Ab incubation (min)	Dilution	CC1 (min)	Ab incubation (min)	Dilution
TS-1	4	16	120	1:100	8 ^a	120	1:100
TS-2	4	16	120	1:100	16 ^a	120	1:100
TS-3	4	16	120	1:100	32 ^a	120	1:100
TS-4	4	16	120	1:100	46 ^a	120	1:100

EBER, Epstein-Barr virus–encoded RNA; ISH, in situ hybridization; IHC, immunohistochemistry; CC1, cell conditioning 1; Ab, primary antibody.

^aParameters indicate changes.

Table 4. Multi-EBER-ISH and IHC staining using optimized protocols in EBV-associated malignancies using a Ventana BenchMark XT immunostainer

	EBER CD20 CD3	EBER CD20 CD56	EBER CD3 CD15	EBER CD30 CD3	EBER CK CD3
First procedure, XT INFORM Probe iVIEW Blue v3					
1. Deparaffinization	S	S	S	S	S
2. ISH Protease 2 (min)	4	4	4	4	4
3. INFORM EBER	S	S	S	S	S
Second procedure, XT OptiView DAB IHC v4					
4. CC1 (min)	16	16	16	16	16
5. Pre-primary peroxidase inhibit	S	S	S	S	S
6. Ab incubation time (min)	120	120	120	120	120
Ab dilution	1:100	1:100	1:100	1:50	1:100
Third procedure, XT UltraView RED v3					
7. CC1 (min)	20	20	20	20	20
8. Ab incubation time (min)	120	120	120	120	120
Ab dilution	1:100	1:25	1:100	1:100	1:100
9. Hematoxylin 2 (min)	16	16	16	16	16
10. Bluing (min)	4	4	4	4	4

EBER, Epstein-Barr virus–encoded RNA; ISH, in situ hybridization; IHC, immunohistochemistry; EBV, Epstein-Barr virus; CC1, cell conditioning 1; S, selected; Ab, primary antibody.

DISCUSSION

This study aimed to identify an optimized multistaining protocol using automated immunostainers and commercially available kits for ISH and IHC to make multiple staining easy to use in pathologic practice. Recently, a proper assessment of the expression of many biomarkers in diagnoses has become increasingly important. In particular, it is essential to accurately determine the immunophenotype of various biomarkers and morphology of cells in diagnosing many benign or malignant diseases associated with EBV infection.⁹ However, the immunophenotyping of atypical cells as well as the EBER-expressing cells is challenging and the various molecular tests frequently needed consume a lot of tissue. Thus, we selected EBV-associated malignancies to be representative examples for establishing optimized multistaining protocols.

We determined that ISH should be performed before IHC during multiple staining. When IHC was administered first, EBER-ISH was not stained, which could be attributed to the complete degradation of mRNA during IHC. Additional baking/depaffinization was not needed for antigen retrieval during IHC, but all of the primary antibodies used in this study required HIER for antigen retrieval. If proteolytic-induced epitope retrieval (PIER) is required for restoring antigenicity, such as with the primary antibody for epidermal growth factor receptor,¹⁰ it may be necessary to determine PIER reaction time during IHC with multistaining because this protease would have already been

applied in ISH. It was expected that staining quality might be worse due to tissue damage when PIER reaction time was the same in multi-ISH/IHC stain as in single IHC. Although a definite mechanism for HIER has yet to be established, it is presumed that the calcium ion of the HIER solution plays a role of opening or closing the cross linkage between proteins through a chelation reaction with a covalent ring-forming metal substance.¹¹ In double IHC, temporarily opened protein cross-linking after HIER is restored to the state before HIER after a certain period of time, and only one HIER is required when the two primary antibodies simultaneously react. However, we needed additional HIER because the primary antibodies were applied in sequence in double IHC.

The OptiView kit and the UltraView kit for IHC are 3-step and 2-step multimer methods, respectively. Because the sensitivity of antigen detection is higher with the OptiView kit than the UltraView kit, the dilution ratio of some antibodies needed to be reduced when used with the UltraView kit. Thus, we obtained better staining with primary antibodies of higher sensitivity using the UltraView kit, while those with lower sensitivity were stained using the OptiView kit when double IHC was performed. In addition, the 3-step multimer method, which maintained good staining quality even when CC1 treatment time was short, was first applied, and then the 2-step multimer method was applied while adjusting appropriate CC1 treatment time. The development of various coloring agents for 3-step multimers would provide more flexibility in protocol design and result

in better quality multi-immunostaining.¹²

ISH-protease and HIER time were found to be the most important parameters for successful multiple staining. The longer the

treatment time of ISH-protease, the more severe the loss of antigen. Longer HIER led to worse tissue condition and poor quality hematoxylin counterstaining, making it difficult to identify tis-

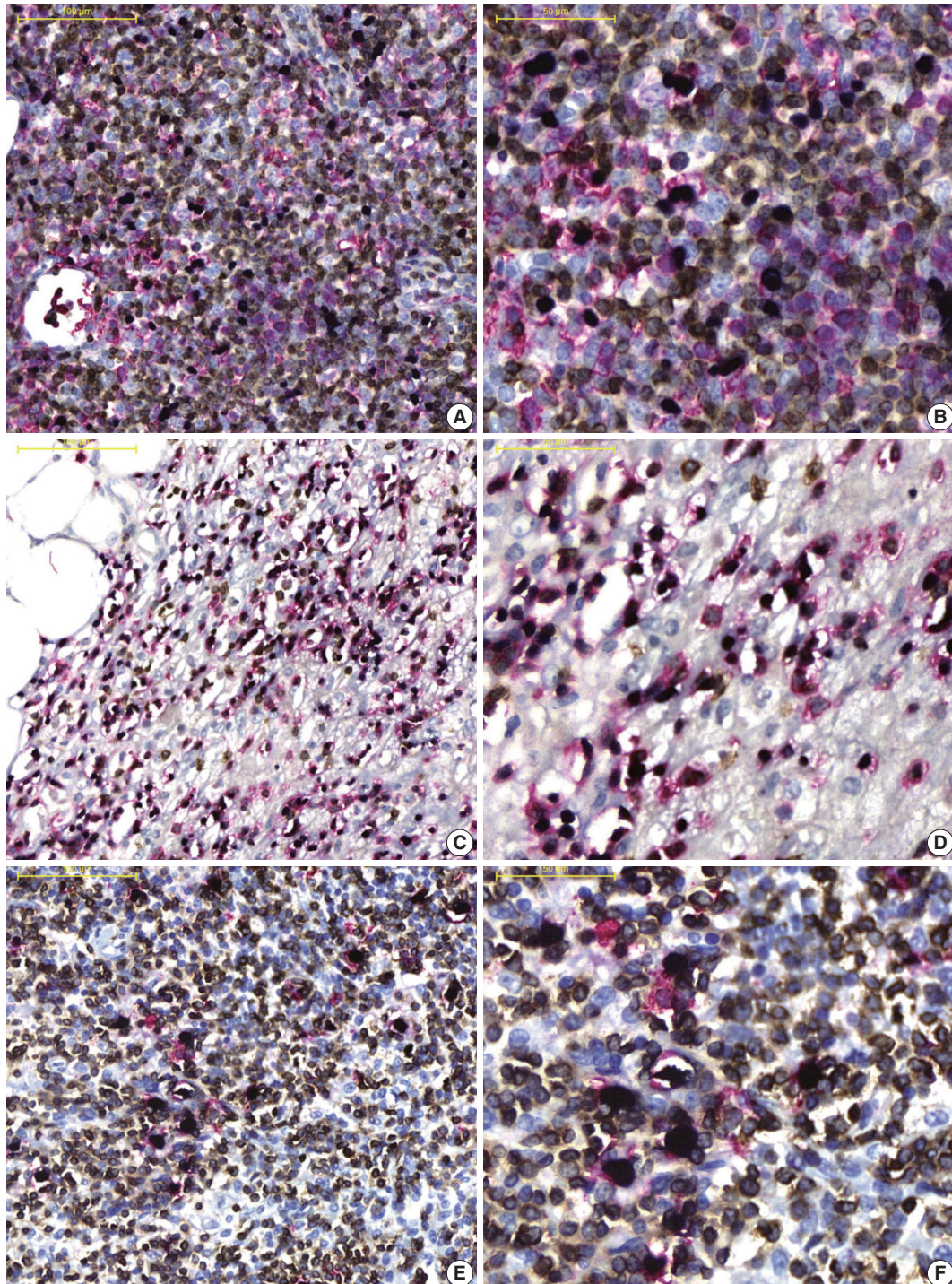


Fig. 2. Application of the optimized multistaining protocol to various Epstein-Barr virus (EBV)-associated malignancies. (A, B) EBV-positive diffuse large B-cell lymphoma (Epstein-Barr virus-encoded RNA [EBER], purple; CD20, red; CD3, brown). (C, D) Extranodal natural killer/T-cell lymphoma, nasal type (EBER, purple; CD56, red; CD3, brown). (E, F) Classic Hodgkin lymphoma stroma (EBER, purple; CD15, red; CD3, brown).
(Continued on the next page)

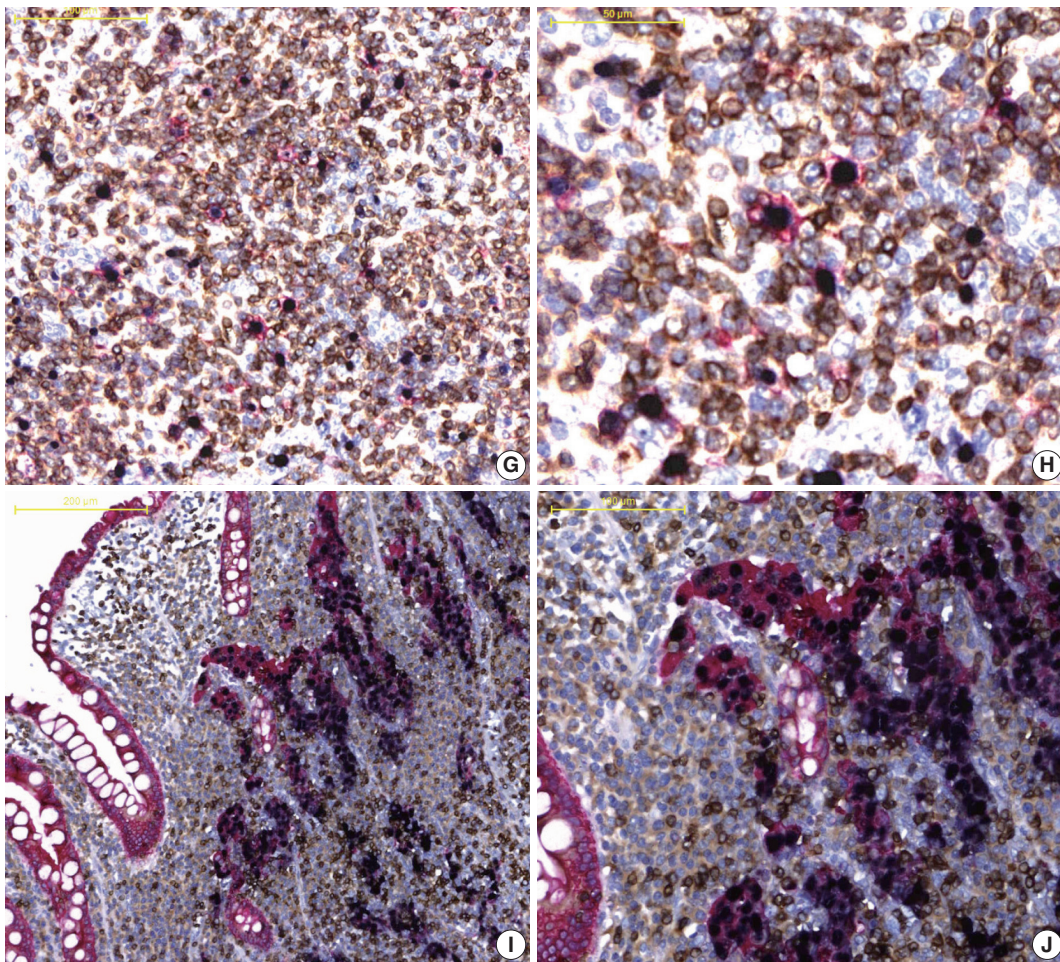


Fig. 2. (Continued from the previous page) (G, H) Angioimmunoblastic T-cell lymphoma stroma (EBER, purple; CD30, red; CD3, brown). (I, J) EBV-positive gastric carcinoma with lymphoid stroma (EBER, purple; cytokeratin, red; CD3, brown).

sue architecture and cell morphology. In the case of multiple ISH/IHC staining, the protease and HIER time proposed in this study could be used to achieve the same quality of staining as single ISH and/or IHC.

Because three staining procedures were sequentially performed for EBER-ISH and double IHC, the kits needed to be replaced at the end of each procedure, and the turnaround time increased. Nevertheless, double EBER-ISH/IHC and triple EBER-ISH/IHCs could be completed within the same day or take up to half a day. Because FFPE tissues and three independent kits were used for triple staining in each procedure, the staining procedures for each marker could be easily added. For example, if double or triple staining was required while reading an EBER-ISH stained slide, the coverslip of the slide could be removed and stained with other biomarkers such as CD20, CD30, and CD15.

In conclusion, EBER-ISH and double IHC could be easily used in pathologic practice by adjusting the treatment time of

the reagents as well as the dilution ratio and reaction time of the primary antibodies, as suggested by the described optimized protocols for currently available automated immunostainers. If more coloring agents are commercialized in the future, more biomarker expression could be evaluated on one slide. In addition, evaluation of the type of cells expressing a particular biomarker and the relevance of multiple biomarkers would be more accurate, while minimizing tissue loss for further ancillary studies.

Electronic Supplementary Material

Supplementary materials are available at Journal of Pathology and Translational Medicine (<https://jpatholtm.org>).

ORCID

Jae Nam Ko: <https://orcid.org/0000-0001-7257-2145>

Jin Kyoung Jung: <https://orcid.org/0000-0002-4993-9305>

Yun Ik Park: <https://orcid.org/0000-0003-4551-5684>
 Hwa Jeong Shin: <https://orcid.org/0000-0002-2873-3850>
 Jooryung Huh: <https://orcid.org/0000-0002-6991-6397>
 Sol Back: <https://orcid.org/0000-0003-0451-4183>
 Yu Jin Kim: <https://orcid.org/0000-0003-0730-5192>
 Jae Ho Kim: <https://orcid.org/0000-0003-3124-0309>
 Heounjeong Go: <https://orcid.org/0000-0003-0412-8709>

Author Contributions

Conceptualization: JNK, HG.
 Data curation: JNK, JKJ.
 Formal analysis: JNK, HG.
 Funding acquisition: HG.
 Investigation: JNK, JKJ, YIP, HJS, SB.
 Methodology: JNK, JKJ, HG.
 Project administration: JH, JHK.
 Resources: JNK, JKJ, YIP, HJS, JH, SB, YJK.
 Supervision: JH, JHK, HG.
 Validation: JNK, JH, JHK, HG.
 Visualization: JNK, JKJ, HG.
 Writing—original draft: JNK.
 Writing—review & editing: JH, JHK, HG.

Conflicts of Interest

The authors declare that they have no potential conflicts of interest.

REFERENCES

1. Swerdlow SH, Campo E, Harris NL, et al. WHO classification of tumours of haematopoietic and lymphoid tissues. Revised 4th ed. Lyon: International Agency for Research on Cancer, 2017.
2. Coiffier B, Lepage E, Briere J, et al. CHOP chemotherapy plus rituximab compared with CHOP alone in elderly patients with diffuse large-B-cell lymphoma. *N Engl J Med* 2002; 346: 235-42.
3. Wu L, Qu X. Cancer biomarker detection: recent achievements and challenges. *Chem Soc Rev* 2015; 44: 2963-97.
4. Isidro RA, Isidro AA, Cruz ML, Hernandez S, Appleyard CB. Double immunofluorescent staining of rat macrophages in formalin-fixed paraffin-embedded tissue using two monoclonal mouse antibodies. *Histochem Cell Biol* 2015; 144: 613-21.
5. Ojima T, Kinami S, Nakamura K, et al. Advantages of the rapid double-staining method for intraoperative detection of micrometastasis in sentinel lymph nodes. *Oncol Rep* 2013; 30: 1067-72.
6. Van der Hauwaert C, Savary G, Gnemmi V, et al. Isolation and characterization of a primary proximal tubular epithelial cell model from human kidney by CD10/CD13 double labeling. *PLoS One* 2013; 8: e66750.
7. Jeziorski E, Senechal B, Molina TJ, et al. Herpes-virus infection in patients with Langerhans cell histiocytosis: a case-controlled sero-epidemiological study, and in situ analysis. *PLoS One* 2008; 3: e3262.
8. Bankfalvi A, Boecker W, Reiner A. Comparison of automated and manual determination of HER2 status in breast cancer for diagnostic use: a comparative methodological study using the Ventana BenchMark automated staining system and manual tests. *Int J Oncol* 2004; 25: 929-35.
9. Weisenburger DD, Savage KJ, Harris NL, et al. Peripheral T-cell lymphoma, not otherwise specified: a report of 340 cases from the International Peripheral T-cell Lymphoma Project. *Blood* 2011; 117: 3402-8.
10. Terragni R, Casadei Gardini A, Sabbatini S, et al. EGFR, HER-2 and KRAS in canine gastric epithelial tumors: a potential human model? *PLoS One* 2014; 9: e85388.
11. Shi SR, Key ME, Kalra KL. Antigen retrieval in formalin-fixed, paraffin-embedded tissues: an enhancement method for immunohistochemical staining based on microwave oven heating of tissue sections. *J Histochem Cytochem* 1991; 39: 741-8.
12. Van der Loos CM. Chromogens in multiple immunohistochemical staining used for visual assessment and spectral imaging: the colorful future. *J Histotechnol* 2010; 33: 31-40.

Amoebic Encephalitis Caused by *Balamuthia mandrillaris*

Su Jung Kum, Hye Won Lee, Hye Ra Jung, Misun Choe, Sang Pyo Kim

Department of Pathology, Keimyung University School of Medicine, Daegu, Korea

We present the case of a 71-year-old man who was diagnosed with amoebic encephalitis caused by *Balamuthia mandrillaris*. He had rheumatic arthritis for 30 years and had undergone continuous treatment with immunosuppressants. First, he complained of partial spasm from the left thigh to the left upper limb. Magnetic resonance imaging revealed multifocal enhancing nodules in the cortical and subcortical area of both cerebral hemispheres, which were suggestive of brain metastases. However, the patient developed fever with stuporous mentality and an open biopsy was performed immediately. Microscopically, numerous amoebic trophozoites, measuring 20 to 25 μm in size, with nuclei containing one to four nucleoli and some scattered cysts having a double-layered wall were noted in the background of hemorrhagic necrosis. Based on the microscopic findings, amoebic encephalitis caused by *Balamuthia mandrillaris* was diagnosed. The patient died on the 10th day after being admitted at the hospital. The diagnosis of amoebic encephalitis in the early stage is difficult for clinicians. Moreover, most cases undergo rapid deterioration, resulting in fatal consequences. In this report, we present the first case of *B. mandrillaris* amoebic encephalitis with fatal progression in a Korean patient.

Key Words: Amoebic encephalitis; *Balamuthia mandrillaris*; Histopathologic features

Received: March 18, 2019 **Revised:** April 29, 2019 **Accepted:** May 14, 2019

Corresponding Author: Sang Pyo Kim, MD, Department of Pathology, Keimyung University School of Medicine, 1095 Dalgubeol-daero, Dalseo-gu, Daegu 42601, Korea
Tel: +82-53-580-3815, Fax: +82-53-580-3823, E-mail: smkim5@kmu.ac.kr

Although amoebic encephalitis is a rare disease, it has a very high mortality rate. There are two distinct forms of representation of this disease. One is the granulomatous amoebic encephalitis caused by *Balamuthia mandrillaris* or *Acanthamoeba* species, which progresses chronically or subacutely, during a period of two weeks to 2 years. The other is the primary amoebic meningoencephalitis caused by *Naegleria fowleri*, which progresses rapidly and fulminantly, resulting in death within a week or less.¹

Unlike the other amoeba species, *B. mandrillaris* affects not only immunocompromised but also immunocompetent people, especially the young and the elderly.² The histopathologic findings showed a wide spectrum of features from acute and subacute to granulomatous inflammation. In addition, the mortality rate is known to be 98%.³ Since 1991, *B. mandrillaris* encephalitis has been reported in more than 200 cases in the world and has predominantly occurred in South America and the United States. However, in East Asia, only nine cases have been reported in Japan⁴ and the present patient is the first case of *B. mandrillaris* encephalitis in the Republic of Korea.

CASE REPORT

A 71-year-old Korean man presented with partial spasm from the left thigh to the left upper limb for a day without any infectious symptoms at that time. He had had rheumatic arthritis for 30 years and had been continuously treated with immunosuppressants such as steroids, methotrexate, and nonsteroidal anti-inflammatory drugs. Initial magnetic resonance imaging (MRI) of the brain revealed several ring-enhancing nodules measuring up to $3.7 \times 3.2 \times 1.8$ cm in size in both cerebral hemispheres, and brain metastasis of unknown origin was suspected (Fig. 1A). The initial blood laboratory test revealed an increased C-reactive protein (CRP) level (7.89 mg/dL) and a normal white blood cell count. The cerebrospinal fluid (CSF) study revealed that the glucose level was within the normal range of 60 mg/dL and that the protein level was elevated at 331.8 mg/dL. A week after, the patient complained of fever and stuporous mentality; a second brain MRI performed at that time revealed a number of nodules that were larger in size (Fig. 1B) compared with the initial MRI.

Therefore, an open biopsy of the brain was performed imme-

diately. During the operation, the frozen sections with squash preparation showed acute inflammation with hemorrhagic necrosis, and no definitive diagnosis could be made. After the operation, the permanent sections showed diffuse or perivascular infiltration of amoebic trophozoites in the background of hemor-

rhage and necrosis (Fig. 2A–C). The trophozoites were ovoid or round and 20–25 μm in size. They each had 1–2 nuclei containing 1–4 nucleoli (Fig. 2D–F). Additionally, some scattered cysts having inner rigid and outer wavy double-layered walls were observed (Fig. 3A–E). These findings were consistent with the

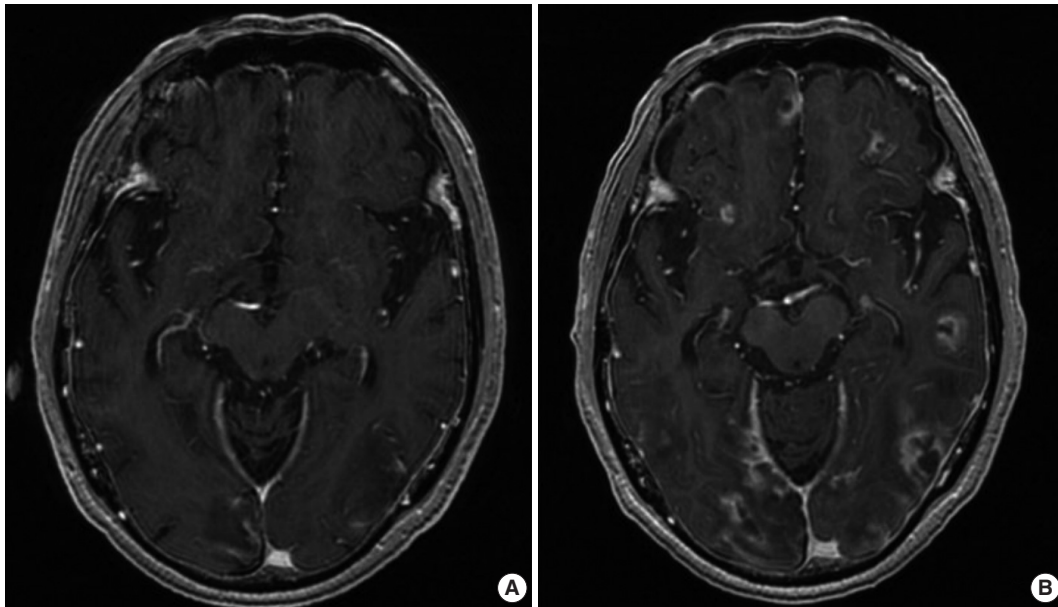


Fig. 1. (A) Initial magnetic resonance imaging (MRI) showing multiple ring-enhancing nodules in the cortical and subcortical areas of both cerebral hemispheres. (B) Second MRI showing an increased number and size of the nodules compared to the initial MRI.

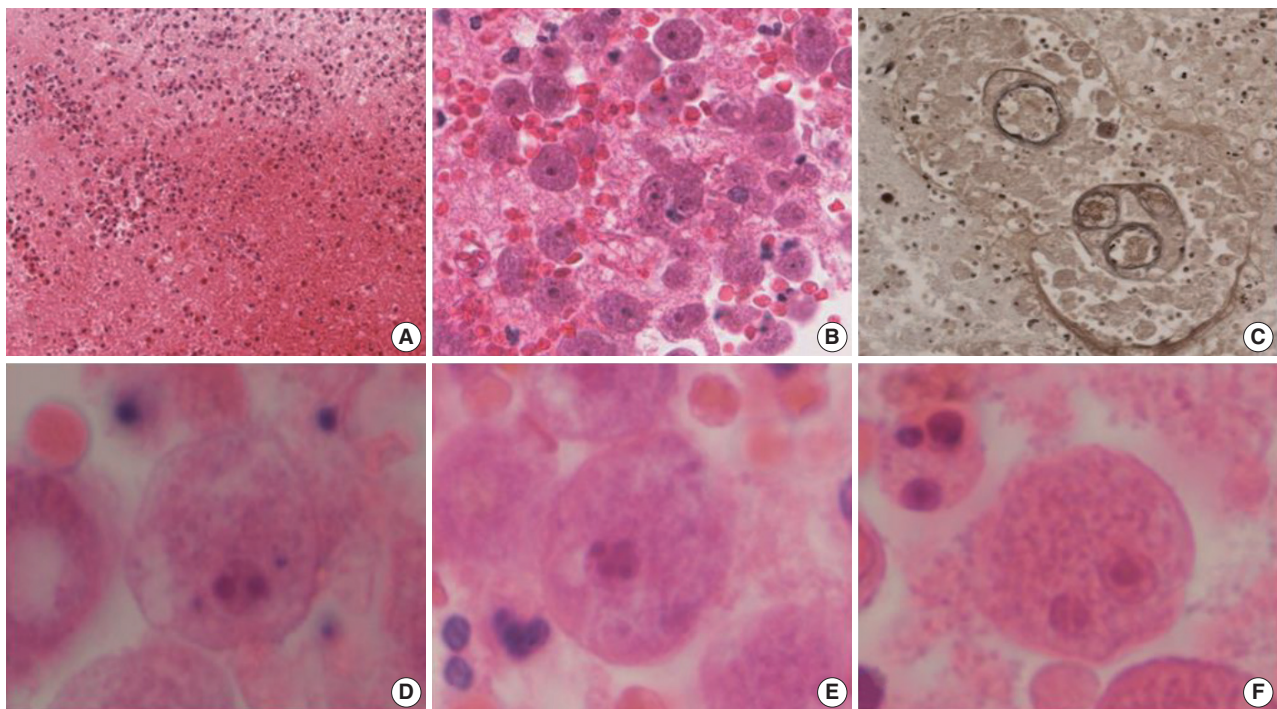


Fig. 2. Hemorrhagic necrosis (A) is associated with diffuse or perivascular infiltration of amoebic trophozoites (B, C). (C) Elastic stain highlights the trophozoites. Ovoid to round trophozoites, measuring 20 to 25 μm in size, with 1–2 nuclei containing 1–4 nucleoli are noted (D–F).

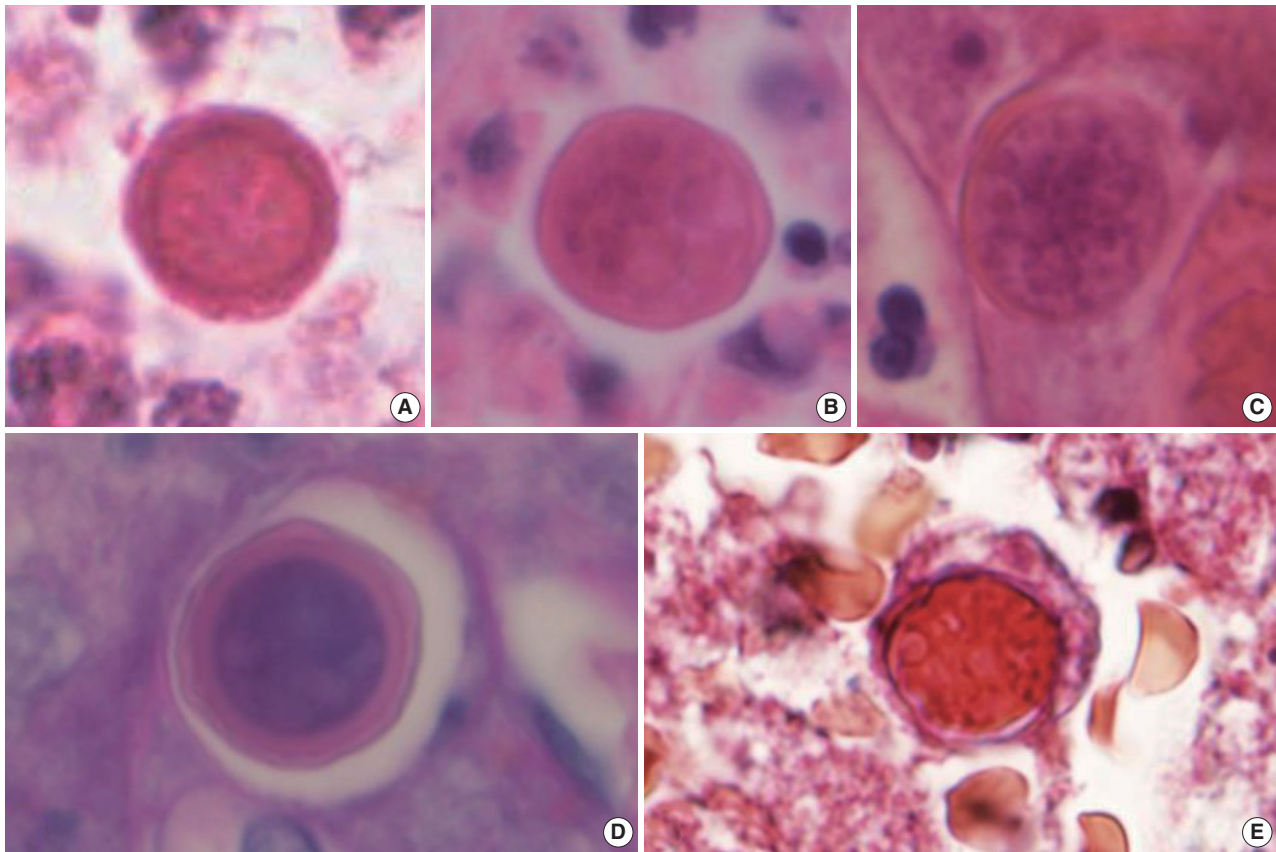


Fig. 3. (A–E) Spherical cysts, measuring 15–20 μm in size, consisting of a rigid double-layered wall are noted. The periodic-acid Schiff (D) and trichrome (E) stains highlight the cysts.

diagnosis of *B. mandrillaris* amoebic encephalitis. Even though the patient was treated with the combination of pentamidine and paromomycin, he died on the 10th day after being admitted to the hospital.

Ethics statement

This study was approved by the Institutional Review Board of Keimyung University Dongsan Medical Center, with waiver of informed consent (IRB No. 2019-02-023).

DISCUSSION

Balamuthia mandrillaris, *Acanthamoeba* species, and *Naegleria fowleri* are known to be free-living amoebae that can cause amoebic encephalitis. *B. mandrillaris* and *Acanthamoeba* species mainly cause granulomatous amoebic encephalitis, which shows subacute to chronic progression, while *N. fowleri* causes primary amoebic meningoencephalitis, which shows a highly acute progression.¹ Unfortunately, all of these amoebae do not have characteristic clinical features; thus, early diagnosis is very difficult for clinicians

and the condition is associated with a high mortality rate of over 90%.⁵

B. mandrillaris amoebic encephalitis is also a fatal condition, and the mortality rate is known to be 98%.³ It affects not only immunocompromised but also immunocompetent individuals, especially the young and the old.² Despite its high mortality rate, the pathophysiology and pathogenesis of *B. mandrillaris* amoebic encephalitis are not clearly understood. However, it is assumed that the main routes of the infections are through the nasal mucosa or hematogenous spread through the respiratory and cutaneous pathways in a manner similar to other amoebic species. The CSF study did not reveal any organism, but showed a normal or slightly low glucose level and an elevated protein level, which are similar to findings with the presence of *Acanthamoeba* species.⁶

Like *Acanthamoeba* species, *B. mandrillaris* also have two life cycle stages: trophozoite and cyst. Histopathologically, trophozoites have a round to ovoid shape and range from 12 to 60 μm in size. They usually only have a single nucleus, but, occasionally, more than one nucleus can be noticed. Each nucleus contains one

Table 1. Differential diagnosis of amoebic encephalitis by histopathologic features

	Present case	<i>Balamuthia mandrillaris</i>	<i>Acanthamoeba</i> spp.	<i>Naegleria fowleri</i>
Trophozoite				
Size (µm)	20–25	12–60	15–50	10–25
Nuclei	1–2	1–3	1	1
Nucleoli	1–4	≥1	1	1
Cyst				
Size (µm)	15–20	15–30	15–25	Not identified
Double layer wall				
Outer	Wavy	Wavy	Wrinkled	Not identified
Inner	Round	Round and rigid	Various shape	Not identified
Background	Acute inflammation Angiitis	Acute to granulomatous inflammation (GAE) Angiitis	Granulomatous inflammation (GAE) Angiitis	Acute inflammation (PAM)
CSF study	Not done	Not identified	Usually absent (if present, in trophozoite form)	Present, in flagellate form
Others				
			Keratitis Skin infection	

GAE, granulomatous amoebic encephalitis; PAM, primary amoebic meningoencephalitis; CSF, cerebrospinal fluid.

to three nucleoli. When they become cysts, they have a triple-layered wall, but, under a light microscope, they are observed to have a double-layered wall: a round and rigid inner wall and wavy outer wall, ranging from 15–30 µm in size.^{7,8} The cysts and trophozoites are prominent in the vascular or perivascular area, in the background of acute to granulomatous inflammation with angiitis, hemorrhage, and necrosis.

In contrast, *Acanthamoeba* species have vegetative trophozoites with cysts in the tissue. Trophozoites are 15–50 µm in size and contain one vesicular nucleus with one large, centrally placed nucleolus. Cysts range from 15–25 µm in size and have a double-layered wall. The outer wall is wrinkled with folds and ripples, while the inner wall varies in shape. On the other hand, *N. fowleri* have only trophozoites without cysts in the brain tissue. Trophozoites are 10–25 µm in size and have one nucleus with one prominent nucleolus in the middle, and are usually observed around vessels, in the background of acute inflammation associated with hemorrhage and necrosis.⁸

For the diagnosis of amoebic encephalitis, it is essential to identify organisms in the tissue or CSF.^{7,9} Differential diagnosis of the three amoebae is possible using each of their characteristic histopathologic findings. In the present case, numerous trophozoites and scattered cysts were found in the vessel wall and perivascular area and were seen in association with acute inflammation and diffuse hemorrhagic necrosis. The trophozoites were in round to ovoid shape, having 1–2 nuclei, and each of them contained 1–4 nucleoli. The cysts were round to ovoid shape, had a double-layered wall, and measured 15–20 µm in size. While the inner layer was round and rigid, the outer layer was wavy, which is consistent with the features of *B. mandrillaris*. The characteristic histopath-

ologic features of the three amoebae are listed in Table 1.

In the CSF study, the glucose level was in the normal range of 60 mg/dL and the protein level was elevated at 331.8 mg/dL, which is consistent with any of the amoebic encephalitis types. Unfortunately, a culture or pathologic smear of CSF was not performed. The CRP level in the blood was increased to 7.89 mg/dL, and the white blood cell count was normal. Additionally, an immunofluorescence study or polymerase chain reaction can be used to identify the specific organism. However, in the present case, using only the amoeba-specific histopathologic features was sufficient to identify *B. mandrillaris*, and this emphasizes the importance of examining the histopathological features of the amoebae.

ORCID

Su Jung Kum: <https://orcid.org/0000-0003-4871-3707>
 Hye Won Lee: <https://orcid.org/0000-0001-8540-524X>
 Hye Ra Jung: <https://orcid.org/0000-0002-1477-6606>
 Misun Choe: <https://orcid.org/0000-0002-1412-5360>
 Sang Pyo Kim: <https://orcid.org/0000-0003-0948-2408>

Author Contributions

Conceptualization: SPK.
 Data curation: SJK.
 Formal analysis: HRJ, MC.
 Investigation: SJK, HWL.
 Project administration: SPK.
 Supervision: SPK.
 Validation: HWL, HRJ, MC.

Writing—original draft: SJK, SPK.

Writing—review & editing: SJK, HWL, HRJ, MC, SPK.

Conflicts of Interest

The authors declare that they have no potential conflicts of interest.

Funding

No funding to declare.

REFERENCES

- Martinez AJ. Infection of the central nervous system due to *Acanthamoeba*. *Rev Infect Dis* 1991; 13 Suppl 5: S399-402.
- Diaz JH. The public health threat from *Balamuthia mandrillaris* in the southern United States. *J La State Med Soc* 2011; 163: 197-204.
- Matin A, Siddiqui R, Jayasekera S, Khan NA. Increasing importance of *Balamuthia mandrillaris*. *Clin Microbiol Rev* 2008; 21: 435-48.
- Itoh K, Yagita K, Nozaki T, et al. An autopsy case of *Balamuthia mandrillaris* amoebic encephalitis, a rare emerging infectious disease, with a brief review of the cases reported in Japan. *Neuropathology* 2015; 35: 64-9.
- Diaz JH. Behavioral and recreational risk factors for free-living amoebic infections. *J Travel Med* 2011; 18: 130-7.
- Kiderlen AF, Laube U. *Balamuthia mandrillaris*, an opportunistic agent of granulomatous amoebic encephalitis, infects the brain via the olfactory nerve pathway. *Parasitol Res* 2004; 94: 49-52.
- Visvesvara GS, Schuster FL, Martinez AJ. *Balamuthia mandrillaris*, N. G., N. Sp., agent of amoebic meningoencephalitis in humans and other animals. *J Eukaryot Microbiol* 1993; 40: 504-14.
- Visvesvara GS, Moura H, Schuster FL. Pathogenic and opportunistic free-living amoebae: *Acanthamoeba* spp., *Balamuthia mandrillaris*, *Naegleria fowleri*, and *Sappinia diploidea*. *FEMS Immunol Med Microbiol* 2007; 50: 1-26.
- Reddy R, Vijayaradhi M, Uppin MS, Challa S, Jabeen A, Borghain R. *Acanthamoeba* meningoencephalitis in an immunocompetent patient: an autopsy case report. *Neuropathology* 2011; 31: 183-7.

Diffuse Involvement of Primary Colorectal Lymphoma Simulating Ulcerative Colitis

Ji-Ye Kim, Sun Hee Chang, Han Seong Kim, Mee Joo

Department of Pathology, Inje University Ilsan Paik Hospital, Goyang, Korea

Diffuse involvement of colorectal lymphoma masquerading as colitis is a very rare presentation of primary colorectal lymphoma. Detecting occult lymphoma is difficult in the setting of diffuse colonic involvement with no definite mass and inflammatory mucosal changes. We encountered a case of diffuse-type primary colorectal lymphoma simulating ulcerative colitis in a previously healthy 31-year-old woman. Despite multiple mucosal biopsies, the biopsy diagnosis was not made due to unawareness of atypical lymphocytes admixed with dense lymphoplasmacytic infiltration. The present case emphasizes the importance of being aware of this rare presentation of primary colorectal lymphoma in order to avoid misdiagnosis.

Key Words: Colorectal lymphoma; Primary; Diffuse type; Colitis

Received: May 17, 2019 **Revised:** July 2, 2019 **Accepted:** July 12, 2019

Corresponding Author: Mee Joo, MD, PhD, Department of Pathology, Inje University Ilsan Paik Hospital, 170 Juhwa-ro, Ilsanseo-gu, Goyang 10380, Korea
Tel: +82-31-910-7141, Fax: +82-31-910-7139, E-mail: mjoo@paik.ac.kr

The incidence of primary colorectal lymphoma is very rare, accounting for 0.2%–0.6% of colorectal malignancies.¹ Primary colorectal lymphomas manifest in a variety of ways, ranging from solitary fungating masses to multiple polyps. In 1968, Friedman et al.² reported four cases of “lymphomatous colitis,” a rare form of primary colorectal lymphoma mimicking ulcerative colitis (UC). Since then, a small number of patients with diffuse-type colorectal lymphoma have been reported, in whom a clinical and/or histological diagnosis of colitis, including inflammatory bowel disease (IBD), was made initially but were subsequently discovered to have diffuse lymphoma involvement of the colon within a short period of time.^{3–17} IBD and immunosuppression have been reported as risk factors for primary colorectal lymphoma.¹⁸ Most IBD-related lymphomas develop late in the course of an extensive longstanding disease. In that respect, these cases differ from most reports of primary colorectal lymphoma as a complication of longstanding IBD. We experienced a case of UC-like primary colorectal lymphoma in a 31-year-old woman who presented with profuse hematochezia, was misdiagnosed with UC, and died of a diffuse lymphoma involving the entire colon 12 months after hematochezia first developed.

CASE REPORT

A 31-year-old woman with no prior history of IBD presented with intermittent abdominal pain and mucoid diarrhea. Five months later, she developed hematochezia and was diagnosed with UC on the basis of endoscopic biopsy. She was treated with oral Pentasa and Pentasa enema. However, she continued to be symptomatic with marked weight loss (20 kg in 4 months). Follow-up colonoscopy revealed continuous mucosal changes from the rectum to the cecum, such as diffuse hyperemia, edematous changes, friability, loss of normal vascularity, and multiple variable-sized ulcers, consistent with UC (Fig. 1A). No mass-forming lesion was present throughout. Abdominal and pelvic computed tomography revealed diffuse edematous wall thickening in the whole colon and multiple enlargements of mesenteric lymph nodes. No hepatosplenomegaly was observed. Multiple biopsies were taken from the terminal ileum, cecum, transverse colon, sigmoid colon, and rectum. All biopsy specimens revealed diffuse infiltration of large, atypical lymphoid cells with a high nucleus-to-cytoplasmic ratio, occasional prominent nucleoli, and mitotic figures (Fig. 1B, C). They expanded the lamina propria, pushed the crypts apart, and invaded the submucosa. By immunochem-

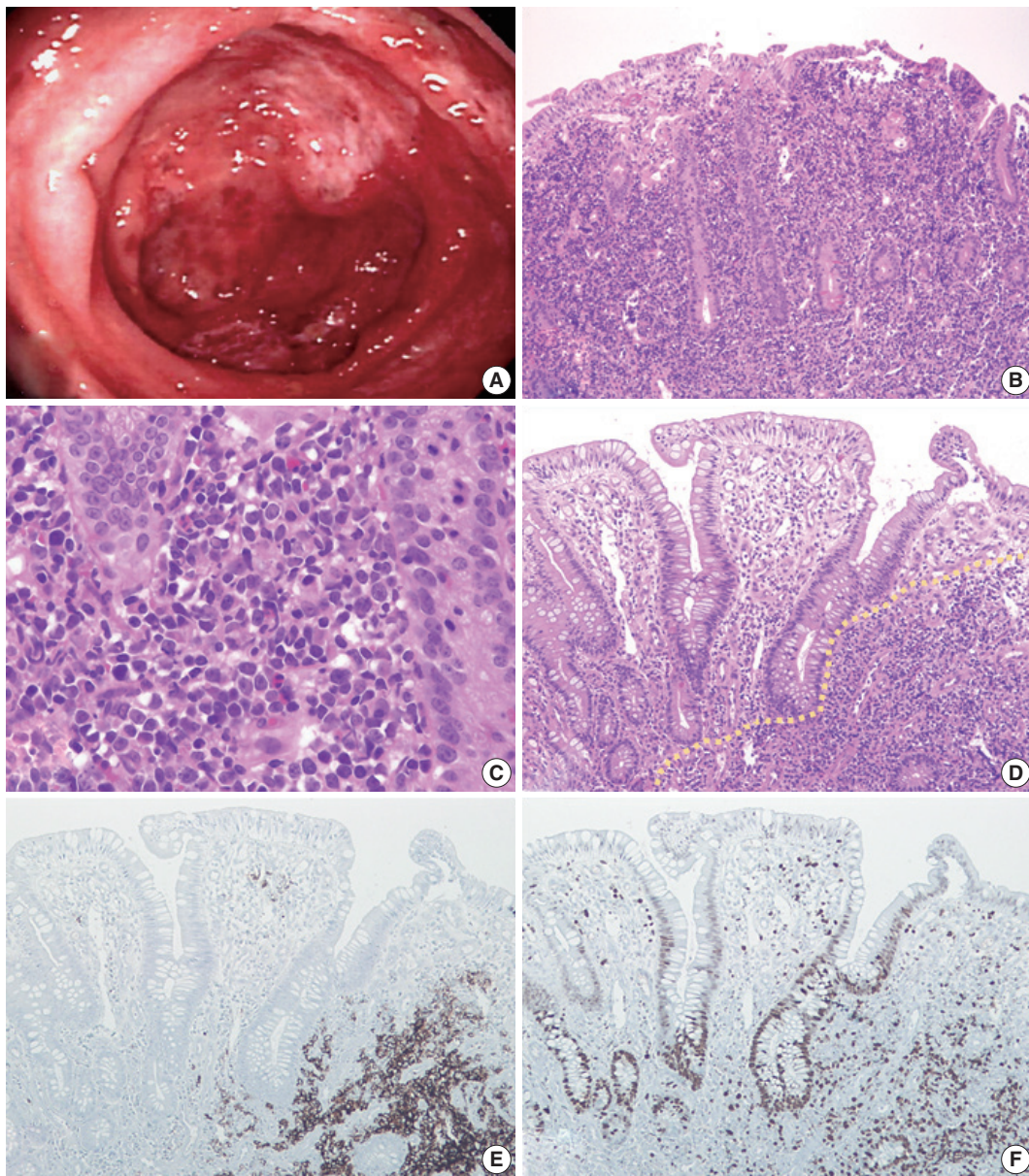


Fig. 1. (A) Colonoscopy reveals diffuse hyperemic inflamed mucosa with total loss of normal vascularity and surface ulceration from the rectum to the cecum. (B, C) Representative microphotographs of diffuse lymphoma involvement on the biopsy specimens. (B) The mucosa and submucosa are diffusely involved by densely packed lymphocytes with the background remnants of colonic crypts. Monotonous large-sized lymphocytes have vesicular chromatin and often membrane-bound nucleoli, resembling centroblasts (C). (D–F) Retrospective examination of initial colonoscopic biopsy. (D) The biopsied colonic mucosa displays crypt architectural distortion and dense inflammatory cell infiltration, resembling chronic colitis. Atypical lymphoid cells are aggregated in the bottom right corner (below the yellow dotted line), which show not only strong expression on CD20 immunostaining (E) but also high Ki-67 labeling index (F).

istry, the tumor cells were diffusely positive for CD20, bcl2, and p53, and negative for CD3, CD5, CD10, and cyclin D1. The Ki-67 labeling index was about 60%. The overall histology and immunophenotype supported a diagnosis of diffuse large B-cell lymphoma. There was no detectable evidence of extra-abdominal lymphadenopathy or lymphomatous involvement elsewhere. Bone marrow evaluation was also negative for lym-

phoma. As no extraintestinal disease was found, we considered it as a primary colorectal lymphoma. The patient died while receiving the second cycle of R-CHOP chemotherapy.

We retrospectively reviewed the colonoscopic biopsy specimens that were initially diagnosed with UC. At low magnification view, the background mucosa displayed crypt architectural distortion and dense inflammatory cell infiltration, resembling chronic

Table 1. Clinical and pathological findings of previously published cases of “colitis-like” diffuse-type colorectal lymphomas in the English literature

Year	Author	Sex/ Age (yr)	Pathologic diagnosis	Endoscopic findings	Revision of initial diagnosis	Superficial LAP at presentation	Extracolonic involvement
1968	Friedman et al. ²	M/37	Reticulum cell sarcoma	UC	No	No	Liver
1968	Friedman et al. ²	F/54	Malignant lymphoma	UC	Yes (colectomy)	No	No
1968	Friedman et al. ²	M/73	Lymphosarcoma	UC	Yes (Bx)	No	No
1980	Weir et al. ³	F/67	Lymphocytic lymphoma	CD	Yes (Bx)	Yes, generalized	BM
1992	McCullough et al. ⁴	M/44	Mantle cell lymphoma	UC	Yes (Bx)	Yes, cervical axillary	Pancreas
1995	Lenzen et al. ⁵	F/53	MALT lymphoma	UC	No	No	Upper GI tract, BM
1996	Robert et al. ⁶	F/71	Mantle cell lymphoma	UC	Yes (colectomy)	No	No
1996	Hirakawa et al. ⁷	M/47	T-cell lymphoma	UC	No	No	Upper GI tract
1997	Son et al. ⁸	F/40	Peripheral T-cell lymphoma	CD	Yes (Bx)	No	No
2003	Isomoto et al. ⁹	M/47	Adult T-cell leukemia/lymphoma	UC	No	Yes, generalized	Stomach, skin
2004	Payne et al. ¹⁰	F/76	High-grade T-cell lymphoma	Colitis	No	Yes, generalized	No
2004	Tamura et al. ¹¹	M/61	Mantle cell lymphoma	Colitis	No	No	Tonsil, upper GI tract
2008	Berkelhammer et al. ¹²	F/82	MALT lymphoma	CD	Yes (Bx)	No	No
2014	Koksal et al. ¹³	M/73	Mantle cell lymphoma	UC	No	No	Stomach
2015	Zaheen et al. ¹⁴	M/74	EBV-negative NK cell lymphoma	Colitis	No	No	BM, pleural effusion
2015	Wu et al. ¹⁵	M/56	T-cell lymphoma	Ulcers	Yes (Bx)	Yes, generalized	No
2016	Cheung et al. ¹⁶	NA/12	EBV-positive T-cell lymphoma	Colitis	No	No	Hepatosplenomegaly
2016	Cheung et al. ¹⁶	NA/6	EBV-positive T-cell lymphoma	CD	No	No	No
2017	Zenda et al. ¹⁷	M/59	Follicular lymphoma	UC	No	Yes, cervical inguinal	Spleen, BM
	Present case	F/32	Diffuse large B-cell lymphoma	UC	Yes (Bx)	No	No

LAP, lymphadenopathy; M, male; UC, ulcerative colitis; F, female; Bx, biopsy; CD, Crohn's disease; BM, bone marrow; MALT, mucosa-associated lymphoid tissue; GI, gastrointestinal; EBV, Epstein-Barr virus; NA, not available.

colitis. However, we found some lymphoma cells, which were admixed with other inflammatory cells or showed focal aggregation in the basal portion of the mucosa (Fig. 1D). Those lymphoma cells were more distinguishable on immunostaining for CD20 and Ki-67 (Fig. 1E, F).

Ethics statement

This study was approved by the Institutional Review Board of Inje University Ilsan Paik Hospital with a waiver of informed consent (IRB No. ISPAIK 2019-05-005) and performed in accordance with the principles of the Declaration of Helsinki.

DISCUSSION

Twenty cases (including the present one) of “colitis-like” diffuse-type colorectal lymphoma were reported in the English literature.²⁻¹⁷ We excluded cases of colorectal lymphoma developed in patients with a longstanding IBD or prior established diagnosis of extracolonic lymphoma. The clinical and pathological findings of these patients are summarized in Table 1. There were 10 men, 8 women, and two children. Their mean age at presentation was 53.2 years (range, 6 to 82 years). The main symptoms were diarrhea/hematochezia (90%), loss of weight (50%), ab-

dominal pain (25%), and fever (10%). Endoscopic findings were consistent with UC (55%), Crohn disease (20%), diffuse colitis (20%), and multiple ulcers (5%); no localized mass-like lesion was present. All cases were non-Hodgkin's lymphoma: eight were B-cell type (four mantle cell lymphomas, two mucosa-associated lymphoid tissue lymphomas, one diffuse large B-cell lymphoma, and one follicular lymphoma), seven were T-cell type, one was natural killer cell lymphoma, and four other unclassified lymphoreticular malignancies (one malignant lymphoma, one reticulum cell sarcoma, one lymphosarcoma, and one lymphocytic lymphoma). Of note, there were nine patients in whom colitis was histologically confirmed with multiple biopsy or colectomy but were subsequently found to have lymphoma involvement in a retrospective review of previous slides. Taken together, diffuse type primary colorectal lymphoma is a very rare disease and is easily misdiagnosed, particularly in reliance on endoscopic biopsy examination alone. The possibility of a hidden lymphomatous involvement would have to be considered in patients with medically refractory and rapidly progressive colitis.

Lymphoma involvement of the gastrointestinal (GI) tract may occur either as an isolated primary neoplasm or as a manifestation of systemic generalized lymphoma. To distinguish between primary and secondary GI lymphoma, Dawson's criteria is generally

applied: (1) no palpable superficial lymphadenopathy at initial presentation, (2) a normal chest X-ray with no mediastinal lymphadenopathy, (3) no evidence of leukemia, (4) a predominant mass in the bowel with only local lymphadenopathy, and (5) no hepatosplenomegaly.¹⁹ When the diagnostic criteria of primary colonic lymphoma are strictly applied, only seven of 20 cases of “colitis-like” colorectal lymphoma are eligible for diffuse-type primary colorectal lymphoma: 13 cases were excluded due to synchronous other organ involvement at initial presentation, such as superficial or generalized lymphadenopathy (six cases), upper GI involvement (five cases), bone marrow involvement (four cases), or hepatosplenomegaly (three cases), etc. Consequently, it is a reflection that “colitis-like” diffuse involvement of colorectal lymphoma seems to be more often secondary. Accurate discrimination between primary and secondary colorectal lymphoma is important for proper staging and management. In conclusion, since primary colorectal lymphoma can rarely manifest as “colitis-like” diffuse colonic involvement, awareness of this rare presentation is important to ensure proper diagnosis and treatment.

ORCID

Ji-Ye Kim: <https://orcid.org/0000-0003-4291-2967>

Sun Hee Chang: <https://orcid.org/0000-0002-7775-4711>

Han Seong Kim: <https://orcid.org/0000-0003-3740-0588>

Mee Joo: <https://orcid.org/0000-0002-5886-0287>

Author Contributions

Conceptualization: MJ.

Investigation: MJ.

Visualization: MJ.

Writing—original draft: JYK, MJ.

Writing—review & editing: JYK, MJ, SHC, HK.

Conflicts of Interest

The authors declare that they have no potential conflicts of interest.

Funding

No funding to declare.

REFERENCES

- Wong MT, Eu KW. Primary colorectal lymphomas. *Colorectal Dis* 2006; 8: 586-91.
- Friedman HB, Silver GM, Brown CH. Lymphoma of the colon simulating ulcerative colitis: report of four cases. *Am J Dig Dis* 1968; 13: 910-7.
- Weir AB, Poon MC, Groarke JF, Wilkerson JA. Lymphoma simulating Crohn’s colitis. *Dig Dis Sci* 1980; 25: 69-72.
- McCullough JE, Kim CH, Banks PM. Mantle zone lymphoma of the colon simulating diffuse inflammatory bowel disease: role of immunohistochemistry in establishing the diagnosis. *Dig Dis Sci* 1992; 37: 934-8.
- Lenzen R, Borchard F, Lübke H, Strohmeyer G. Colitis ulcerosa complicated by malignant lymphoma: case report and analysis of published works. *Gut* 1995; 36: 306-10.
- Robert ME, Kuo FC, Longtine JA, Sklar JL, Schrock T, Weidner N. Diffuse colonic mantle cell lymphoma in a patient with presumed ulcerative colitis: detection of a precursor monoclonal lymphoid population using polymerase chain reaction and immunohistochemistry. *Am J Surg Pathol* 1996; 20: 1024-31.
- Hirakawa K, Fuchigami T, Nakamura S, et al. Primary gastrointestinal T-cell lymphoma resembling multiple lymphomatous polyposis. *Gastroenterology* 1996; 111: 778-82.
- Son HJ, Rhee PL, Kim JJ, et al. Primary T-cell lymphoma of the colon. *Korean J Intern Med* 1997; 12: 238-41.
- Isomoto H, Furusu H, Onizuka Y, et al. Colonic involvement by adult T-cell leukemia/lymphoma mimicking ulcerative colitis. *Gastrointest Endosc* 2003; 58: 805-8.
- Payne S, Phillips M, Reffitt D, et al. An unusual case of colitis. *Gut* 2004; 53: 1824.
- Tamura S, Ohkawauchi K, Yokoyama Y, et al. Non-multiple lymphomatous polyposis form of mantle cell lymphoma in the gastrointestinal tract. *J Gastroenterol* 2004; 39: 995-1000.
- Berkelhammer C, Mohammed A, Zalzaleh G, Grella J, Blumstein A, Stein R. Spontaneous multiperforation in lymphomatous colitis masquerading as Crohn’s disease: 2 cases. *Inflamm Bowel Dis* 2008; 14: 1172-3.
- Koksal AS, Taskiran I, Kalkan IH, Kayacetin E. A rare endoscopic appearance of primary gastrointestinal mantle cell lymphoma resembling ulcerative colitis. *Bratisl Lek Listy* 2014; 115: 800-1.
- Zaheen A, Delabie J, Vajpeyi R, Frost DW. The first report of a previously undescribed EBV-negative NK-cell lymphoma of the GI tract presenting as chronic diarrhoea with eosinophilia. *BMJ Case Rep* 2015; 2015: bcr2015212103.
- Wu PH, Chu KE, Lin YM, Huang SH, Wu CC. T-cell lymphomas presenting as colon ulcers and eosinophilia. *Case Rep Gastroenterol* 2015; 9: 246-52.
- Cheung FM, Tong Y, Wang Y, et al. Epstein-Barr virus-positive T-cell-associated colitis mimicking inflammatory bowel disease: clinicopathological study of two cases. *Histopathology* 2016; 68: 465-8.
- Zenda T, Nakagawa N, Maruyama H, et al. Follicular lymphoma-related colitis resembling ulcerative colitis. *Clin J Gastroenterol*

2017; 10: 147-53.

18. Farrell RJ, Ang Y, Kileen P, et al. Increased incidence of non-Hodgkin's lymphoma in inflammatory bowel disease patients on immunosuppressive therapy but overall risk is low. *Gut* 2000; 47: 514-9.
19. Dawson IM, Cornes JS, Morson BC. Primary malignant lymphoid tumours of the intestinal tract. Report of 37 cases with a study of factors influencing prognosis. *Br J Surg* 1961; 49: 80-9.

Human Papillomavirus–Related Multiphenotypic Sinonasal Carcinoma with Late Recurrence

Bokyung Ahn, Eojin Kim, Harim Oh, Yang-Seok Chae, Chul Hwan Kim, Youngseok Lee, Jeong Hyeon Lee, Yoo Jin Lee

Department of Pathology, Korea University Anam Hospital, Korea University College of Medicine, Seoul, Korea

In 2013, Bishop et al.¹ introduced a newly-described human papillomavirus (HPV)–related sinonasal carcinoma, referred to as “HPV-related carcinoma with adenoid cystic carcinoma-like features,” and it is provisionally included in the 2017 World Health Organization (WHO) classification of head and neck tumors.² In 2017, Bishop et al.³ suggested a change in the name to ‘HPV-related multiphenotypic sinonasal carcinoma’ to encompass its broader histologic features.¹ We report a case of recurrent ‘HPV-related multiphenotypic sinonasal carcinoma’ with the second-longest follow-up time and an unusual HPV genotype with abrupt keratinization.

CASE REPORT

A 66-year-old man underwent surgical resection for a polypoid lesion in his right nasal cavity, and he was diagnosed with adenoid cystic carcinoma, solid variant. He received no additional postoperative treatment, and he did not have any routine follow-up visits for 16 years until he presented to the Otorhinolaryngology Department of our institution due to 12 months of right nasal obstruction. A new fungating mass in the right nasal cavity was found, and a piecemeal removal was performed.

Microscopically, the tumor showed highly cellular proliferation of basaloid cells with a predominantly lobular growth pattern and comedonecrosis (Fig. 1A). There were several foci of cribriform growth pattern aligned around cylindromatous microcystic spaces filled with mucopolysaccharide-like basophilic

material, resembling adenoid cystic carcinoma (Fig. 1B, C). The tumor cells showed relatively large, uniform, round nuclei with prominent nucleoli and scant granular cytoplasm. Frequent squamous differentiation with abrupt keratinization (Fig. 1D) and varying degrees of dysplasia of the overlying surface squamous epithelium were noted (Fig. 1E). Neither lymphovascular nor perineural invasion was present. On immunohistochemical staining, the tumor cells were diffusely positive for cytokeratin and p63, but they were negative for CD117 immunostain in both the solid and cribriform areas. As a surrogate marker for the presence of HPV, p16 immunostain showed strong and diffuse reactivity in nearly the entire tumor, except the dysplastic surface squamous epithelium (Fig. 1F). We further confirmed the presence of HPV genotype 33 and 51 by quantitative HPV-specific polymerase chain reaction (Anyplex II HPV28 Detection, Seegene Inc., Seoul, Korea).

The combination of the microscopic findings, the immunoprofile, and the HPV testing results allowed us to reclassify the formerly diagnosed adenoid cystic carcinoma to the newly-emerging entity, HPV-related multiphenotypic sinonasal carcinoma.

Ethics statement

Study approval was obtained from the Institutional Review Board of Korea University Anam Hospital (IRB No. 2019AN 0012), and informed consent was waived.

DISCUSSION

Until now, 56 cases of HPV-related carcinoma with adenoid cystic carcinoma-like features have been reported.^{1,3-6} The tumor is defined as a sinonasal carcinoma with the morphologic features of a salivary gland tumor including admixed ductal and myoepithelial elements, surface squamous epithelial dysplasia,

Received: January 29, 2019 Revised: March 27, 2019
Accepted: April 2, 2019

Corresponding Author: Yoo Jin Lee, MD
Department of Pathology, Korea University Anam Hospital, Korea University
College of Medicine, 73 Incheon-ro, Seongbuk-gu, Seoul 02841, Korea
Tel: +82-2-920-5590, Fax: +82-2-920-6576, E-mail: yujinn87@korea.ac.kr

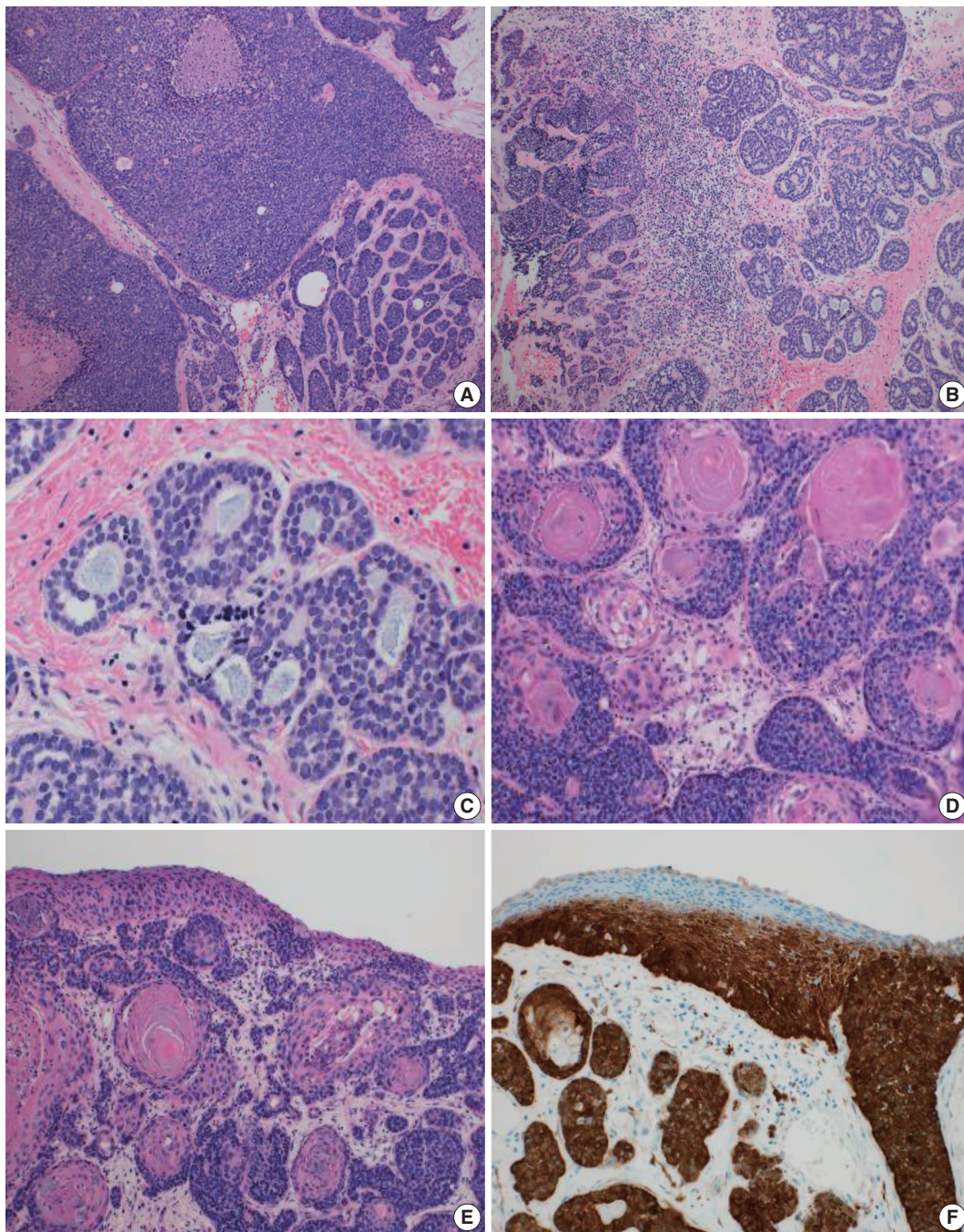


Fig. 1. Microscopic findings of an human papillomavirus–related multiphenotypic sinonasal carcinoma. (A) Basaloid cells with predominant solid, lobular pattern and comedonecrosis. (B, C) A few foci of cribriform architecture resembling adenoid cystic carcinoma. (D) Frequent squamous differentiation with abrupt keratinization. (E) Varying degree of surface epithelial dysplasia. (F) Diffuse, strong positive p16 immunostain sparing the dysplastic surface epithelium.

association with high-risk HPV (particularly type 33), and no *MYB* gene fusion. A new terminology, HPV-related multiphenotypic sinonasal carcinoma, has been recently suggested due to the tumor's diverse morphology, including anaplastic giant cells, clear cells, sarcomatoid cells, chondroid structure, osseous differ-

entiation, and hemangiopericytoma-like blood vessels.³

Although this tumor was classified under the non-keratinizing squamous cell carcinoma category in the 2017 WHO classification of head and neck tumors, only a few cases showed squamous differentiation and abrupt keratinization.^{2,3,7} A total

of nine cases demonstrated scattered foci of squamous differentiation,³ with two cases showing abrupt keratinization,⁸ and our case is another with abrupt keratinization. Given these various morphological features, keratinization alone cannot be a differential point from conventional squamous cell carcinoma.

This tumor was suggested to have an indolent behavior with a better prognosis than other carcinomas.^{3,6} While the reported mean follow-up time is 42 months, frequent local recurrence (13 patients), rare distant metastasis (2 patients), and no tumor-related death were noted.^{1,3-6} One former report introduced a recurrent case after a 30-year disease-free interval,⁶ and our case has the second-longest follow-up of any published reports, supporting the tumor's characterization of being indolent yet having potential for late recurrence. Due to the small number of reported cases and limited clinical follow-up, more clinical data are needed to better understand the tumor prognosis and treatment options.

Another interesting point of our case is that, to our knowledge, this is the first case of HPV-related multiphenotypic sinonasal carcinoma that showed the high-risk HPV genotype 51. HPV 51 is included in the WHO-categorized cancer-causing HPV types and is a high-risk carcinogen in head and neck cancer.⁹ However, its oncogenic implication or the tumor characteristics associated with HPV 51 infection have not been determined. One study reported HPV 51 to be one of the predominant genotypes in squamous cell carcinoma of the oral cavity and larynx,¹⁰ although none of the HPV-related multiphenotypic sinonasal carcinomas have shown HPV 51 thus far.

To better understand the clinicopathologic features of this rare disease, more data on such rare cases need to be collected. We report a case of HPV-related multiphenotypic sinonasal carcinoma with abrupt keratinization and a rare HPV type that recurred after a long indolent period of 16 years.

ORCID

Bokyung Ahn: <https://orcid.org/0000-0002-0229-2276>
 Eojin Kim: <https://orcid.org/0000-0003-3111-6754>
 Harim Oh: <https://orcid.org/0000-0003-4904-4015>
 Yang-Seok Chae: <https://orcid.org/0000-0002-8801-0910>
 Chul Hwan Kim: <https://orcid.org/0000-0003-2026-8824>
 Youngseok Lee: <https://orcid.org/0000-0002-9762-4957>
 Jeong Hyeon Lee: <https://orcid.org/0000-0003-2041-4617>
 Yoo Jin Lee: <https://orcid.org/0000-0003-3830-7051>

Author Contributions

Conceptualization: BA.

Data curation: YJL.

Formal analysis: BA, YJL.

Investigation: BA, HO, EK.

Methodology: JHL, YL, CHK, YSC.

Project administration: YJL, CHK.

Resources: YJL.

Supervision: YJL.

Validation: YJL, CHK.

Visualization: BA, YJL.

Writing—original draft: BA.

Writing—review & editing: YJL.

Conflicts of Interest

The authors declare that they have no potential conflicts of interest.

Funding

No funding to declare.

REFERENCES

- Bishop JA, Ogawa T, Stelow EB, et al. Human papillomavirus-related carcinoma with adenoid cystic-like features: a peculiar variant of head and neck cancer restricted to the sinonasal tract. *Am J Surg Pathol* 2013; 37: 836-44.
- El-Naggar AK, Chan JK, Grandis JR, Takata T, Slootweg PJ. WHO classification of head and neck tumours. 4th ed. Lyon: IARC Press, 2017.
- Bishop JA, Andreasen S, Hang JF, et al. HPV-related multiphenotypic sinonasal carcinoma: an expanded series of 49 cases of the tumor formerly known as HPV-related carcinoma with adenoid cystic carcinoma-like features. *Am J Surg Pathol* 2017; 41: 1690-701.
- Chouake RJ, Cohen M, Illoreta AM. Case report: HPV-related carcinoma with adenoid cystic-like features of the sinonasal tract. *Laryngoscope* 2018; 128: 1515-7.
- Ruangritchankul K, Jitpasutham T, Kitkumthorn N, Thorner PS, Keelawat S. Human papillomavirus-related multiphenotypic sinonasal carcinoma: first case report associated with an intermediate-risk HPV type and literatures review. *Hum Pathol Case Rep* 2018; 14: 20-4.
- Shah AA, Lamarre ED, Bishop JA. Human papillomavirus-related multiphenotypic sinonasal carcinoma: a case report documenting the potential for very late tumor recurrence. *Head Neck Pathol* 2018; 12: 623-8.
- Bishop JA, Westra WH. Human papillomavirus-related multiphenotypic sinonasal carcinoma: An emerging tumor type with a unique

- microscopic appearance and a paradoxical clinical behaviour. *Oral Oncol* 2018; 87: 17-20.
8. Hang JF, Hsieh MS, Li WY, et al. Human papillomavirus-related carcinoma with adenoid cystic-like features: a series of five cases expanding the pathological spectrum. *Histopathology* 2017; 71: 887-96.
 9. Kashif M, Afzal N, Tayyab MA, Shahzad F, Jahan S. Human papilloma virus: important etiological factor in head and neck squamous cell carcinogenesis. *J Cancer Biol Res* 2016; 4: 1081.
 10. Snow AN, Laudadio J. Human papillomavirus detection in head and neck squamous cell carcinomas. *Adv Anat Pathol* 2010; 17: 394-403.

Liquid-Based Cytology Features of Papillary Squamotransitional Cell Carcinoma of the Uterine Cervix

Yangkyu Lee*, Younghwa Choi*, Kiryang Lee¹, Youngeun Lee¹, Hyojin Kim,
Ji-Young Choe², Hye Seung Lee, Yong Beom Kim³, Haeryoung Kim¹

Department of Pathology, Seoul National University Bundang Hospital, Seoul National University College of Medicine, Seongnam;

¹Department of Pathology, Seoul National University Hospital, Seoul National University College of Medicine, Seoul;

²Department of Pathology, Hallym University Sacred Heart Hospital, Hallym University College of Medicine, Anyang;

³Department of Obstetrics and Gynecology, Seoul National University Bundang Hospital, Seoul National University College of Medicine, Seongnam, Korea

Papillary squamotransitional cell carcinoma (PSTCC) of the uterine cervix is an uncommon variant of cervical squamous cell carcinoma (SCC).¹ Here we describe the SurePath liquid-based cytology (LBC) findings of a case of PSTCC which showed a combination of cytological features of low-grade papillary urothelial carcinoma (LGPUC) and SCC.

CASE REPORT

A 77-year-old previously healthy woman presented with bloody vaginal discharge at the outpatient clinic. A colposcopy revealed a 2.5 cm-sized papillary mass (Fig. 1), and a punch biopsy was performed. After the possibility of a PSTCC or papillary SCC was suggested on the biopsy, she underwent a total abdominal hysterectomy with bilateral salpingo-oophorectomy. Two years later, she returned to the clinic complaining of vaginal discharge. A 6-mm-sized enhancing nodular lesion was noted at the right vaginal stump on pelvic computed tomography, and a cervicovaginal smear and punch biopsy was taken to confirm recurrence. However, further treatment of the vaginal lesion was not performed, as imaging incidentally revealed a pancreatic tail neoplasm with peritoneal seeding. The patient was subsequently referred to hospice care.

At low-power magnification, the LBC preparation was highly cellular, showing a few small hyperchromatic crowded groups (HCGs) in a background of abundant scattered cells (Fig. 2A). At higher magnification, the HCGs were 3-dimensional irregularly-shaped papillary fragments containing fibrovascular cores. The atypical cells lining the papillary clusters were relatively uniformly distributed with mild nuclear overlapping (Fig. 2B). The nuclei were smaller than those of parabasal cells, and were round-to-oval with smooth nuclear membranes. Nucleoli were small and almost inconspicuous. Mitotic figures were only occasionally seen. Similar-looking atypical cells were individually scattered in the background (Fig. 2B, C). Some cells were spindle-shaped with long and tapered cytoplasmic processes (Fig. 2C). Altogether, most of the neoplastic cells demonstrated the cytological features of LGPUC. There were also a few interspersed cells with increased nuclear-to-cytoplasmic ratio, hyperchromasia and nuclear membrane irregularity, suggestive of high-grade squamous intraepithelial lesion (HSIL) (Fig. 2D). A small cluster of dyskeratotic cells was seen (Fig. 2E, F). Tumor diathesis was not identified.

The biopsied tissue demonstrated papillary excrescences containing fibrovascular cores (Fig. 3A). The lining epithelium showed hybrid features of LGPUC and SCC (Fig. 3B, C). The LGPUC-like component was seen towards the basal layers and showed mild cytological atypia. Towards the surface of the papillary structures, there was evidence of keratinization and high-grade cytological atypia. Koilocytosis was focally seen (Fig. 3D). Although stromal invasion was not observed in the biopsied tissue, the subsequent hysterectomy specimen demonstrated residual tumor with stromal invasion and vascular invasion in the parametrial vessels. Immunohistochemistry revealed diffuse nuclear p63 expression, and the

Received: May 9, 2019 Revised: May 28, 2019

Accepted: June 5, 2019

Corresponding Author: Haeryoung Kim, MD, PhD

Department of Pathology, Seoul National University College of Medicine, Basic Science Building #101, 103 Daehak-ro, Jongno-gu, Seoul 03080, Korea
Tel: +82-2-740-8322, Fax: +82-2-765-5600, E-mail: haeryoung.kim@snu.ac.kr

*Yangkyu Lee and Younghwa Choi contributed equally to this work.

tumor cells were cytokeratin 7 (CK7)-positive and CK20-negative. A human papillomavirus (HPV) test (LG AdvanSure GenoBlot Assay, LG Life Sciences, Seoul, Korea) detected “other type” HPV. The histologic findings of the recurrent tumor were similar to



Fig. 1. Colposcopy reveals a friable papillary mass in the cervical canal.

that of the initial tumor.

Ethics statement

This case study was approved by the Institutional Review Board of Seoul National University Bundang Hospital (IRB approval number B-1710-427-702) and informed consent was waived.

DISCUSSION

PSTCC was first reported in 1986 by Randall et al.¹ as a variant of SCC showing varying degrees of urothelial-like differentiation. Due to the predominantly exophytic nature of these tumors, invasion may not be detected on small biopsies or cervicovaginal cytology. However, despite the surface papillary growth pattern, PSTCCs have been frequently associated with deep invasion, local recurrence and distant metastasis.¹⁻³

While the clinicopathological features of PSTCC have been discussed in several case reports, the cytological findings of PSTCC have only been described in two reports: one study described the

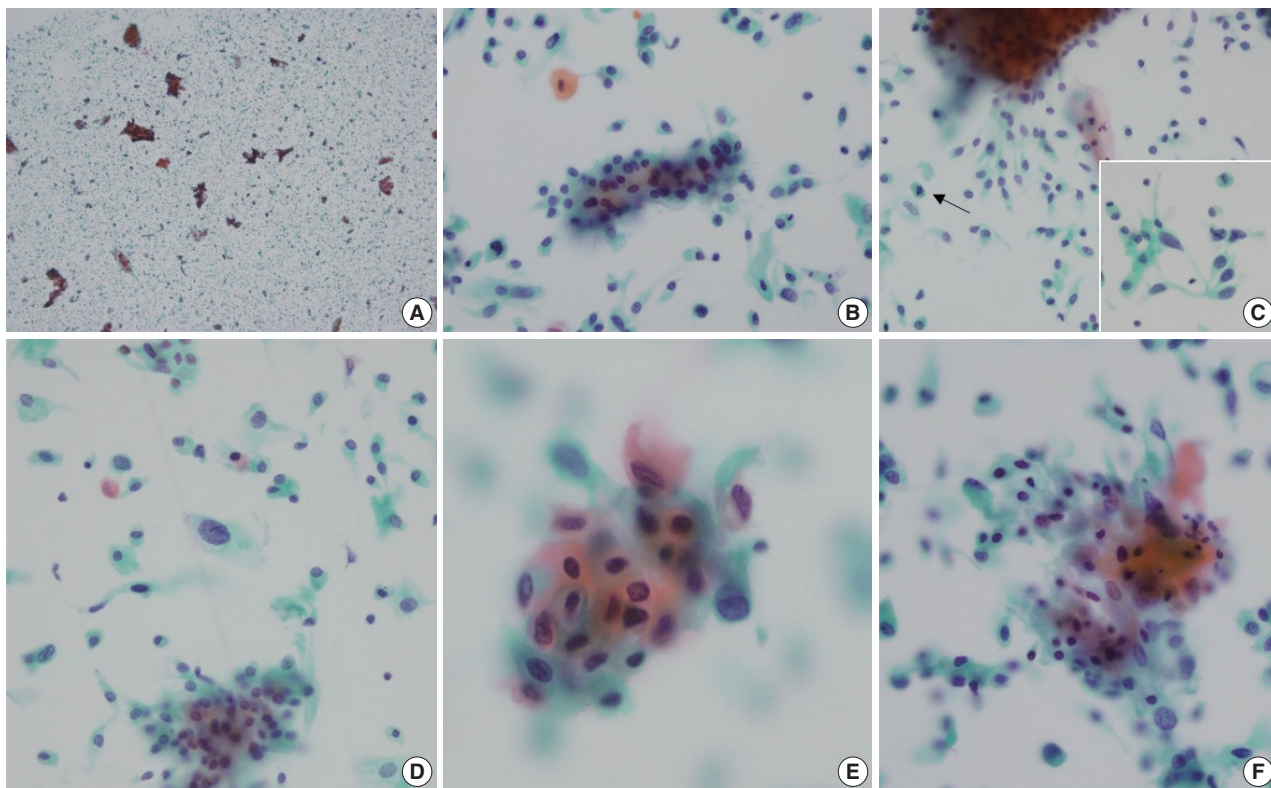


Fig. 2. Liquid-based cytology findings. (A) Low-power magnification shows some scattered hyperchromatic crowded groups and abundant individually scattered cells. (B) A papillary cluster (center) is lined by small neoplastic cells with round-to-oval nuclei and minimal nuclear atypia. (C) The scattered neoplastic cells demonstrate similar features, with eccentrically located, round-to-oval nuclei. Long cytoplasmic processes are seen in some neoplastic cells (“cercariform” cells) at the edge of papillary fragments (C, inset). A mitotic figure is seen (arrow). (D) A high-grade squamous intraepithelial lesion cell with coarse chromatin and irregular nuclear membrane (center) is seen among the scattered low-grade urothelial carcinoma-like cells. (E, F) Dyskeratotic cells and focal koilocytotic atypia are occasionally seen.

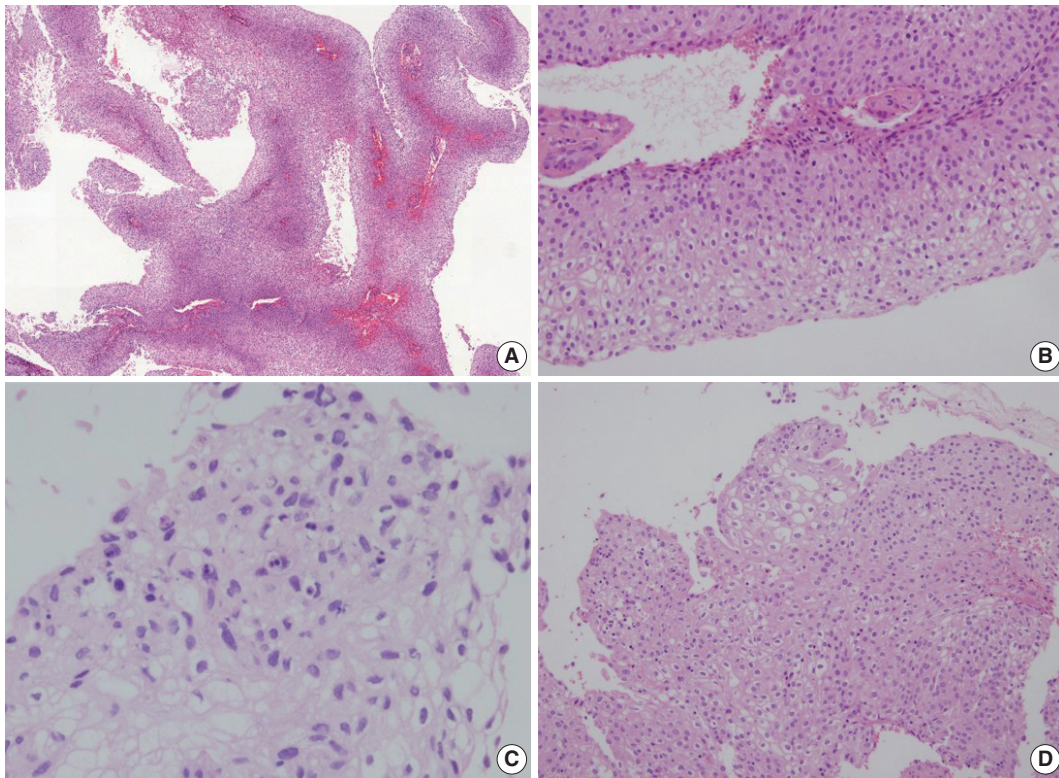


Fig. 3. Histological findings. (A) Low-power view demonstrates papillary structures with fibrovascular cores. (B) The papillae are mostly lined by urothelial-like cells. (C, D) Focal areas of keratinization (C) and koilocytotic atypia (D) are seen in the surfaces of the papillae.

LBC features of six cases,⁴ and the other one is a single case report describing the conventional smear features.⁵ The LBC features of PSTCC in this case could be summarized as follows: (1) a moderate-to-high cellularity, (2) HCGs characterized by 3-dimensional papillary fragments with branching architecture, (3) urothelial-like features, and (4) loosely dispersed hyperchromatic parabasal-like cells in the background.^{4,5}

The differential diagnosis of PSTCC includes a spectrum of lesions ranging from reactive to neoplastic, including papillary immature metaplasia and HSIL with papillary configuration.^{6,7} Immature metaplastic and repair cells are immature parabasal-like cells with cytoplasmic projections, 2-dimensional sheets and fine chromatin, while PSTCCs frequently demonstrate 3-dimensional HCG with papillary architecture and hyperchromatic nuclei. Although papillary architecture may be seen in HSILs, the papillary fragments of PSTCC have been described to show more complex arborizing patterns.⁴ In addition, the presence of horizontally aligned cells on the surface of papillary structures—similar to that seen in LGPUC in urine cytology—has been shown to be a characteristic cytological feature of PSTCC.^{4,8}

Despite the urothelial-like features, PSTCCs have been suggested to be metaplastic variants of SCC. The CK7+/CK20–

profile of PSTCC (including this case) is identical to that of müllerian epithelium.³ Moreover, similarly to SCC, HPV and allelic losses at 3p have been implicated in the pathogenesis of PSTCCs, while chromosome 9 alterations (common in bladder cancer) were not detected.^{3,9,10}

ORCID

Yangkyu Lee: <https://orcid.org/0000-0002-6008-7713>

Younghwa Choi: <https://orcid.org/0000-0002-1425-9422>

Kiryang Lee: <https://orcid.org/0000-0003-3769-001X>

Youngeun Lee: <https://orcid.org/0000-0002-0000-1615>

Hyojin Kim: <https://orcid.org/0000-0001-9201-8328>

Ji-Young Choe: <https://orcid.org/0000-0001-7967-8487>

Hye Seung Lee: <https://orcid.org/0000-0002-1667-7986>

Yong Beom Kim: <https://orcid.org/0000-0003-1196-369X>

Haeryoung Kim: <https://orcid.org/0000-0002-4205-9081>

Author Contributions

Conceptualization: HK (Haeryoung Kim).

Data curation: YL (Yangkyu Lee), YC.

Investigation: YL (Yangkyu Lee), KL, YL (Youngeun Lee).

Methodology: YL (Yangkyu Lee), HK (Haeryoung Kim).

Resources: HK (Hyojin Kim), JYC, HSL, YBK, HK (Haeryoung Kim).

Supervision: HK (Haeryoung Kim).

Visualization: YL (Yangkyu Lee), HK (Haeryoung Kim).

Writing—original draft: YL (Yangkyu Lee), YC, KL.

Writing—review & editing: YL (Yangkyu Lee), KL, HK (Haeryoung Kim).

Conflicts of Interest

The authors declare that they have no potential conflicts of interest.

Funding

No funding to declare.

REFERENCES

1. Randall ME, Andersen WA, Mills SE, Kim JA. Papillary squamous cell carcinoma of the uterine cervix: a clinicopathologic study of nine cases. *Int J Gynecol Pathol* 1986; 5: 1-10.
2. Al-Nafussi AI, Al-Yusif R. Papillary squamotransitional cell carcinoma of the uterine cervix: an advanced stage disease despite superficial location: report of two cases and review of the literature. *Eur J Gynaecol Oncol* 1998; 19: 455-7.
3. Koenig C, Turnicky RP, Kankam CF, Tavassoli FA. Papillary squamotransitional cell carcinoma of the cervix: a report of 32 cases. *Am J Surg Pathol* 1997; 21: 915-21.
4. Ng WK. Thin-layer (liquid-based) cytologic findings of papillary squamotransitional cell carcinoma of the cervix. Review of cases over a 4-year period with emphasis on potential diagnostic pitfalls. *Acta Cytol* 2003; 47: 141-8.
5. Vesoulis Z, Erhardt CA. Cytologic diagnosis of vaginal papillary squamotransitional cell carcinoma. A case report. *Acta Cytol* 2001; 45: 465-9.
6. Kokka F, Verma M, Singh N, Faruqi A, Yoon J, Reynolds K. Papillary squamotransitional cell carcinoma of the uterine cervix: report of three cases and review of the literature. *Pathology* 2006; 38: 584-6.
7. Kim HS, Seon MI, Kim YJ, Kim HS. Cytologic features of papillary immature metaplasia of uterine cervix. *Korean J Cytopathol* 2002; 13: 21-7.
8. Chung YR, Won JK, Park IA, et al. Cytomorphological characteristics of low-grade papillary urothelial carcinoma for differential diagnosis from benign papillary urothelial lesions: logistic regression analysis in SurePath(TM) liquid-based voided urine cytology. *Cytopathology* 2016; 27: 83-90.
9. Fujimoto T, Sakuragi N, Shimizu M, et al. Papillary squamous cell carcinoma of the uterine cervix: a report of two cases with human papillomavirus 16 DNA. *Acta Obstet Gynecol Scand* 2002; 81: 176-8.
10. Maitra A, Wistuba, II, Gibbons D, Gazdar AF, Albores-Saavedra J. Allelic losses at chromosome 3p are seen in human papilloma virus 16 associated transitional cell carcinoma of the cervix. *Gynecol Oncol* 1999; 74: 361-8.

RETRACTION

Journal of Pathology and Translational Medicine 2019; 53: 345
<https://doi.org/10.4132/jptm.2019.09.06>

JPTM

RETRACTION: eNOS Gene Polymorphisms in Perinatal Hypoxic-Ischemic Encephalopathy

Journal of Pathology and Translational Medicine Editors

This article¹ has been retracted at the request of the Editors. *Journal of Pathology and Translational Medicine*, formerly known as *The Korean Journal of Pathology* (1967–2014), requires that Institutional Review Board (IRB) approval is received for all studies on human subjects and that authors follow guidelines for research and publication ethics.

Concerns were raised about unjustified authorship and false statements regarding IRB approval. After evaluating the concerns carefully, we asked the corresponding author to provide an explanation for the concerns. The corresponding author notified the Journal that IRB approval from the author's institution was not obtained for the human subjects research described in the article. In addition, the corresponding author stated that the five co-authors (MC, KSH, DCC, IYC, and MJK) were attributed as authors without having made intellectual contributions to this study, and therefore agreed with changing the five persons' co-authorship to contributorship. In Korea, unjustified authorship is construed as a type of research misconduct (Ministry of Science and Technology, directive No. 236, enacted 2007.2.8.).

As a consequence, the Editors of *Journal of Pathology and Translational Medicine* retract this article. The corresponding author agrees to the retraction and apologizes to the Korean Society of Pathologists for any inconvenience caused by the publication and retraction of this article.

REFERENCE

1. Cho M, Hyun KS, Chung DC, Choi IY, Kim MJ, Chang YP. eNOS gene polymorphisms in perinatal hypoxic-ischemic encephalopathy. *Korean J Pathol* 2009; 43: 306-11.

